# Patch clamp experiments with human neuron-like cells under different gravity conditions

Thesis presented in fulfilment of

the thesis requirement for the degree of

Doctor of Philosophy in Natural Sciences (Dr. rer. nat.)

Faculty of Natural Sciences

Universität Hohenheim

Institute of Physiology (230)

Department of Membrane Physiology (230b)

presented by

Florian Peter Michael Kohn

from Stuttgart, Germany

2010

| | |
|---|---|
| Dean: | Prof. Dr. Heinz Breer |
| Reviewer: | Prof. Dr. Wolfgang Hanke |
| Co-reviewer: | Prof. Dr. Reinhardt Hilbig |
| Submitted: | 11th June 2010 |
| Oral defence (viva voce): | 04th August 2010 |

This submission was accepted on 20th July 2010 by the Faculty for Natural Sciences at the Universität Hohenheim as „Thesis presented in fulfilment of the thesis requirement for the degree of Doctor of Philosophy in Natural Sciences (Dr. rer. nat.)".

*If I have seen further than others, it is by standing upon the shoulders of giants.*

- Isaac Newton

This piece of work is dedicated to Ms. Hausmann, my former biology tutor.

I sincerely thank her for inspiring me!

# 1 Introduction

Gravity is the weakest force of the four fundamental interactions of nature (strong interaction, weak interaction, electromagnetic force and gravity). Nevertheless it is responsible for the formation of stars and planets as the Sun or Earth (Montmerle et al. 2006). During the ages, many properties on Earth as solar irradiation, temperature, composition of the atmosphere, humidity and other, changed. Earth's gravity field itself however did not change significantly after the final stages of planet formation, therefore it was (and is) constant during evolution and life adapted to 1*g*. This permanent physical stimulus led to the formation of gravity perceiving systems in many organisms which influence growth or behaviour.

For plants, gravitropism, the growth in response to gravity, plays an important role during germination and growth. The root grows towards the gravitational pull (positive gravitropism) to gain nutrients, water and stability. The stem grows against the gravitational pull (negative gravitropism). The adaptation to the gravity field can only be achieved by growth. Growth has a delay of several minutes (root orientation) to longer periods (longitudinal growth) since the nucleus is involved. Recent experiments indicate the existence of fast electric signals in root cells during gravity stimuli, but the function of this process is not clear (personal correspondence with S. Mancuso[1] during an ESA meeting in Noordwijk 2009, and D. Volkmann[2] at the Gravimeeting 2009).

For mobile organisms, fast gravity perceiving systems exist. Along with the different organisms, the mechanics of the gravity perceiving systems vary.

Probably the most investigated system in animals (and humans) is the vestibular organ (*Organon vestibulare*) of vertebrates. It is the most important component in the balance system beside the visual system and proprioreception. The conjugated vestibular organ is located in the inner ear. In general, it consists of two small chambers, *Sacculus* and *Utriculus,* filled with endolymp and three semicircular canals (lateral, anterior and posterior) which are aligned approximately orthogonally to each other. The semicircular canals are responsible for the perception of angular acceleration. Each of the semicircular canals is filled with endolymp and contains a specialized area (*cupula*) where sensory hair cells transduct the

[1] International Plant Neurobiology Laboratory, University of Florence, Italy
[2] Rheinische Friedrich-Wilhelms-University, Bonn, Germany

mechanical movement of the endolymp into electrical signals. *Utriculus* and *Sacculus,* the otolithic organs*,* are responsible for the detection of linear acceleration. They are aligned orthogonally to each other. *Utriculus* perceives horizontal acceleration, *Sacculus* vertical stimuli. The stereocilia of hair cells protrude into an otolithic membrane with small particles (statoconia). The movement of these particles deflects the stereocilia of the hair cells and this stimulus is transduced into an electric signal.

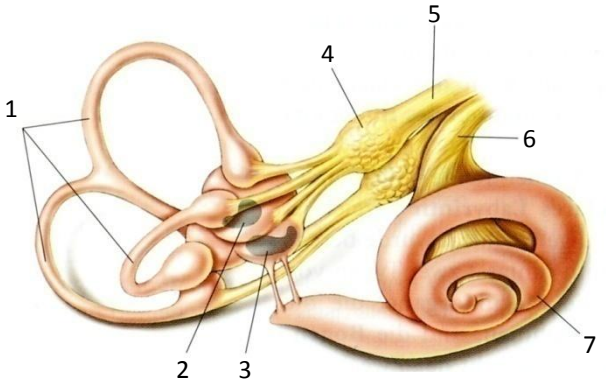


Figure 1.1: Human vestibular system and cochlea.

1- Semicircular canals
2 Utriculus
3 Sacculus
4 Ganglion vestibularis
5 N. Vestibularis
6 N. Cochlearis
7 Cochlea

(from Neurowissenschaften, 3rd ed.; modified)

Fishes and amphibians in general have a similar system. They possess three semicircular canals and three macular organs (Utriculus, Sacculus and Lagena) with, compared to humans, large otoliths (Lapillus, Sagitta, and Asteriscus). The increased size can probably be affiliated with the need for a more sensitive vestibular system in their aquatic habitat where gravity is compensated by buoyant force. Beside the reception of movement and acceleration, the system is also used for hearing.

Some unicellular organisms as *Paramecium* or *Euglena* are capable of orienting in Earth's gravity field (gravitaxis) without identified sensory systems as they exist in complex organisms. This raises the question how these unicellular organisms detect gravity. The organelles in the cytosol could have a similar function as the statoliths in root tips or the vestibular system but this is not verified. In *Paramecium*, mechanosensitive ion channels ($Ca^+$ and $K^+$) can be found in the cell membrane. They are located asymmetrically along the anterior-posterior axis. If a paramecium subsides, the changed density in the surrounding medium compared to the density of the cytosol activates the mechanosensitive ion channels which change the membrane potential. This receptor potential, together with intracellular calcium controls the three-dimensional oscillations of the cilia and flagellums and enables orientation in Earth's gravity field (Machemer 1998).

This indicates that the cell membrane, membrane proteins and the membrane potential are involved in the reception of gravity of unicellular organisms. These components are also the

essential elements of the properties of neuronal tissue therefore the question arises if and how neuronal tissue is influenced by gravity. Neuronal tissue (from the complete brain to single cells) fulfils all requirements to be treated as an excitable medium, as the generation of ordered structures, pattern formation and the generation of excitation-depression waves (Hanke et al. 1998). "*It exhibits the behaviour of non-linear thermodynamical systems" (*Hanke et al 1998*)* and therefore the properties depend on the parameters (temperature, etc…) and on weak external forces as gravity (Hanke et al. 2006).

The reaction of neuronal tissue to altered gravity is examined intensively on different levels. The behaviour of the brain is examined with non invasive methods as EEG, for example with recordings of slow cortical potentials (SCP) which reflect the excitability of the brain (Elbert 1993). It was shown in 2 parabolic flight campaigns that the SCP of the subjects are clearly gravity dependent whereby the polarity of the DC shifts depend on each individual brain (Wiedemann et al. 2010).

The retina, as an easy accessible part of the central nervous system, was used to investigate the gravity dependence of excitable tissue. The retinal spreading depression (rSD) is a propagating excitation depression wave and is well described (Leao 1944, Hanke 1999). The propagating rSD can easily be observed with the naked eye since the intrinsic optical signal (IOS) is changing (due to a change in the cell volume which alters the light scattering). The velocity of the propagation wave ($V_p$) is increasing under hypergravity and is decreasing under microgravity (Wiedemann et al. 2006).

The properties of action potentials (AP) are also gravity dependent. Experiments with isolated rat nerve fibres (*n. ischiadicus*) showed that the propagation velocity of action potentials is increasing under hypergravity and decreasing under microgravity compared to 1*g* (Meissner et. al 2005). The frequency of AP generated by spontaneous spiking leech neurons is increasing under microgravity (Meissner et al. 2005).

How can this finding be explained? Several interpretations are possible. The latency of the action potential, the time between the membrane potential crosses the AP threshold after a stimulus, could become shorter. This can be achieved by an increasing excitability of the membrane, leading to a lowered AP threshold, or by a decreasing refractory period after an action potential which leads to a faster recovery of the excitability of the membrane.

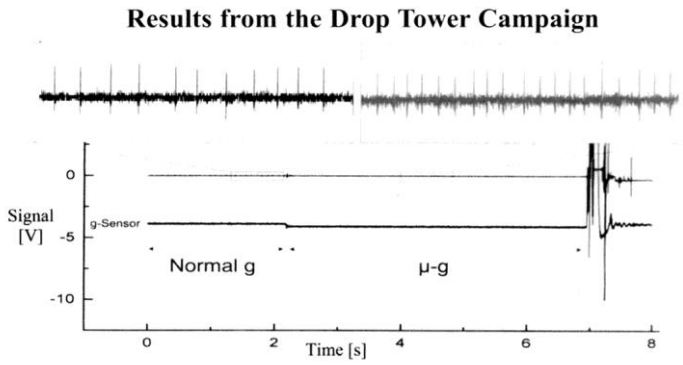


Figure 1.2: Recording from a spontaneous spiking neuron from leech in a drop tower experiment. The number of AP increases under microgravity (from Meissner et al. 2005)

These findings were confirmed by fluorescence experiments with single cells. SF21 cells were treated with Di-4-ANEPPS, a dye which reacts to changes in the membrane potential (the light intensity decreases continuously approx. 10% / 100mV hyperpolarization), and the fluorescence was recorded during a drop tower campaign (Meissner 2004). The fluorescence of the treated SF21 cells increased under microgravity which indicates a depolarization of the membrane. An increased depolarization leads to an increased excitability of the membrane.

It is still unclear if the membrane itself or the membrane proteins are responsible for the physiological reactions. To approach the molecular principle of the interaction of ion channels and membranes, a simplified system of artificial lipid bilayer with alamethicin, a polypeptide (20 amino acids) from the fungus *Trichoderma viride* whose aggregates (4-6 molecules) form voltage dependent ion-pores, was used in microgravity experiments (drop tower and parabolic flight) and hypergravity experiments (centrifuge). The alamethicin induced ion current is noticeably decreasing under microgravity after a delay of several hundred milliseconds (Klinke et al. 2000, Wiedemann et al. 2003).

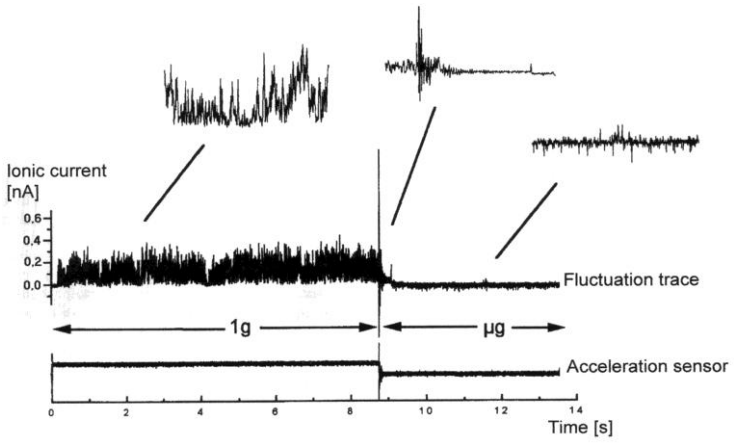


Figure 1.3: Ion channel activity of alamethicin under 1g (left) and microgravity (right). The ion current is clearly reduced under microgravity (from Klinke et al. 2000)

To investigate the reaction of native ion channels, porin ion channels derived from E. coli (strain MRE-600) were reconstituted in artificial lipid bilayer to investigate their electrophysiological properties under different gravity conditions. It was shown that the open state probability of the porin channels is significantly reduced under microgravity and is significantly increasing with higher g-values. The effect is completely reversible for hyper- and microgravity, as soon as the gravity is back to 1*g*, the open state probability goes back to normal activity (Goldermann et al. 2001).

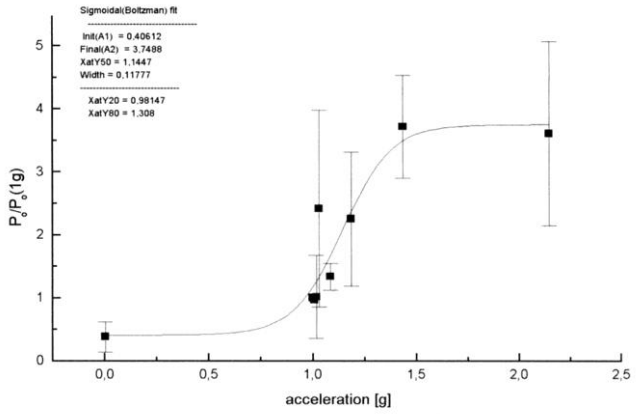


Figure 1.4: Dependency of the normalized integral open state probability of porin channels on gravity (from Goldermann et al. 2001)

These results indicate that gravity detection might be an intrinsic property of biological membranes and/or of its ion channels. To examine single channel activities the patch clamp technique, developed by Erwin Neher and Bernd Sakmann in 1976, is used. Nowadays it is a common tool in electrophysiology and is used in laboratories around the world. To use this technique with microgravity research platforms it had to be adapted. Drop tower experiments were successfully performed with leech neuron cells with intracellular recoding electrodes (Meissner 2004), which technically wasn't "real" patch clamping. A classic patch clamp setup was adapted to be used in parabolic flights. Due to the mechanical disturbance during the flights, the recordings had a low signal-to-noise ratio and were hard to interpret. Even with filtering, spectrographic analysis and ground controls only hints of ion channel activity could be obtained. The project was not continued as the weakness of the patch clamp technique, vibrations which destroy the patch, could not be compensated in the aircraft (Meissner 2004).

Since the late 1990s, the patch clamp technique advanced. Different research groups and companies designed automated patch-clamp setups, mainly for the pharmaceutical industry. As regulations changed and new drugs had to be tested against unwanted targets to minimize the risk of adverse reactions, for example with hERG $K^+$-channels in cardiomyocytes (e.g. the life-endangering acquired Long-QT syndrome, where the repolarization of the heart is delayed). For these automated patch clamp setups the theory of planar patch clamp, which was developed in the 1970s (Kryshtal et al. 1975), was taken up again. Approximately since 2005, the planar patch clamp technique has become an established technology in academic and industrial research.

For microgravity research, planar patch clamp, in this case the Port-a-Patch device from Nanion has several interesting features:

- The resistance to vibration. Since there are no movable parts and the cells can attach to the surface of the planar patch electrode the system is very stable.
- Reduced size. The system can be operated without optical control, therefore the microscope and lighting can be omitted which furthermore reduces the size of the Faraday cage to a minimum. The Patch clamp module only consists of the headstage, the electrodes and a small pump.
- Reduced need for liquids. This is an important safety aspect which facilitates the use of the hardware in space research as parabolic flight campaigns. The Port-a-Patch only needs several µl of electrophysiological solutions.

Objective of the present work was to adapt a planar patch clamp device to be usable in microgravity research (parabolic flight) and to perform first recordings with suitable cells to contribute to the exploration of the molecular principle of gravity detection in the human nervous system.

In respect of long-term residence in weightlessness, as on the international space station today, and future manned space flights, as planned trips to Moon and Mars, the influence of weightlessness on neuronal cells must be investigated. Furthermore, the comprehension of the interaction between the membrane and ion channels under different gravity conditions can be used to further improve the understanding of neuronal processes on Earth.

# 2 Material and methods

## 2.1 Available gravity research platforms

Different gravity research platforms can be used by the scientist, depending on the aim of the experiment. In the following a short summary will be given with the focus on the viability for biological experiments.

To obtain hypergravity different types of centrifuges are used. For small experiments, a standard centrifuge in the lab can be adapted. For larger experiments various centrifuges are provided by the space agencies (e.g. European Space Agency or German Aerospace Center).

For obtaining microgravity, different platforms exist, each with its own conditions concerning the duration of microgravity, consequential hypergravity, access during execution (grade of needed automation), availability and the costs.

The ZARM drop tower in Bremen (Germany) provides microgravity for 4.5 seconds (or 9 seconds with catapult start). It can provide probably the best microgravity quality which is possible on Earth ($10^{-6}$g). The experiment must be completely automated, but since the drop tower is used by only one team at a time, the capsule with the experiment will be dropped only if the researchers give a signal. This is a big advantage compared to other platforms. The deceleration load of up to 40g has to be considered during the design of experiments. It can be used for biological research since the high g-load only occurs at the end of the drop. A typical drop tower campaign takes 2 weeks with 2 to 3 drops per day. The preliminary work requires several weeks or months.

Parabolic flights repeatedly provide up to 22 seconds of microgravity. Since it is a major part of this work, the detailed description will follow in the subsequent chapters.

For microgravity up to one minute, atmospheric balloons have been used (MICROBA –microgravity research balloon). They had to be fully automated and needed a good thermal isolation against low temperatures at high altitudes. Due to the long ascend the balloon had a restricted usability for biological research.

Sounding rockets can provide microgravity for up to 12 minutes, but with high g-loads during the launch and at the end of the flight. This is the longest period of microgravity available on Earth. But again, the experiment must be completely automated and the hardware (and the

specimen) must withstand high g-loads which are limiting factors for biological research. The preliminary work before a sounding rocket experiment may take up to two years.

Last but not least, the platforms which provide “real” microgravity are satellites, scientific payload in shuttles and the international space station (ISS). Microgravity can be obtained for days (shuttles to and from the ISS) to weeks (satellites, such as the Russian FOTON or the Chinese Shenzhou) to months (ISS).

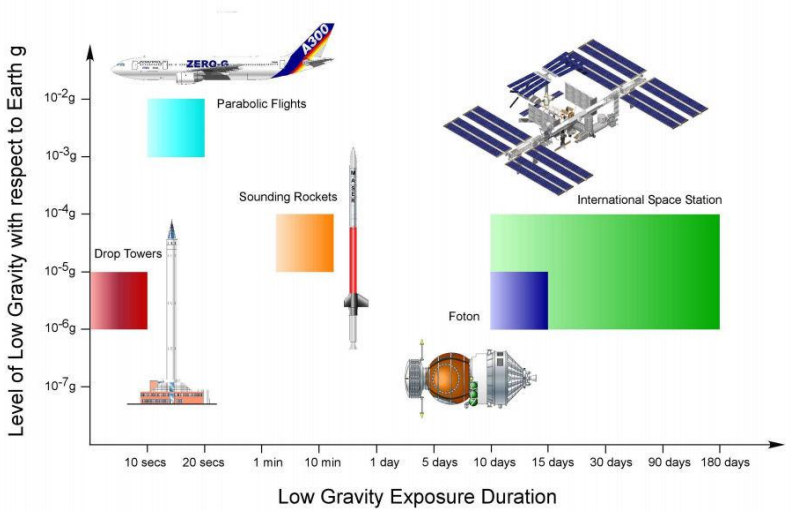


Figure 2.1: Magnitude and continuous duration of microgravity for different platforms (from ESA 2007)

These 3 orbital platforms share with each other preliminary work of several years, the need for extremely reduced mass and weight and an extremely high grade of autonomy. On the ISS the time of the astronauts is limited which is another limiting factor for performing experiments.

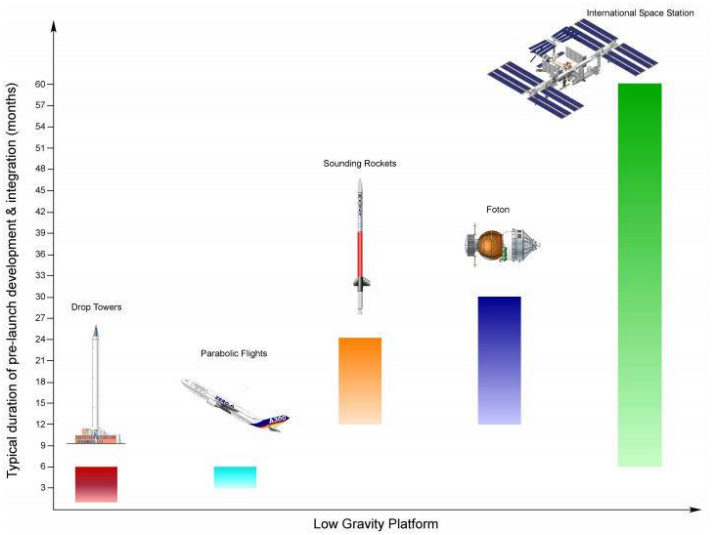


Figure 2.2: Duration of the preliminary work required for microgravity research platforms (from ESA 2007)

## 2.2 Parabolic flight

In contrary to the previously summarized research platforms, the greatest advantage of parabolic flights is the fact that the experiment can be performed by the scientist. No special hypergravity training is needed, 1.8g can be beard. For each campaign 10 to 15 different experiments can be performed in the aircraft with an overall maximum of 40 scientists per flight day. Parabolic flights offer the opportunity to realize rather complex experiments, like patch clamp, with standard equipment already used in the laboratory. The experiment can be performed during consecutive flights with the possibility to modify it between the flights to optimize the data output.

Preliminary work starts about 6 months before a campaign. This time may vary depending on the complexity of the experiment. The first participation of a new hardware certainly needs more time. Each scientific team is assigned to an engineer from Novespace. The engineers support the teams during the design and construction processes and they make sure the hardware and the ground procedures comply with the mandatory safety regulations.

### 2.2.1 The aircraft

Novespace is a French company which owns and operates the European aircraft used for parabolic flights. Since 1997 the parabolic flights are performed with a modified Airbus A300 called *A300 Zero-G*. The A300 Zero-G never was used in scheduled flights. It was always used as a testing facility for new aviation hardware by the manufacturer and other companies.

Figure 2.3: Illustration of the Zero-G interior (from Novespace)

The major part of the interior is occupied by the experiment area. The seats for the crew and the scientists are located at the nose and at the tail of the plane with the experiment area between. It is bordered by safety nets on both ends in the x-axis of the aircraft to prevent free floating objects (and scientists) to leave the area which could endanger the cockpit crew or people sitting in the seats. The floor, the ceiling and the walls of the experiment area are upholstered with protective padding to reduce the danger of injuries

### 2.2.2 The facilities

The home base of the A300 Zero-G is the Airport Bordeaux-Mérignac in France. Most of the campaigns are carried out from there with regular exception for campaigns at aeronautic exhibitions as the Paris Air Show or the "*Tag der Luft- und Raumfahrt*" (Day of Aerospace) in Cologne (Germany).

The Novespace facility contains the Novespace offices and rooms for the leading space agencies representatives and a medical office as well. The major part of the building is designed to fulfil the needs of the science teams: workshops (which take most of the available space), 2 clean rooms which can be used as laboratories, storage facilities and a large common room. Every science team gets an allocated section of the workshop to arrange the experiment and the equipment. If requested a section in one of the laboratory rooms is also reserved for the team.

All needed equipment has to be brought by the science teams themselves which can be quite an effort. For the patch clamp experiment we had to transport the experiment itself and all the needed cell culture equipment including a sterile work bench (for details please refer to section 2.10.3).

## 2.3 The parabolic flight campaign

The patch clamp experiment was performed during 5 parabolic flight campaigns. In the following, a short summary about the course of a parabolic flight campaign will be given.

| Name | Date |
|---|---|
| 11th DLR PFC | November 2007 |
| 12th DLR PFC | April 2008 |
| 13th DLR PFC | March 2009 |
| 50th ESA PFC | May 2009 |
| 52nd ESA PFC | May 2010 |

Table 2.1: List of used parabolic flight campaigns

A parabolic flight campaign took 2 weeks with different core themes. The first week was designated to final safety checks before the experiment is loaded on board the A300 Zero-G and to the preparation of the experiment.

The second week started with the final safety review on board the A300 for every experiment. Monday afternoon a mandatory safety briefing for all participants took place. During the meeting detailed explanations how the parabolic flight manoeuvre is performed, what safety rules have to be considered and how motion sickness can be prevented during the flight were given.

Usually there were 3 flight days[3] scheduled for a parabolic flight campaign (Tuesday, Wednesday, Thursday) with Friday as a backup day if a flight must be delayed (due to bad weather conditions or technical issues).

Directly after the last flight, the experiments are unloaded and the science teams pack up their equipment. After a last debriefing, the campaign is concluded and the teams return home.

[3] More flight days could be requested by the space agencies in advance

Figure 2.4: Operational cycle for the 2 weeks of the parabolic flight campaign (from ESA 2005, modified)

### 2.3.1 The flight days

In the hours before the takeoff the experiments were prepared at the Novespace workshop and laboratories. One hour before the closing of the door, the voluntary (but recommended) medication[4] was dispensed by the flight doctor.

Usually the door closing was scheduled for $9^{00}$ in the morning. Approximately 30 minutes after the doors were closed the aircraft taxied to the runway.

During takeoff and the ascent the experiments were powered off and the passengers were at their seats. After arriving at the designated flying area and a first evaluation of the flight conditions, the researchers were allowed to leave their seats and to power on their experiments.

10 minutes before the first parabola, which was announced by the pilots, the patch clamp process was performed until a gigaseal was established (please refer to section 2.10.1 and 3.3 for a detailed description).

Each parabola was announced with the same identifiable commands from the cockpit crew.

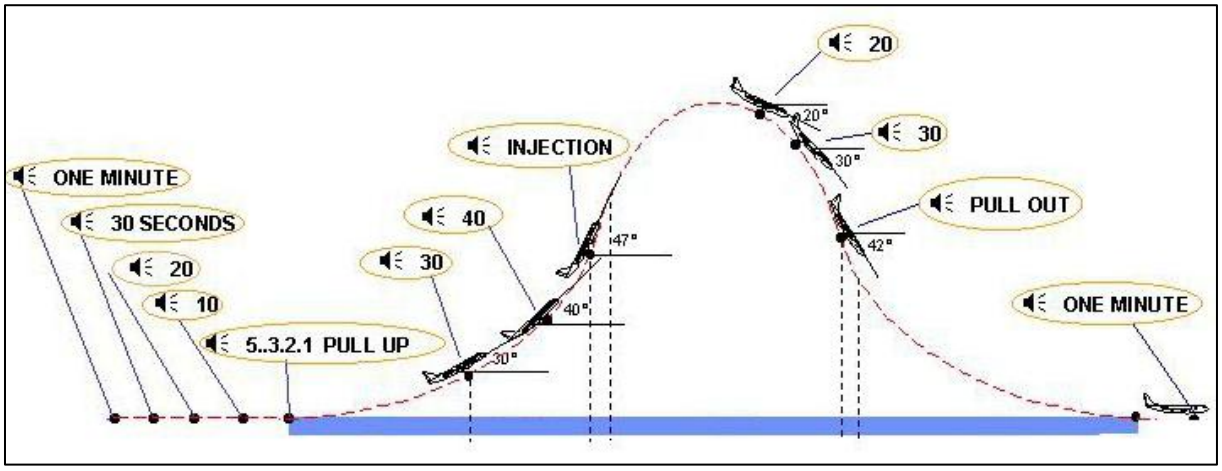


Figure 2.5: Announcements from the cockpit crew for a single parabolic manoeuvre (from Novespace safety briefing; modified)

The parabolas were executed in sets of 5 with a parabola “0” as a test parabola for the pilots and for the first flyers to familiarize with the manoeuvre and the perceptions during hyper- and microgravity. Each set was followed by a prolonged 1g-phase, usually 4, 5 or 8 minutes where the scientists could change samples or perform modifications. The breaks could be extended or shortened to a certain degree by request.

[4] Two types of medication against motion sickness are available (at the time of 2009). Scopolamine in different administration forms (Pill, subcutaneous injection, patch) and Nautamine pills (active agent: diphenhydramine monoacefyllinate)

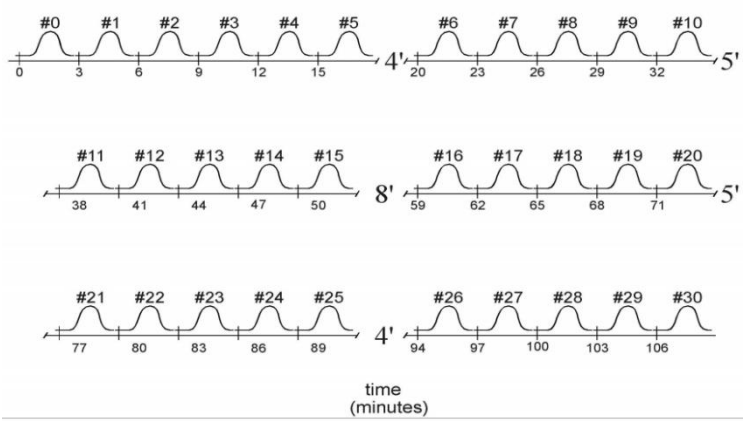


Figure 2.6: Sequence of parabolas during a flight day with the indicated breaks (from Novespace)

After the last parabola the experiments were powered off and the aircraft returned to Mérignac Airport. A debriefing was held after the flight and the participating groups (pilots, safety crew, Novespace crew, science teams) could give a feedback on the flight and have requests for the next flight day. The experiments were accessible in the A300 on ground to prepare the next flight day.

| Number of parabolas | Time of hypergravity | Time of microgravity |
|---|---|---|
| 1 | 2 x Ø 20 seconds | Ø 20 seconds |
| 31 | 1240 seconds | 620 seconds |
| | ≈20 minutes | ≈10 minutes |

Table 2.2: Total achieved time of the different gravity phases during a flight

| Number of flight days | Number of parabolas | Time of hypergravity | Time of microgravity |
|---|---|---|---|
| 3 | 93 | 3270 seconds | 1860 seconds |
| | | ≈ 62 minutes | = 31 minutes |
| 4 | 124 | 4960 seconds | 2480 seconds |
| | | ≈ 83 minutes | ≈ 41 minutes |

Table 2.3: Summary of a flight campaign with 3 or 4 flight days

## 2.4 The parabolic flight manoeuvre

The parabolic flight manoeuvre begun with the aircraft flying in a steady horizontal altitude (approx. 6000m; 825km/h) with a gravity level of 1g. At a given point, the aircraft was pulled up and started climbing. During the ascent an acceleration of up to 1.8g could be monitored for about 20 seconds. At an altitude of 7500 meters the pitch angle was about 47 degrees with a reduced speed of 580km/h. The thrust of the engines was reduced to the force which was needed to compensate the air-drag. At this point the aircraft followed a free fall ballistic flight path which could not be interrupted (20-22 seconds). The altitude of the highest point was around 8500 meters. The two pilots shared the controls during the complete manoeuvre. While the first pilot was responsible only for the elevator, the second pilot only controlled the rudder to optimize the level of microgravity and to reduce the unwanted forces during the manoeuvre. At the end of the microgravity phase, at approximately 7500 meters, the engine thrust was increased to pull out of the flight path with another 20 seconds of hypergravity, followed by horizontal flight at 1g until the next parabola.

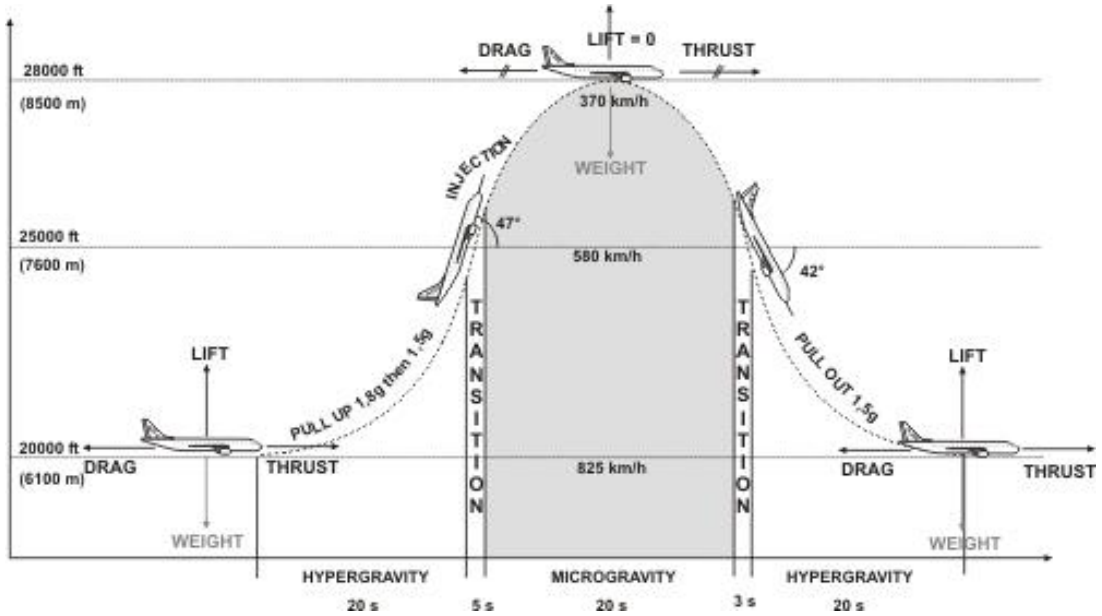


Figure 2.7: The parabolic flight manoeuvre in details (from Novespace safety briefing; modified)

The interplay of starting altitude, speed, angle of attack (=max. pitch angle) with the resulting g-loads and times must be assessed for every type of aircraft. A jet fighter, for example, can perform the manoeuvre with longer microgravity phases but at the cost of higher and longer hypergravity-loads. For the A300, the limitation is the certification of the aircraft to a maximum of 1.8g (ESA 2005).

### 2.4.1 Aircraft dynamics during the flight

The following coordinate system was used for the subsequent calculations:

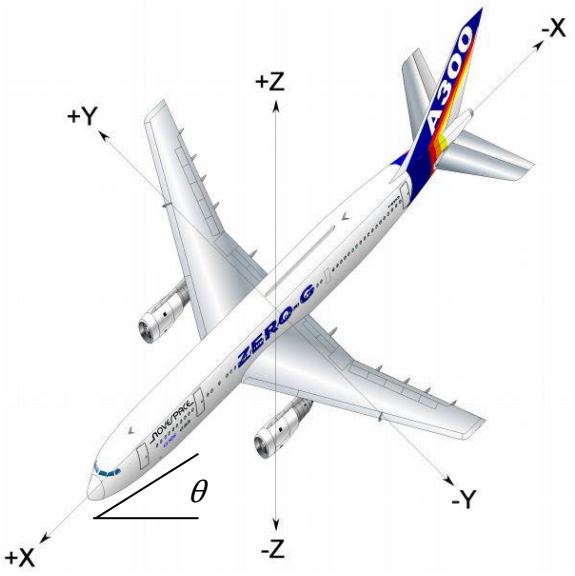


Figure 2.8: Coordinate system of the aircraft (from ESA 2005, modified)

| | |
|---|---|
| *x-axis*: | longitudinal axis (nose to tail) |
| *y-axis*: | transverse axis (wing to wing) |
| z-axis: | vertical axis (ceiling to floor) |
| $\theta$: | pitch angle of the aircraft related to earth horizontal |

For an optimal microgravity phase the aircraft must be controlled exactly to approach freefall conditions as near as possible. The following parameters can be modulated by the pilots: Lift (L) and the pitch angle $\theta$ with the elevators and wings, thrust (T) with the engines. Drag (D) depends on many factors, such as airspeed and altitude.

| | |
|---|---|
| $m_p$ | mass of the aircraft |
| $W$, $W_x$, $W_y$, $W_z$ | Axial weight of the aircraft with $W = m_p \cdot g$ |
| $a$, $a_x$, $a_z$ | Axial acceleration of the aircraft |

In the z-axis during the 1.8g phase:

$$L - \mathrm{W_z} = L - W \cdot \cos\theta = \mathrm{m_p} \cdot \mathrm{a_z} = \mathrm{m_p}(1.8 - \cos\theta)g$$

$$L = W \cdot \cos\theta + \mathrm{m_p}(1.8 - \cos\theta)g = W(\cos\theta + 1.8 - \cos\theta) = 1.8W$$

$$L = 1.8W$$

Throughout the whole 1.8g phase a constant lift is held, regardless of the pitch angle which varies during the manoeuvre.

In the z-axis during the microgravity phase:

$$L - \mathrm{W_z} = L - W \cdot \cos\theta = \mathrm{m_p} \cdot \mathrm{a_z} = \mathrm{m_p}(-\cos\theta)g$$

$$L = W \cdot \cos\theta + \mathrm{m_p}(-\cos\theta)g = W(\cos\theta - \cos\theta) = 0W$$

$$L = 0W$$

Similar to the 1.8g phase, a constant “lift” is held during the microgravity phase regardless of the changing pitch angle.

During the parabolic manoeuvre, the airspeed decreases until the top of the parabola. Concurrently the lift generated by the wings is decreasing, which is counterbalanced by deflection of the elevators (controlled by a pilot). Increasing deflection of the elevators leads to an increased aerodynamic drag (D). To maintain the parabolic manoeuvre the thrust (T) of the engines is adjusted to counter drag. In the x-axis of the aircraft, the acceleration is set as $a_x$:

$$T - D - W_\mathrm{x} = m_\mathrm{p} \cdot a_\mathrm{x}$$

$$T - D - W \cdot \sin\theta = m_\mathrm{p}(g \cdot \sin\theta)$$

$$T - D - W \cdot \sin\theta = W \cdot \sin\theta$$

$$T - D = 0$$

$$T = D$$

Which means that engine thrust counters air drag.

(Karmali F., Shelhamer M.: The dynamics of parabolic flights: Flight characteristics and passenger percepts; Acta Astronautica 63, pp. 594-602, 2008)

### 2.4.2 Forces during the parabolic flight manoeuvre on the participants

For the pilots the hardest challenge is to minimize the forces on the experiment(ers) for valuable microgravity phases. Longitudinal and transversal forces must be reduced to zero in order to have a system with only one degree of freedom where the participants are only affected by forces in vertical direction. Unfortunately this can only be achieved by approximation due to the challenging flight manoeuvre and unpredictable flight conditions, but experienced pilots can get very close to optimal conditions.

To derive the different forces the following coordinate systems was used:

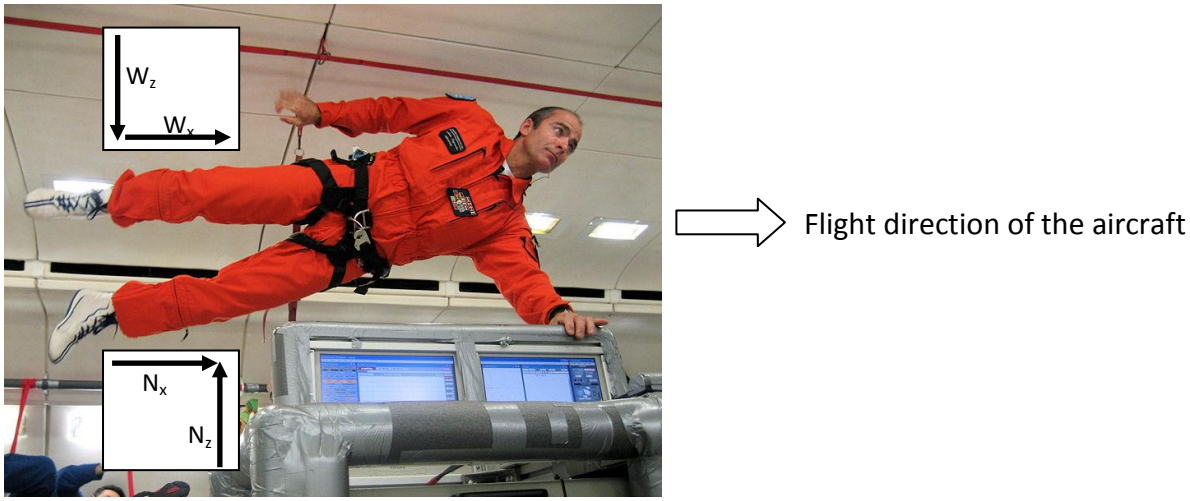


Figure 2.9: Forces on the participant

| | |
|---|---|
| $W, W_x, W_z$ | weight of the participant along the aircraft axis at constant 1$g$ of Earth's gravity field with |
| $W = m \cdot g$ | |
| $m$ | mass |
| $g$ | acceleration of gravity |
| $N, N_x, N_z$ | normal force between participants' feet and the aircraft along the aircraft axis |
| $a, a_x, a_z$ | Acceleration of the participant along the aircraft axis |

### Forces along the vertical axis of the aircraft

During the parabolic flight manoeuvre $N_z$ and $a_z$ are reduced to near zero during the microgravity phase.

$$\sum F_z = m \cdot a_z = -W_z + N_z = W_z \cdot \cos\theta + N_z$$

During the hypergravity phase (1.8g) the normal force is $N_z = 1.8W$,

$$\sum F_z = m \cdot a_z = -W \cdot \cos\theta + 1.8W$$
$$a_z = (1.8 - \cos\theta)g$$

During the microgravity phase (0g) the normal force is $N_z = 0W$,

$$\sum F_z = m \cdot a_z = -W \cdot \cos\theta + 0W$$
$$a_z = (0 - \cos\theta)g$$
$$= -g \cdot \cos\theta$$

### Forces along the longitudinal axis of the aircraft

The forces on the scientists (and the experiments) along the longitudinal axis should be reduced as much as possible to avoid the generation of drift movements during microgravity.

$$\sum F_x = m \cdot a_x = W_x + N_x = W_x \cdot \sin\theta + N_x$$

During the hypergravity phase the normal force is $N_x = 1.8W$,

$$\sum Fx = m \cdot a_x = W \cdot \sin\theta + 1.8W$$

$$a_x = (1.8 - \sin\theta)g$$

During the microgravity phase, the scientists should not move along the floor to avoid generating *g* acceleration, we assume $N_x = 0$ (not 0W)

$$\sum F_x = m \cdot a_x = W \cdot \sin\theta + 0$$
$$a_x = g \cdot \sin\theta$$

The last equation shows the relationship between the pitch angle (sin θ) and the acceleration ($a_x$) of the aircraft. The thrust of the engines must be exactly controlled to reduce the unwanted longitudinal forces on the scientists.

## Rotation forces

Since not all experiments are located at the aircraft's center of gravity, additional forces across the axes, generated by rotation of the plane, must be considered. The rotational forces vary dependent on the distance from the plane's center of gravity and can be divided into three forces. At the center of gravity only torques are generated by rotation. With increasing distance, a centripetal acceleration towards the center of gravity and an increasing acceleration along the vertical axis occur. During the parabolic flight manoeuvre, the aircraft's pitch changes from 45° nose-up to 45° nose down in approximately 30 seconds (see fig. 2.7). The average angular velocity ω is

$$\omega = \frac{\Delta\theta}{\Delta t} = \frac{45° - (-45°/s)}{30s} = 3°/s$$

The angular acceleration at the center of gravity generates a centripetal along the aircraft's length. With 27m as the maximum lever (based on 54m total length of the A300) the centripetal acceleration ($a_c$) is

$$a_c = \omega^2 r = (3°/s \times \frac{\pi}{180} rad/deg)^2 \cdot 27m$$

$$= 0.074\, m/s^2 = 7.4 \cdot 10^{-3} g$$

The vector of this reaction force acts in the nose-tail direction which can be experienced as friction force during 1.8g. A 70kg scientist would experience a force of approximately 5N.

During the transition from 1.8g to 0g and from 0g to 1.8g (see fig 2.7) there is a change in the angular velocity as the aircraft pitch is changing from nose-up to nose-down (and vice versa). According to recordings from Novespace this transition takes between 3 and 5 seconds, resulting in an average angular acceleration of

$$\alpha = \frac{\Delta\omega}{\Delta t} = \frac{3°/\text{s-(-3°}/s)}{4s} = 2°/s^2$$

This is just about at the threshold of detection of the vestibular organ and normally is hardly perceived by the participants (Karmali et al. 2008).

The transition phases of the aircraft have to be considered since the angular velocity inverts from upwards to downwards (and vice versa) affecting the participants depending on their location in the aircraft. At the nose of the aircraft the normal force increases during the ascent and decreases during the descent (again vice versa way at the tail of the aircraft). For an experimenter at the tail or the pilots in the cockpit this generates a tangential acceleration of

$$a_{\text{tang}} = \alpha \cdot r = (2°/s \times \frac{\pi}{180} rad/deg) \cdot 27m$$

$$= 0.95\ m/s^2 = 7 \cdot 10^{-3} g$$

This tangential acceleration increases or decreases the normal force of the participants depending of the position of the participant and if the plane is ascending or descending. The pilots' normal force for example increases during the 1.8g-0g transition and decreases during the 0g-1.8g transition.

This tangential acceleration has to be considered if the experiment is running during the transition phases. If this is the case it is advised to use an accelerometer which is coupled with the data acquisition to monitor possible influence.

(Karmali F., Shelhamer M.: The dynamics of parabolic flights: Flight characteristics and passenger percepts; Acta Astronautica 63, pp. 594-602, 2008)

## 2.5 Classic patch clamp technique

The hypothesis that nerves and muscles communicate with electrical signals exist since the 18th century. But it was not before the late 1970s until real-time recordings of single ion channels were performed for the first time. For the development of the patch clamp technique, Erwin Neher and Bernd Sakmann received the Nobel Prize in Physiology or Medicine in 1991 (Hamill et al. 1981; Single Channel Recording 1983).

The main challenge in recording single channel events is to reduce the electric background noise of the experiment to a level which is below the electric current generated by the flow of ions through an ion channel. With the patch clamp technique, a small "patch" of the cell membrane is electrically isolated from the surroundings with a small glass pipette (the famous "*gigaseal*") to record the small currents of single ion channels.

The following subchapters cover the different aspects of patch clamping.

### 2.5.1 Basic principle

Most of the patch clamp experiments are based on the voltage clamp technique which was invented in the 1930s. The purpose of the voltage clamp is to prevent changes of the membrane potential. A electronic feedback system is used where a defined potential (holding potential) is compared with the measured membrane potential. Any deviation from the holding potential is instantly compensated by a current injection. This current (but opposite in algebraic sign) represents the ionic current over the membrane.

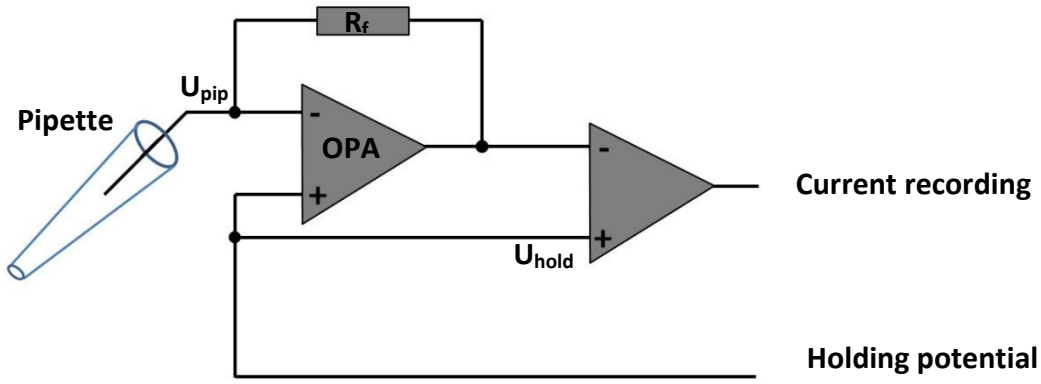


Figure 2.10: simplified circuit diagram of a patch clamp amplifier. OPA = operational amplifier; $R_f$= Feedback resistor; $U_{pip}$= Recorded potential at the pipette; $U_{hold}$= holding potential

The command voltage (holding potential) can be varied, from simple stepwise changes to rather complex protocols to study the general electrical properties of a cell or specific

channel properties. Additional correction circuits are integrated in the patch clamp amplifier to maintain a time resolution of microseconds ($10^{-6}$ sec).

The appearance of patch clamp setups in different laboratories varies, however the functions of the core components are identical.

### 2.5.2 Supporting systems

Two possible problems must be considered during the positioning of a patch clamp setup: vibrations and electric interferences.

#### Vibration dampening

Since the patch clamp electrode and the membrane interact on a microscopic level, even small vibrations can influence the patch clamp recording. In the worst case the established seal breaks and the recording cannot be continued. The building itself is exposed to wind, traffic passes nearby and numerous other causes (e.g. earth movements or industrial vibrations) and therefore it oscillates. Inside the building various sources for vibrations exist: power generators, ventilation systems, electrical equipment and, of course, the people. The amount of banging doors is directly proportional to the number of people in the building (subjective observation) and inversely proportional to the durability of a patch clamp seal.

In general, a good place for a patch clamp setup is in the lowest floor. If that is not possible the setup should be placed in a corner, at a load-bearing wall or at a supporting column since there, the oscillations of the structure, are reduced.

With vibration-isolation tables, the external vibrations can be compensated to a large extent. Low-frequency oscillations can only be compensated by a large (inert) mass, for example tabletops made from concrete or metal. Vibration-cushioned tables exist in many forms from self-made tables to manufactured hardware from various companies, from passive systems to actively dampening systems (electrical and/or pneumatic). On the table the microscope, the micromanipulator and the preamplifier are placed. To avoid accidental contact during the recording, an outer “table” is built around the anti-vibration table. This structure must be completely detached from the inner table.

In addition a Faraday cage is attached to the outer table, which leads to the next paragraph, the electrical shielding of the patch clamp setup.

## Electrical shielding

A good electrical shielding can make the difference between delicate patch clamp recordings and high quality recordings with a good signal-to-noise-ratio. Patch clamp is very sensitive to electrical interferences for two reasons. First, the targeted currents from single cells or single ion channels are several magnitudes smaller (nano- or pico-ampere) than the unwanted interferences and second, high-resistance circuits ($R_f$ and OPA) are used to record these small currents.

The patch clamp setup should be placed in a room with little electromagnetic interferences (from internal sources, or surrounding rooms and equipment), but often this cannot be done. Therefore a Faraday cage is used to protect the interior against external electric fields and electrostatic discharges. For optimal protection, the cage should be closed on all sides, which can be realized with a door or a metal curtain in the front to be able to operate the setup. In many setups, the front is left open with no metal shielding since a door can generate unwanted vibrations. The attenuation of shielding of the Faraday cage depends on the type and diameter of the conductive material and the mesh size (if solid walls are rejected due to the weight). The smaller the mesh size the smaller wavelengths can be dampened. Inside the cage, only the actually needed electrical consumers should be placed as their electromagnetic emissions are not blocked by the cage.

The cage and all equipment must be grounded. Non-conducting parts (many metal objects are varnished, e.g. microscopes) must be connected to the overall grounding (by exposing the bare metal in a spot and attaching a cable to it). To avoid grounding loops, since they can act as induction coils and pick up interferences, all grounding cables should be joined in a single point, avoiding cable crossings. Often a metal block with attachment points is used.

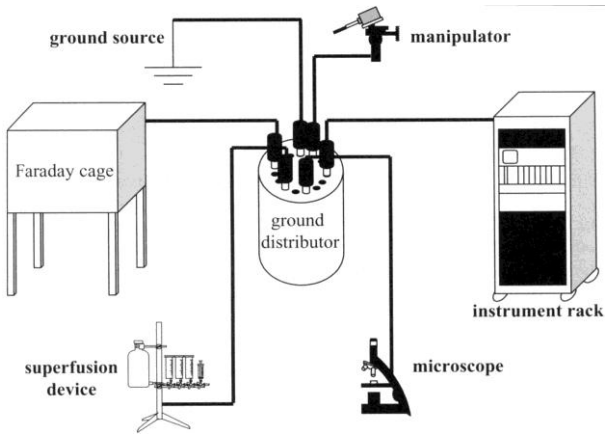


Figure 2.11: Optimal grounding schematic with a central ground distributor (from Molleman A., Patch Clamping, an introductory guide)

If possible, a discrete circuit for the sensitive patch clamp amplifiers should be used and another circuit for the "dirty" consumers like light sources, monitors and others. The optimum would be a complete galvanic separation of the patch clamp hardware by an isolating transformer to avoid external noise, for example by using an uninterruptible power supply (UPS) which will be of peculiar interest in a following chapter about patch clamp in the A300, where electrical shielding is addressed again. There are many forms of electrical noise, the three most commons forms are:

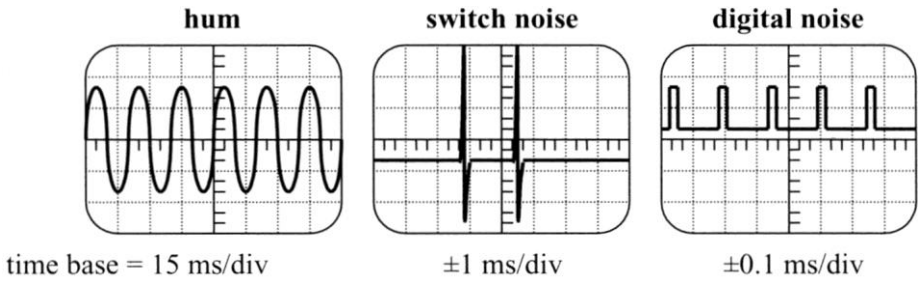


Figure 2.12: Common types of electric noise (from Molleman A., Patch Clamping, an introductory guide)

- Hum. It is generated by the alternating current of the power grid with 50Hz in Europe. Hum generates the biggest noise problems since it is generated by the power grid. It can be reduced with proper grounding and shielding.
- Switch noise. Consumers which need high currents generate inductive surges and drops in the power grid which must be kept away from the patch clamp amplifier. This can be done by separating the patch clamp power grid from such devices or by using surge protectors.
- Digital noise. Many modern devices generate regular, high-frequency clock pulses.

### 2.5.3 The microscope

There are two types of optical microscopes, “upright” microscopes with the objectives above the microscope table and the lighting below and “inverted” microscopes with the objectives below the microscope table and the lighting above. For patch clamp experiments with single cells, the inverse microscope is preferred as it offers several advantages. To focus the cells, the objective is moved, not the microscope table with the cells, reducing direct vibrations at the cells. A condenser with a good working distance can be used to get enough space over the microscope table for the preamplifier and the electrode (and a perfusion system if needed).

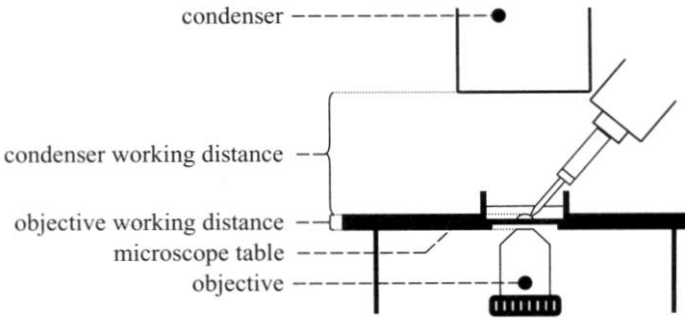


Figure 2.13: Working distance on a inverted microscope (from Molleman A., Patch Clamping, an introductory guide)

A total magnification between 200 and 600 with phase contrast is sufficient in most cases and a photo or video camera can be attached to the microscope.

### 2.5.4 The patch clamp amplifier

The central component is the patch clamp amplifier. It contains the measuring and clamping systems. In the past, most of the amplifiers were self-made, today various companies offer patch clamp amplifiers. A patch clamp amplifier has a small extension, the headstage or probe, which is the interface between the amplifier and the patch clamp target. The probe is mounted on a micromanipulator and the pipette holder with the recording electrode is directly attached to it. The patch clamp amplifier receives the data from the probe and processes the various experimental commands, such as voltage steps or holding potential. Modern patch clamp amplifiers are controlled by a computer. External components can be

attached to the amplifier for special needs, such as additional filters, pulse generators or sensors.

For this work the EPC-10 amplifier from HEKA (HEKA Elektronik Dr. Schulze GmbH; Lambrecht, Germany) with the Patchmaster software on a standard Windows XP computer was used. The computer was adapted to work under microgravity (for details please refer to the results).

### 2.5.5 The micromanipulator

The patch pipette must be positioned precisely on a micrometer scale. For this purpose different types of micromanipulators are available: mechanical, hydraulic (oil or water) and electrical (motor- or piezo-driven). Each type has its own advantages and disadvantages. Hydraulic manipulators do not generate electrical noise but in return electrical manipulators can be programmed e.g. to quickly move the electrode to a predefined position. A combination of different systems is often used, e.g. a fast electrical system for a quick approach to the cell and an attached oil-hydraulic for accurate positioning of the pipette on the membrane. The micromanipulator is attached to the microscope table, whereby the mass of the construct must be considered, or to a supporting frame which is attached to the dampened table.

### 2.5.6 Electrodes

For a patch clamp recording, two electrodes are needed, the recording electrode and a second electrode in the bath solution. Both electrodes are connected to the headstage. The properties of the two electrodes, material, length and diameter, should be similar to reduce offset potentials. To reduce the polarization of the electrode for optimal recording properties, platinised platinum or silver/ silver chloride wires are used. To chlorinate silver wires, different methods exist.

For this work, the following electrophoresis protocol was used:

- Smooth the silver wire with abrasive paper (1000 grain)
- Clean with 70% ethanol
- Insert the wire in 3M KCl
- Connect the wire to the cathode (+ pole) of a 12V DC source with 1kΩ resistor (= 12mA)
- A second wire is connected to the anode (- pole) and inserted into the solution
- Wait until the patch clamp electrode has a smooth grey coating

During the electrophoresis, the negatively charged chloride ions bind to the cathode and hydrogen gas forms at the anode.

### 2.5.7 Patch pipettes

Patch pipettes are used to reduce the contact area of the patch electrode with the cell membrane to a microscopic level. They are filled with salt solutions to connect the silver wire with the cell membrane. The properties of the pipettes must be selected according to the planned recording. A single-channel recording, for instance, needs a smaller tip diameter than a whole-cell recording. Since it would be rather complex to measure the tip diameter of each electrode by hand, the pipette resistance $R_{pip}$ is used as criterion of the tip diameter. $R_{pip}$ is determined by the thickness of the glass and the tip diameter. It is always verified at the beginning of the patch clamp process.

$$R_{\mathrm{pip}} = U/I$$

$U$= applied potential, $I$= recorded current

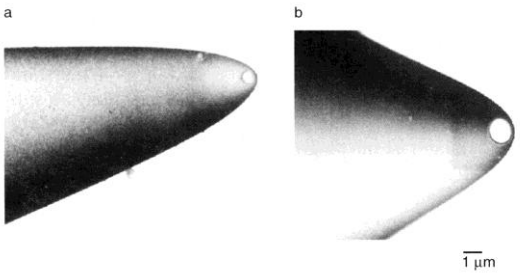


Figure 2.14: Electron microscopic image of the pipette tip of a single channel pipette with high resistance (from Numberger M.; Draguhn A.; Patch-Clamp-Technik)

The glass electrodes are made with an electrode puller which can be programmed to produce a defined tip opening (in our lab a DMZ puller, Zeitz, Martinsried, Germany).

### 2.5.8 Pipette holder

The patch pipette and the electrode wire are combined to an operative microelectrode with the pipette holder. The pipette holder is directly attached to the headstage. A high quality holder is required for an optimal signal-to-noise-ratio, in many cases it is delivered with the patch clamp amplifier. To apply pressure (de- and overpressure) to the inside of the microelectrode, a lateral port for a flexible tube is integrated. The tube must be attached carefully or else it can conduct vibrations to the headstage.

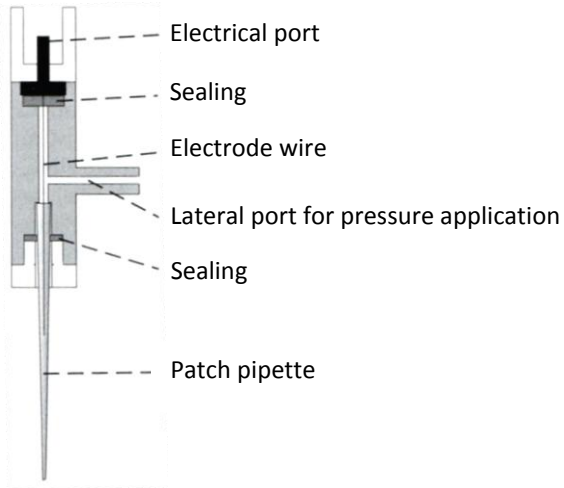


Figure 2.15: Schematic of a pipette holder (from Numberger M.; Draguhn A.; Patch-Clamp-Technik; modified)

## 2.6 Patch clamp configurations

To investigate ion channels, the patch clamp technique offers various recording configurations for different applications. The desired configuration must be selected before the recording, since the ionic composition in the microelectrode (and the bath) must be chosen accordingly.

The first step for the subsequently described configurations is the cell-attached configuration. The microelectrode is in contact with the membrane, forming a very tight connection with high resistance. The membrane stays intact with possible deformation due to the negative pressure in the microelectrode. The intracellular side of the cell keeps its physiological properties and ion channels in the patch can be studied with limited scope of influence, e.g. it is complicated to exchange the media.

### 2.6.1 Whole cell recording

With the whole cell configuration, the macroscopic currents of the cell can be recorded. The microelectrode acts as an extension of the cell membrane, therefore the pipette medium must be adjusted to the intracellular milieu. The extracellular side of the cell can easily be superfused with modified bath solution (e.g. ion substitutes like $Cs^+$ instead of $K^+$, or pharmacological substances as tetrodotoxin or tetraethylammonium).

To obtain the whole cell configuration, the membrane under the micropipette, from the cell-attached configuration, must be ruptured, without destroying the seal, to connect the electrode directly to the cytoplasm. This can be done by negative pressure at the micropipette, or short voltage pulses (called “zapping”; 800mV, 1-2msec). Before rupturing the cell, a negative holding potential must be applied, at best near the approximate resting potential of the cell, otherwise, the cell can be damaged by the depolarization.

The so called series resistance $R_{series}$ ($R_{pip}$ and $R_{acc}$) and the capacitance of the membrane ($C_m$) form a significant RC circuit which can delay any modification in the holding potential. Therefore it is important to compensate $R_{series}$ as good as possible.

### 2.6.2 Single channel recording

There are 3 recoding configurations to study single ion channels. The first configuration, cell-attached, was previously described. The second and third configuration, inside-out and outside-out, excise a patch from the cell membrane, a process where the seal often is destroyed. These configurations offer complete control over the environment of the patch. Furthermore, the seal becomes more resistant to vibrations since the membrane is only connected to the microelectrode with no connection to a second surface.

For the inside-out configuration, the microelectrode is moved away from the membrane after a good cell-attached gigaseal was established. If the patch stays intact, the cytosolic side of the patch membrane faces to the bath and the inner side of ion channels can be manipulated.

For the outside-out configuration, the microelectrode is moved away after the-whole cell configuration was established. If this is done carefully, the membrane folds back to a patch covering the pipette with a good $R_{patch}$. In this configuration, the extracellular side of the membrane faces to the bath and the outer side of the ion channels can be manipulated.

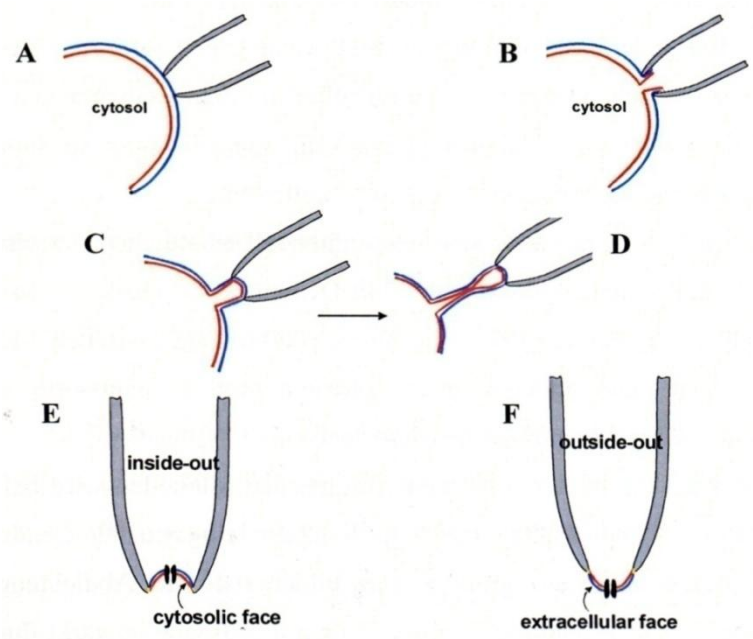


Figure 2.16: Patch clamp configurations. The extracellular side of the membrane is shown in blue, the cytosolic side in red. The cell-attached configuration is the initial configuration (A) for all following variations. For the whole-cell configuration (B) the membrane under the pipette must be ruptured. By slowly moving the microelectrode away from the membrane (C, D), the excised patch configurations (E, F) are achieved (E from A; F from B). (Picture kindly provided by Dr. Hinrich Luehring)

Great care must be taken on applying holding potentials to the patch, since the orientation of the membrane must be considered. In the outside-out configuration, the patch potential is the membrane potential. In the inside-out configuration, the patch potential is reversed. This sign convention must also be applied to the recorded currents.

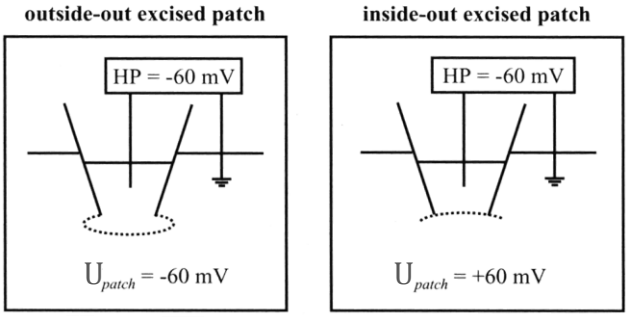


Figure 2.17: The impact of applied holding potentials on the cell potential in excised patch configurations (from Molleman A., Patch Clamping, an introductory guide; modified)

## 2.7 Practical execution

First, the culture dish with the cells is placed into the notch on the microscope table and the bath electrode is carefully inserted into the culture dish to connect the headstage with the bath. Afterwards, a suitable cell is chosen with a magnification of 200. The patch pipette is filled with the electrolytic solution and is attached to the headstage with the recording electrode. To prevent a clogging of the pipette tip, a slight overpressure is applied to the microelectrode during the manoeuvre in the bath. After insertion of the microelectrode, $R_{pip}$ is determined.

The microelectrode is moved near the cell and carefully placed onto the membrane with simultaneous application of a negative pressure to the microelectrode. Beside the visual control, a small test pulse is applied (square wave, 10mV, 20msec) to verify the formation of a high resistance seal. The seal resistance for the cell-attached configuration should come to several gigaohms (gigaseal).

From the cell-attached configuration, the previously described configurations can be achieved. The test pulse is switched off and the real pulse protocols can be applied.

A new electrode must be used for each patch clamp attempt.

## 2.8 Planar patch clamp technique

In the last years the need for high-throughput electrophysiology increased, especially at pharmaceutical companies. Manual patch clamping is rather time consuming. Therefore several companies emerged with different approaches to automated patch clamp systems.

For this work, the semi-automated Port-a-Patch from Nanion Technologies GmbH (Munich, Germany) was used.


Figure 2.18: The Port-a-Patch (from product sheet; Nanion)

### 2.8.1 Basic principle

While the patch clamp amplifier, protocols and procedures are similar for classic and planar patch clamp (as described in section 2.5), the principle, how the seal is obtained, is different. In classic patch clamp, a manoeuvrable microelectrode is moved to a static cell/tissue, whereas this principle is “inverted” for the planar approach. Here an unattached cell, in a cell suspension, is attracted to a stationary, planar (“chip-like”) electrode. Since the electrode cannot be moved, no excised patch configurations can be used. Cell attached, perforated patch and whole cell recordings can be performed.

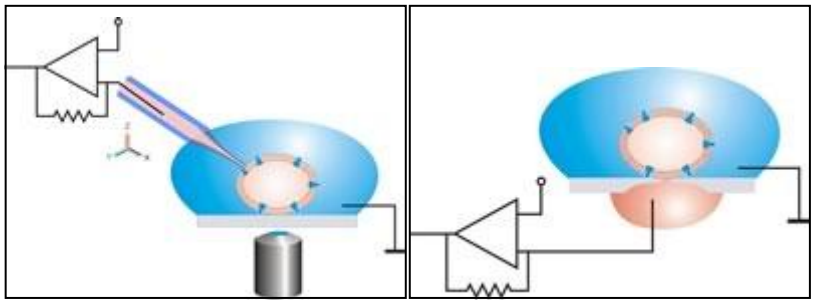

Figure 2.19: Schematic of the classic patch clamp configuration (left) and the planar patch clamp configuration (right). Compared to the classic configuration, the planar configuration is more resistant to vibrations as the cell attaches to the planar electrode. (from Wikipedia, both images released under GNU Free Documentation License)

### 2.8.2 The hardware

The patch hardware for the Port-a-Patch is much smaller than a classic patch clamp setup. Many of the previously described components are not used.

The headstage from the EPC-10 amplifier is integrated in the small Port-a-Patch casing. Since there are no mechanical parts, no microscope is used for optical control of the patch. The patch clamp process is solely observed and validated by the electrical properties.

For an experiment which is not part of this work, I integrated a video-microscope with a magnification between 200 and 400 to observe if *Euglena gracilis* could be attracted to the aperture, so therefore a microscope could be integrated to the system, at least in the laboratory. Up to now this was not done for parabolic flights.

Since the cell is attached only to a single surface, there is no need for a large vibration-dampening system. The Faraday cage is reduced to a small shield which encloses the NPC-1

chip (Nano-Patch-Chip) and the recording electrode. The bath electrode is connected to the Faraday shield. The chip mount is also connected to a USB-controlled pump to apply pressure between -300 and +300 mbar.

The PatchControl software from Nanion is an extension of Patchmaster, so the familiar patch clamp software can be used with expanded control panels. The software can run automated patch clamp procedures only the laboratory work has to be performed by the scientist. The automated protocol applies pulse protocols, constantly monitors the resistance which is used as feedback parameter for the small pump.

For this work, only semi-automated protocols were used. Since the conditions during a parabolic flight could change very quickly, the actual patch clamp process was done manually.

### 2.8.3 The NPC-1 chip

The surface of the NPC-1 (Nano-Patch-Clamp) chip is made from borosilicate glass, which is also often used for classic patch clamp electrodes. It is mounted on a twist cap with an inner rubber sealing. The aperture in the glass is made in several steps. First the glass is thinned from one side with hydrofluidic acid. Afterwards a single heavy ion is shot through, leaving a so-called ion track. This ion track is etched much faster by a second hydrofluidic acid treatment than the surrounding glass, forming a smooth-rimmed opening (Fertig et al. 2001). The chips can be produced with different $R_{pip}$ similar to classic patch clamp pipettes.

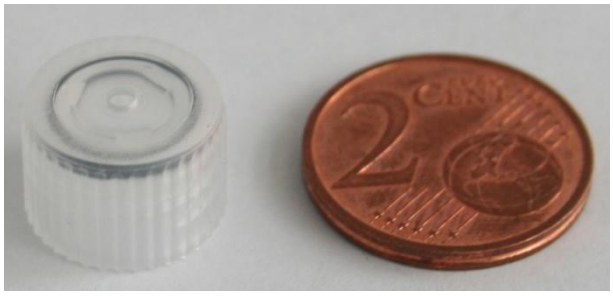

Figure 2.20: The NPC-1 chip

### 2.8.4 Cell culture

Special care had to be taken during the preparation of the cells for the experiments. They had to be separated to ensure that a single cell sealed onto the aperture, since no optical selection of the preferred cell could be performed. Cell clusters had to be avoided. The detailed procedures of the cell culture work are listed in section 2.9.

### 2.8.5 Patch clamp solutions

The following electrophysiological solutions were used for this work, the recipe was kindly provided by Nanion Technologies. All used chemicals were provided by Sigma-Aldrich or Fluke.

#### Internal patch clamp solution

##### For potassium channels

| | |
|---|---|
| 50mM | KCl |
| 10mM | NaCl |
| 60mM | K-fluoride |
| 20mM | EGTA |
| 10mM | HEPES/ NaOH pH 7.2 |
| Osmolarity: | 285mOsmol |

##### For sodium channels

| | |
|---|---|
| 50mM | CsCl |
| 10mM | NaCl |
| 60mM | Cs-fluoride |
| 20mM | EGTA |
| 10mM | HEPES/ CsOH pH 7.2 |
| Osmolarity: | 285mOsmol |

#### External patch clamp solution

| | |
|---|---|
| 140mM | NaCl |
| 4mM | KCl |
| 1mM | $MgCl_2$ |
| 2mM | $CaCl_2$ |
| 5mM | D-glucose monohydrate |
| 10mM | HEPES/ NaOH pH 7.4 |
| Osmolarity | 298mOsmol |

#### Seal enhancer

| | |
|---|---|
| 80mM | NaCl |
| 3mM | KCl |
| 10mM | $MgCl_2$ |
| 35mM | $CaCl_2$ |
| 10mM | HEPES/ NaOH pH 7.4 |
| Osmolarity: | 298mOsmol |

### 2.8.6 Practical execution

First, the cells had to be prepared according to the protocol (please refer to section 2.9.8). For each recording, a new chip had to be used. 5µl of the patch clamp solution were pipetted onto the inner side of the aperture before the chip was fixed onto the chip mount. The recording electrode needed contact with the liquid and the sealing had to be clearly visible as a black ring to ensure a tight connection. The Faraday shield was pulled over the chip and the automated adjustment protocols were started. 10µl of the extracellular patch clamp solution (bath solution) were pipetted onto the outer side of the aperture whereby the bath electrode must have contact to the solution. If everything was done correctly, $R_{chip}$ was automatically determined and the software was ready to start the patch clamp process. 5-10µl of the cell suspension were added to the bath solution and the patch clamp protocol was started. This could be done automatically, whereby the automated protocols needed to be adjusted to the type of cell, or it could be done manually for complete control over the patch process. The automated process could be stopped at any time for manual control (and vice versa).

The software-controlled pump applied a suction protocol to the inside of the chip to position a single cell onto to the aperture.

Just as for classic patch clamping, the first planar patch configuration was always the cell attached configuration. To obtain whole cell access, a suction protocol was applied.

The seal was very stable, since the cell attached to the glass surface of the chip.

## 2.9 Cell culture

### 2.9.1 Primary culture of human muscle cells

Primary cultures of human skeletal muscle cells (HSKMC) and human cardiac muscle cells (HCM) from Provitro (Berlin) were tested for the project. They could not be cultivated properly at Novespace (2008) due to the limited laboratory conditions therefore they were not used for the project.

### 2.9.2 SH-SY5Y cell line

SH-SY5Y is a neuroblastoma cell line which was first reported in 1978 (Biedler et al., 1978). It is a subclone from the cell line SK-N-SH which originates from a bone marrow metastasis from a 4 year-old girl with a metastasizing neuroblastoma which was established in 1971 (Biedler et al., 1973). The SH-SY5Y cells have two distinct phenotypes. The neuroblastoma cells, with small, spherical cell bodies and a small percentage of epithelia-like cells with larger, flat cell bodies (Ross et al., 1983). By treating the cells with retinoic acid (RA), the neuroblastoma cells can be differentiated to neuron-like cells. The receptors for RA in the nucleus act as transcription factors and trigger the differentiation (Abemayor, 1992, Sidell et al., 1998). The neuron-like cells can be identified by the development of large neurites (Pahlmann et al., 1984).

### 2.9.3 SNB19 cell line

SNB19 is an astrocytoma cell line (Gross et al. 1988). Little is known about their channel repertoire. During the 52$^{th}$ ESA PFC they were used because of their good sealing probability and seal stability which was observed at the laboratory. More details can be found in the discussion.

### 2.9.4 Cultivation

The SH-SY5Y and SNB19 cells were cultivated in Ham's F-12 liquid medium with stable glutamine 10% FBS and 1.2% Penicillin/Streptomycin at 37°C with 6.5% $CO_2$ atmosphere.

#### Used products

- Culture flasks (65ml) with filter cap
  (neoLab Migge Laborbedarfs-Vertrieb GmbH, Cat.No. C-8003)
- Petri Dishes ø 35 mm with airvent
  (Nunc GmbH & Co. KG, Cat.No. 153066)
- Ham's F-12 liquid medium with stable glutamine
  (Biochrom AG, Cat.No. FG4815)
- Fetal bovine serum (FBS)
  (Biochrom AG, Cat.No. S0115)
- Penicillin/ Streptomycin 10000U/10000 µg/ml
  (Biochrom AG, Cat.No. A2212)
- Trypsin-EDTA 0.05%/0.02% in PBS w/o $Ca^{2+}$/$Mg^{2+}$
  (Biochrom AG, Cat.No. L2123)
- Biotase-EDTA 0.0042%/ 0.02% in PBS w/o $Ca^{2+}$/$Mg^{2+}$
  (Biochrom AG, Cat.No. L2193)

### 2.9.5 Splitting

The cells were divided into smaller populations at a confluence of 70-80% to prevent the formation of large cell clusters and tissue-like structures. This was done approximately once per week. The following protocol was used:

- Preheat all used liquids to 37°C
- Remove the old cell culture medium
- Add 2ml Trypsin-EDTA for 3-5 minutes at 37°C until the cells detach
  or
  Add 2ml Biotase-EDTA for 5-7 minutes at 37°C until the cells detach
- Add 6ml of HamF12 to neutralize the Trypsin
- Centrifugation; 10 minutes at 1300 rpm and 4°C
- Remove the supernatant
- Resolve the pellet in 1ml HamF12, gently pipette up and down 10-20x to separate the cells
- The cell suspension was diluted between 1:10 and 1:20 (depending on the number of cells) with HamF12 and distributed into new culture flasks
- Disseminate 5 ml per flask in new culture flasks.

### 2.9.6 Differentiation

To differentiate the SH-SY5Y cells 2µl of a 30mM retinoic-acid stock solution (in DMSO) were added per ml of culture medium. The cells are incubated for 4 - 6 days, with regular check of the viability of the cells.

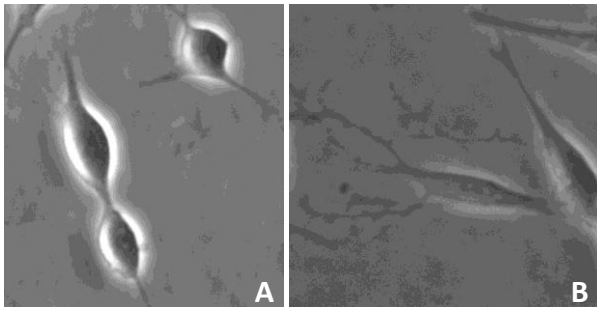


Figure 2.21: SH-SY5Y cells. (A) Undifferentiated, (B) after 5 day treatment with 2µl/ml 30mM retinoic acid in DMSO

#### Used products

- All-trans retinoic acid, $C_{20}H_{28}O_2$, $M_w$ 300.44
  (Fluka, Cat.No. 95152)
- Dimethyl sulfoxide (DMSO)
  (Sigma Aldrich, Cat.No. D4540)

### 2.9.7 Viability check

The viability of the cells was regularly checked with a 0.5% trypan blue solution. The following protocol was used:

- 80 µl of the 05% trypan blue are added to 20µl of the cell-HamF-12 solution
- 20 µl of the suspension are transferred onto a haemocytometer
- Wait 1-2 minutes
- Count the total number of cells and the blue stained cells
- The percentage of unstained cell is equivalent to vital cells
-

SH-SY5Y samples were seeded onto culture dishes in parallel to the culture flasks and the trypan blue was added at certain points during the differentiation for quick optical viability checks.

#### Used products

- Trypan blue 0.5%
  (Biochrom AG, Cat.No. L6323)

### 2.9.8 Cell harvesting for planar patch clamp

The used protocol (provided by Nanion; modified):

- Wash 1x with 5ml PBS (w/o $Ca^{2+}$ and $Mg^{2+}$)
- Add 2ml Trypsin-EDTA for 3-5 minutes at 37°C until the cells detach
  or
  Add 2ml Biotase-EDTA for 5-7 minutes at 37°C until the cells detach
- Add 6ml HamF12, aspirate cells gently 10-20x
- Centrifugation; 2 min at 100g
- Remove supernatant
- Resuspend the cells in 1ml external recording solution
- Centrifugation; 2 min at 100g
- Discard the supernatant
- Resuspend the cells in approx. 200µl external recording solution (End concentration: $1x10^6$ – $5x10^7$ cells/ml)
- Storage in a 1.5ml reaction vessel

Under the microscope, single cells with smooth membranes should be visible.

#### Used products

- Phosphate buffered saline (PBS) without $Ca^{2+}$/$Mg^{2+}$
  (Biochrom AG, Cat.No. L1825)

## 2.10 Adaptations for microgravity research

In this paragraph, the procedures are listed which had to be adapted to parabolic flight campaigns.

### 2.10.1 Planar patch clamp pulse protocols

While the details of the recording protocols varied during the parabolic flight campaigns, the protocols were always arranged in groups of 5 subsequent recordings based on the experiences from the first campaign:

- 1g before the parabola as the reference
- 1.8g upwards
- microgravity
- 1.xg downwards
- 1g after the parabola as a control of the patch clamp parameters
  (Seal resistance, series resistance, slow capacity, fast capacity).

To utilize most of the 20-22 seconds of each section of the parabola, the protocols were programmed accordingly (e.g. multiple repeats or long pulse protocols) to a maximum of 18 seconds. 2-3 seconds at the beginning and the end of each section were calculated for orientation and movement of the scientist to start the experiment and to avoid the transition phases of the manoeuvre.

The detailed protocols are presented in the results.

### 2.10.2 Cell culture

#### Transportation

The cells were transferred to a $CO_2$-independent culture medium in culture flasks with closed caps directly before the transportation to Bordeaux. The flasks were filled to a high level (~50ml) to ensure that the cells do not dry up during the (bumpy) transport. They were fixed in a to 37°C adjusted container which was connected to a 12V plug in the van. Since 2009, a certified cell culture transportation box was used with 80g $CO_2$-capsules and HamF12 medium.

##### Used equipment

- Transport trolley with temperature control
  230V & 12V
- Cell trans 4016 transportation box
  (Labotect Labor-Technik-Göttingen GmbH, Cat.No. 13867)
  230V & 12V, stable 37°C even without power, 5% $CO_2$ atmosphere
- Dennerle $CO_2$ Nano-Set
  (Dennerle GmbH; Cat.No. 5940)
  with pressure reducer, use of 80g $CO_2$ capsules
- Pressure reading
  (Unknown manufacturer, from our laboratory)
  subsequently connected to the $CO_2$ pressure reducer

### 2.10.3 Equipment

No laboratory equipment was provided during a parabolic flight campaign therefore the complete equipment must be brought by the science team. The focus had to be on the size

of the equipment, since space at Novespace (and the van) was limited. A mobile cell culture lab was established with small and robust equipment:

- Incubat 85 (270x180x420 mm)
  (Melag Apparate GmbH)
  Since no $CO_2$ was allowed (until 12/2009), a small heating cabinet was used
- Titan PCR vertical laminar flow clean bench (338x626x975 mm)
  (Scanlaf A/S, Denmark)
- Microscope Leica DM IL
  (Leica Microsystems GmbH)
- Incubation bath Type 1002 (325x395x255 mm)
  (Gesellschaft für Labortechnik mbH)
- Labofuge A centrifuge (until 12/2009) (295x295x315 mm)
  (Heraeus)
  no cooling unit to reduce size and weight
- EBA20 Centrifuge (since 01/2010) (216x231x292 mm)
  (Andreas Hettich GmbH & Co.KG)

The amount of the lab equipment (Pipettes …) and consumables was reduced to a minimum.

### 2.10.4 Cultivation

Since the safety regulations did not allow the use of a $CO_2$-incubator (until 12/2009), the cells had to be cultivated in a culture medium which does not require $CO_2$ for a stable pH. Therefore HEPES-buffered Dulbecco's modified eagle medium (DMEM) was used instead of HamF12 and the cells were stored in an incubator without $CO_2$.

Since the DMEM preparation medium is only suitable to a limited extent to be used in long-term cultivation, backup cells always were brought to the team during the first weekend of the parabolic flight campaign. Further details about the safety regulations will be reviewed in the technical results and in the discussion.

#### Used products

- DMEM with 4.5 g/l D-Glucose, with L-Glutamine
  (Biochrom AG; Cat.No. T043)
- HEPES
  (Sigma-Aldrich; Cat.No. H4043)
- $NaHCO_3$
  (Sigma-Aldrich; Cat.No S5761)

Per liter DMEM (in aqua bidest) 2.4g HEPES (10mM) and 0.37g NaHCO3 (4mM) were added. The pH was adjusted to 7.4 with NaOH. After sterile filtration it was usable for 6 months.

### 2.10.5 Time schedule

Approximately 90 minutes before the scheduled closing of the aircraft doors, the cell culture was prepared. This took about 30 to 45 minutes. The cell culture works was performed as short as possible before takeoff to reduce the time where the prepared cells could form clusters of multiple cells or aggregate to the walls of the reaction vessel.

### 2.10.6 Storage during flight

The reaction vessels containing the specimen cells and the patch clamp solutions were stored at 37°C as long as possible. During the takeoff the reaction vessels were stored in a double containment in the laboratory box (for details of the flight hardware, please refer to the results). Depending on the temperature in the A300 (which could be below 11°C, depending on the season of the year), the cells were stored in a zipper bag (a mandatory double compartment) in the breast pocket of the flight suit until the start of the experiment where the vessels were transferred to the laboratory box.

## 2.11 Used software

For the patch-clamp experiments, PatchMaster (Heka Elektronik) with the PatchControl extension (Nanion Technologies) was used. The data was analyzed with Fitmaster (Heka). The statistical analysis and the graphical presentation were performed with Prism 5 (Graphpad Software).

The hardware was constructed with the freeware version of SketchUp 7 (Google Inc.).

# 3 Results


Figure 3.1: Project logo

## 3.1 Design of a planar patch clamp setup for microgravity research

A parabolic flight campaign is classified as an experimental environment. All participants, procedures and especially the hardware must comply with strict safety rules in order to be used onboard the A300 Zero-G.

The hardware was designed according to *Novespace A300 Zero-G Rules and Guidelines*. Adaptations during the project were made according to the latest update of the guidelines. The focus of the guidelines for the designed hardware lied on:

- Mechanical stability and weight
- Electrical safety
- Liquid handling under microgravity

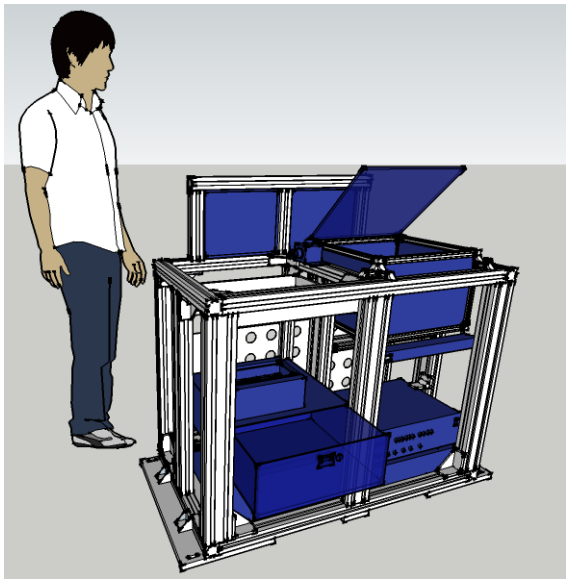

Figure 3.2: Schematic of the complete patch clamp setup

The hardware was designed to be operated by 2 scientists, one scientist operated the software the second scientist performed the patch clamp procedures.

### 3.1.1 Mechanical structure

The structure was made from 45x45mm and 45x90mm t-groove aluminium profiles (Bosch Rexroth) with proper brackets, connectors and screws. The intersected base plate was made from a solid 20mm aluminium plate. The transfixion of aluminium profiles, which

was used for this hardware, is no longer allowed for new hardware according to the updated design guidelines. The hardware was certified in a parabolic flight before the new guideline was set, therefore it could be used for the complete project period. Nevertheless, transfixed attachment points were replaced by groove connections where it was possible during the period of the project.

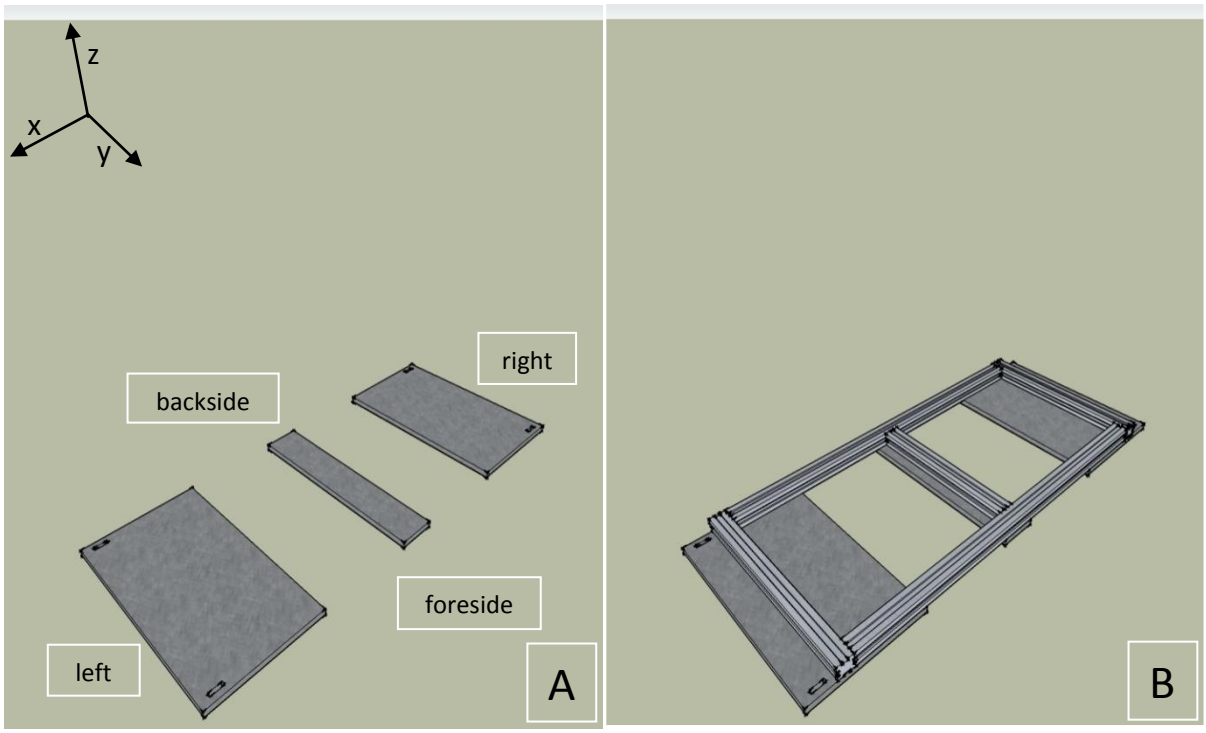


Figure 3.3: (A) The intersected base plate. (B) The bottom framework (45x45mm aluminium profiles)

4 slotted holes in the base plate were used to attach the experiment to the aircraft rails. It was intersected to reduce the overall weight. The base plates were attached to the bottom frame with 17 (7-3-7) M8 screws and slotted blocks. For a smooth contact face to the aircraft all screws holes were recessed.

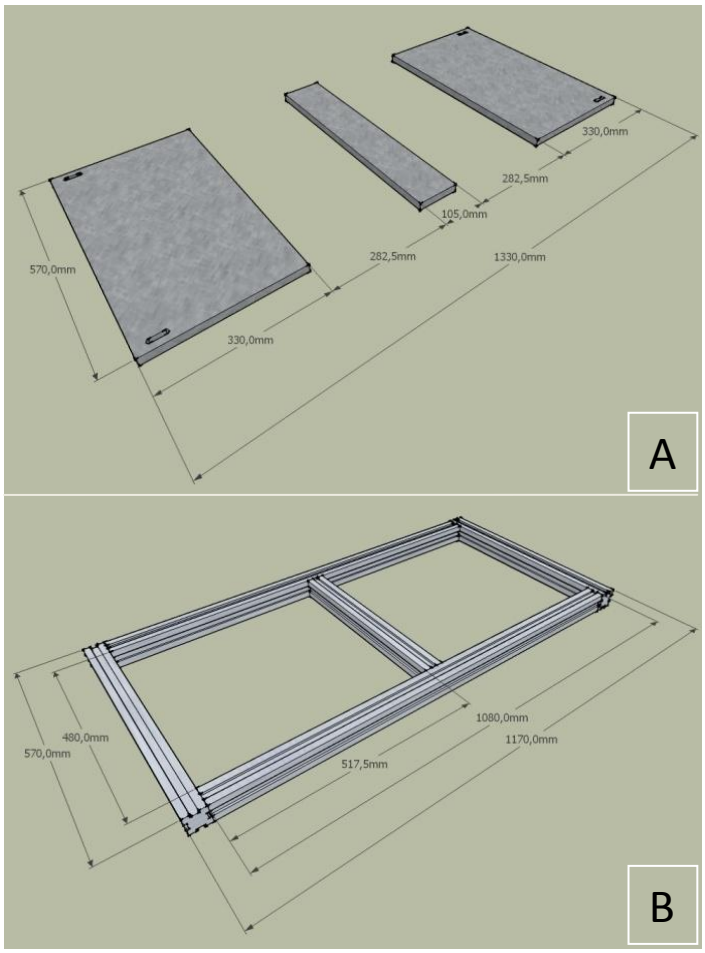


Figure 3.4: Dimensions of (A) the intersected base plate and (B) the bottom frame

The distance of the slotted holes in the y-axis was 503mm to fit in the strait attachment rails of the aircraft.

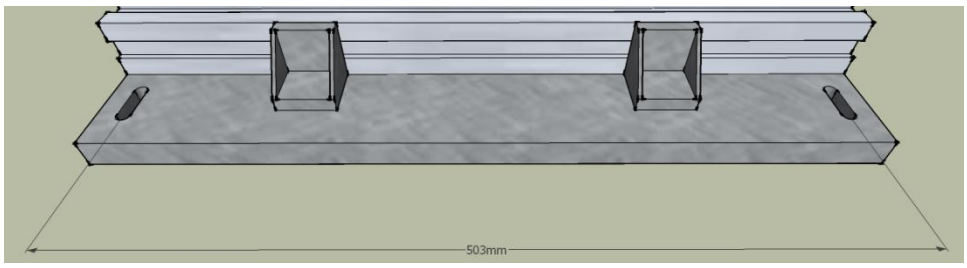


Figure 3.5: Distance of the fixation holes in the y-axis.

Slotted holes in the x-axis were used to simplify the attachment as the distance of the attachment points must be a multiple of 1 inch (2.54 mm). The experiment may only be attached to the aircraft by Novespace or CEV personnel. The attachment points in the x-axis had a distance of 48 inches.

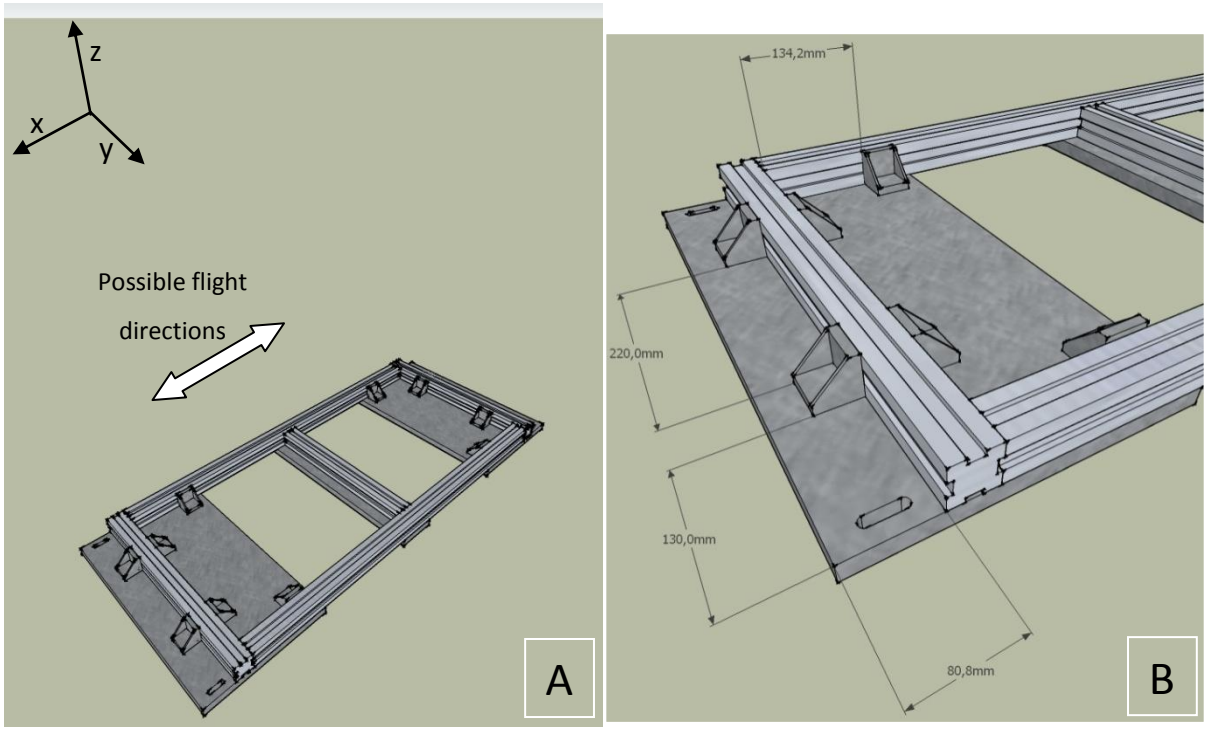


Figure 3.6: (A) Additional brackets, 6 in the x-axis, 4 in the y-axis. (B) Distances of the brackets on the left base plate (similar on the right side without the outer brackets).

The bottom frame was secured with 6 additional brackets in the x-axis to allow the integration of the setup with the left or the right side in flight direction.

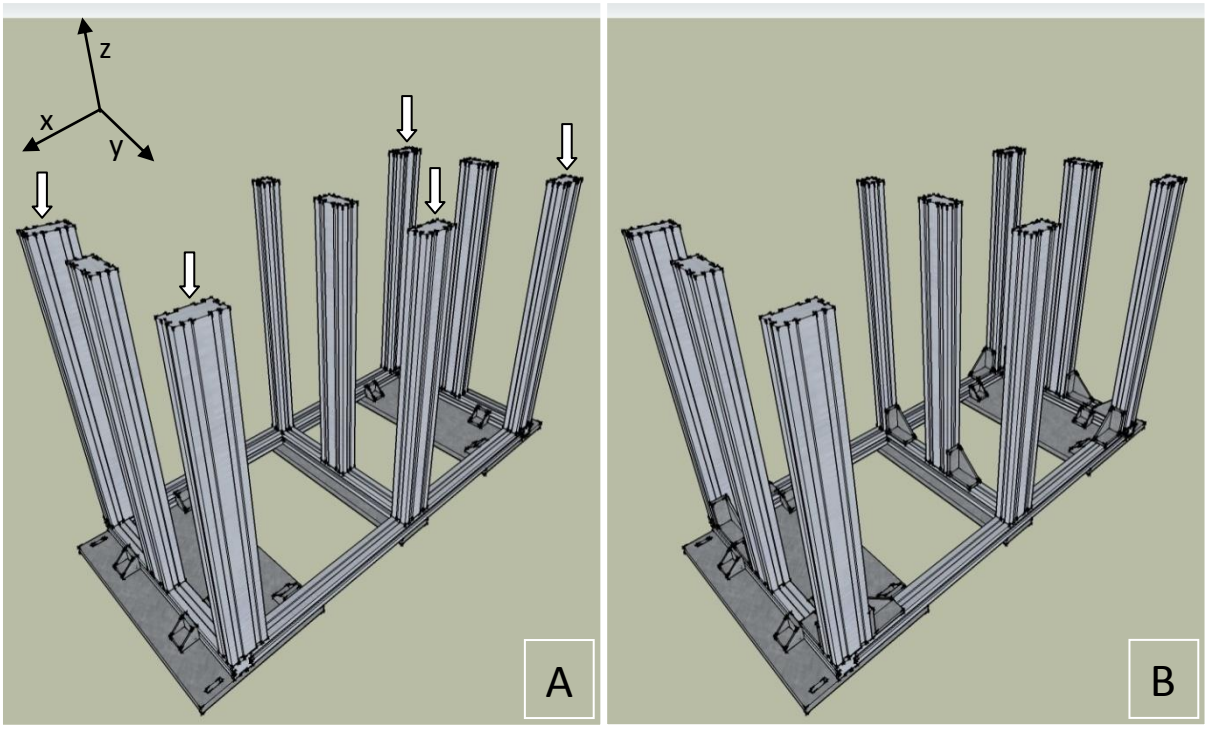


Figure 3.7: (A) The 9 upright profiles, 8 45x90x775mm and 1 45x45x775mm. (B) 12 additional 90mm brackets

The uprights profiles were made from 8 45x90mm profiles and 1 45x45mm profile. To evenly distribute the bending moments of the profiles ($W_x$, $W_y$), with a slight focus on the flight direction, 5 profiles faced $W_x$ in flight direction and 3 in the y-axis. To reinforce the structure against torsion stress, dual bolt connectors connected the outer uprights to the top and bottom frame (indicated by arrows in fig. 3.7A). The unmarked uprights were connected to the top and bottom frame by M8 screws bolted into the central cylinders.

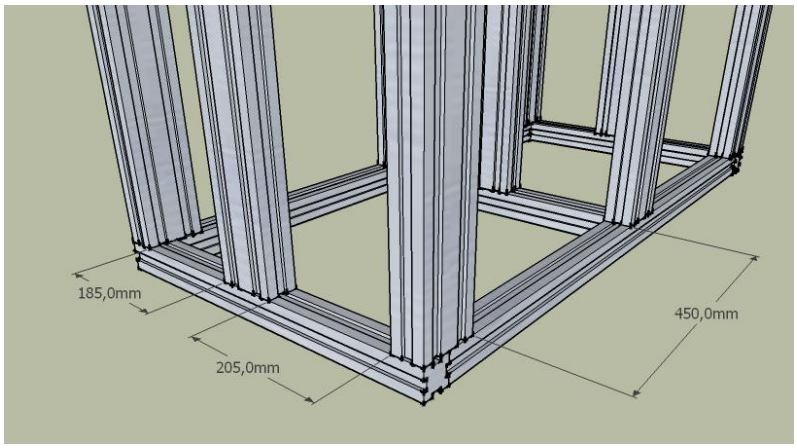

Figure 3.8: Distance of the uprights.

A 19 inch distance of the uprights in the x-axis was chosen to enable the use of standard 19''-rackmount hardware which was attached to the corresponding grooves. The 3 middle uprights were not exactly centred for easier access to the front uprights where the experiment hardware was attached.

The dimensions of the top framework were similar to the bottom framework. It was secured by M8 screws, dual bolt connectors (fig. 3.7A) and 12 brackets.

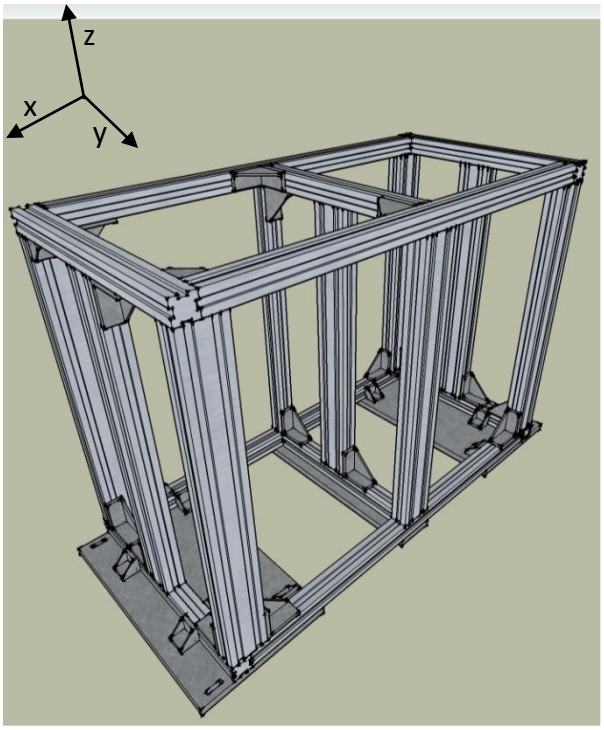


Figure 3.9: The upper framework is additionally fortified with 12 brackets (45 and 90mm, not all visible)

On the top frame, the monitor framework was attached. It was secured by 2 90mm brackets and a flat aluminium bracket. The inner groove was widened to incorporate the monitors.

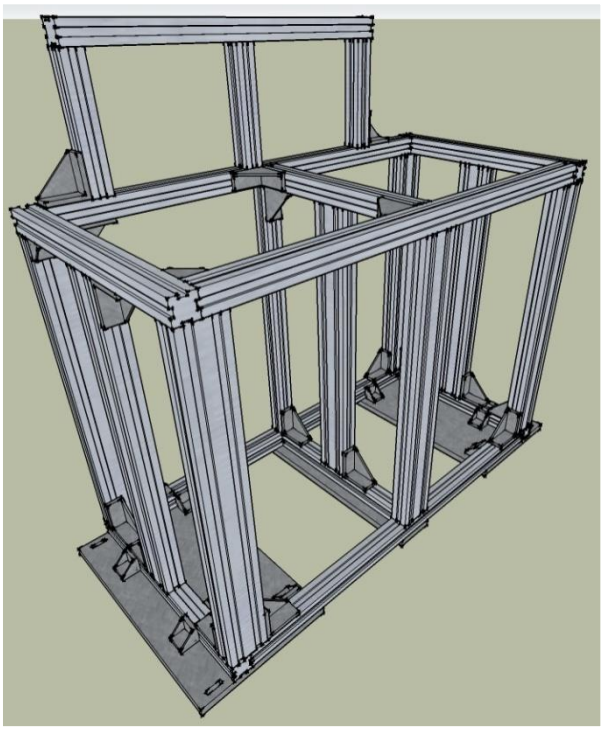

Figure 3.10: The monitor framework

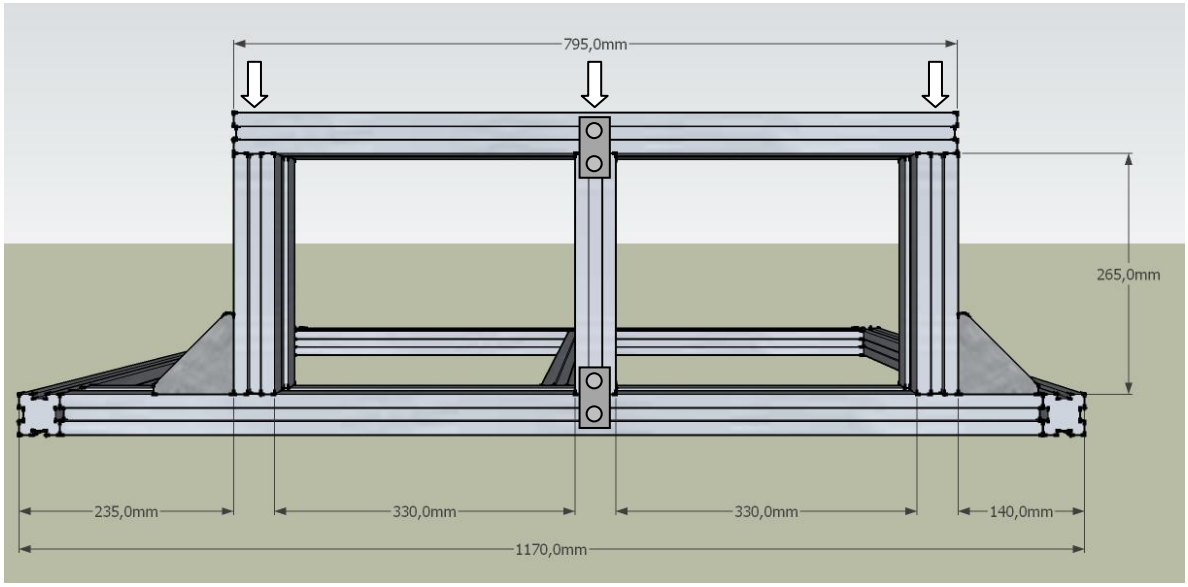


Figure 3.11: Dimensions of the monitor framework. Arrows indicate M8 screws bolted into the central cylinder of the profile. Two flat brackets at the middle upright reinforced the structure.

The last structural components are a lockable rackmount keyboard drawer, which was additionally secured by an aluminium profile at the backside to reduce rattling and 2 slotted steel sheets to protect the cables at the backside of the experiment since it was located directly at the central passageway of the experiment area. The keyboard drawer was always used in the locked position.

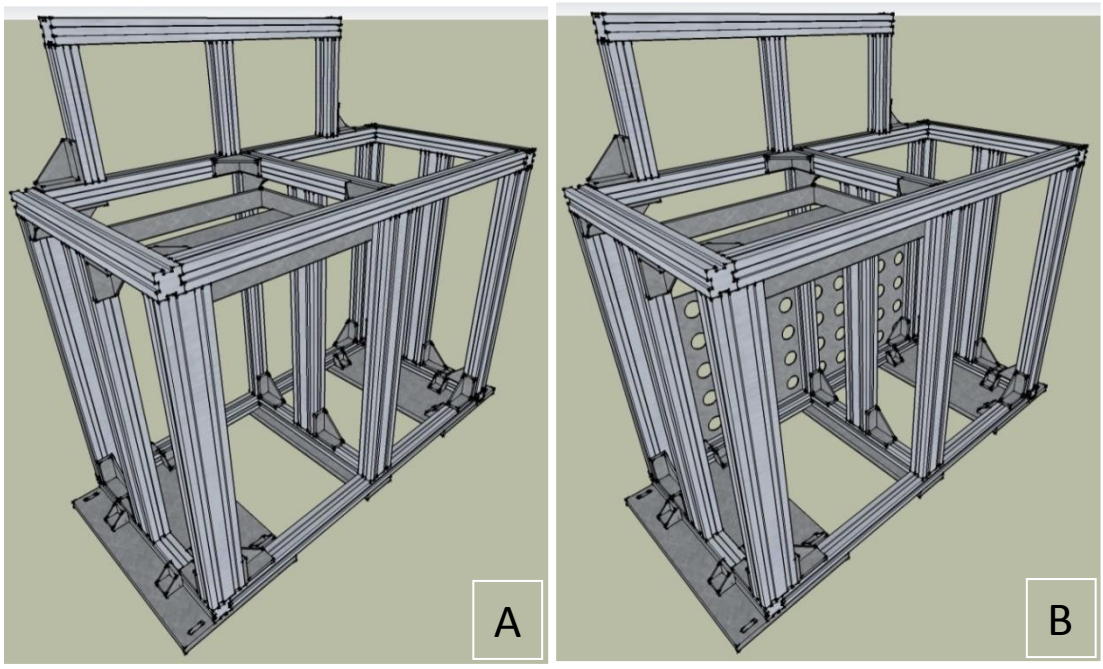


Figure 3.12: (A) The 19'' drawer for the computer keyboard (B) 2 slotted steel sheets to protect the backside.

### 3.1.2 Calculation of the structural properties

The calculations were performed according to *Novespace A300 Zero-G Rules and Guidelines.*

#### Computing linear load

| Weight of the setup [kg] | Number of attachment points | Calculated $M_{attach}$ [kg] | Center of gravity from ground [mm] | Distance between attachment points [inch] |
|---|---|---|---|---|
| 165 | 4 | 41.25 | 340 | 48 |

Table 3.1: Linear load

According to Novespace A300 ZERO-G Rules and Guidelines, page 34, table 6: Maximum allowable rail linear loading over one linear meter, the rail linear loading must be smaller than 100kg ($RL \leq 100kg$).

$M_{attach} = 41.25kg \leq 100kg$

#### Characteristics of the rack

| Overall dimension (X x Y x Z) [mm] | Mass [kg] | Center of gravity height [mm] | Number of attachment points |
|---|---|---|---|
| 1330 x 550 x 1195 | 165 | 340 | 4 |

Table 3.2: Overall characteristics of the rack

| Distance between holes (x-axis) [mm] | Profile dimensions [mm x mm] | Material | Ultimate strength $R_m$ [N/mm²] | Number of vertical uprights | Section modulus $W_x$ [mm³] |
|---|---|---|---|---|---|
| 1219.2 | 45x90<br>90x45<br>45x45 | Aluminium | 250 | 5<br>3<br>1 | $W_x$ 27700<br>$W_y$ 14600<br>$W_{45}$ 6050 |

Table 3.3: Characteristics of the used aluminium profiles

## Computing the shear strength on the experiment attaching screws

| | |
|---|---|
| $W$ | Weight of experiment in kg |
| $N$ | Number of attachment points to the aircraft rails for a given rack |
| $g$ | 9.81m/s$^2$ acceleration |
| $F_c = \frac{9 \cdot g \cdot W}{N}$ | Shear load in newton |
| $F_{adm} = 34800\ N$ | max. acceptable load applied to a screw in newton |
| $SF$ | Safety factor, must be greater than 1.5 = $F_{adm}/F_c$ |

| | W | N | $F_c$ | $F_{adm}$ | SF |
|---|---|---|---|---|---|
| **Rack #1** | 169 | 4 | 3730,3 | 34800 | 9,33 |

Table 3.4: Shear strength on the attaching screws

## Computing the tensile load of the experiment attaching screws

| | |
|---|---|
| $W$ | Weight of experiment in kg |
| $h$ | Height in mm of the rack's center of gravity |
| $N$ | Number of rear attachment points of a given rack to the aircraft rails |
| $g$ | 9.81m/s$^2$ acceleration |
| $d$ | Distance in mm between the furthest front and rear attachment points of a rack. Must be an inch multiple. |
| $Ft = \frac{9 \cdot g \cdot W}{N \cdot d}$ | Tensile load in newton |

| | W | h | N | d | $F_t$ |
|---|---|---|---|---|---|
| **Rack #1** | 169 | 340 | 2 | 1225 | 2070.67 |

Table 3.5: Tensile load on the attaching screws

| | |
|---|---|
| $F_{cs} = 28300N$ | Tightening load of the screws in Newton |
| $F_{adm} = 58000N$ | Max. acceptable load applied to a screw in Newton |
| $SF = Fadm/F$ | Safety factor, must be greater than 1.5 |

| | $F_t$ | $F_{cs}$ | $F = F_t + F_{cs}$ | $F_{adm}$ | SF |
|---|---|---|---|---|---|
| **Rack #1** | 2070.67 | 28300 | 30370.67 | 58000 | 1.91 |

Table 3.6: Calculated safety factor

## Computing the rack uprights' flexural strength in the event of a crash

| | Part number | Section cross-section (mm x mm) | Material | Ultimate strength $R_m$ (N/mm²) | Moment of intertia Ix (cm⁴) | Section modulus Wx (mm³) |
|---|---|---|---|---|---|---|
| **Rack #1** | 3842992432 | 45x90 | Aluminium | 250 | 125 | $W_x$ 27700 mm³<br>$W_y$ 14600mm³<br>$W_{45}$ 6050 mm³ |

Table 3.7: Characteristics of the rack uprights

| | Weight (kg) W | Center of gravity height (mm) h | Number of uprights participating in the rack's flexural strength N |
|---|---|---|---|
| **Rack #1** | 169 | 340 | 9* |

Table 3.8: Flexion crash characteristics of the rack

| | |
|---|---|
| $W$ | Weight of experiment in kg |
| $h$ | Height in mm of the rack's center of gravity from the ground |
| $N$ | Number of vertical uprights participating in the flexural strength |
| $g$ | 9.81m/s$^2$ acceleration |
| $Mf = \frac{9 \cdot g \cdot W \cdot h}{N}$ | Bending moment on an upright in N·mm |
| $Mf_{\text{adm}} = R_m \cdot W$ | Maximum acceptable bending moment applied to an upright in N·mm. The value is calculated based on the section manufacturer's technical data. $R_m$ is the ultimate strength of the material (N/mm$^2$) and W the section's section modulus (mm$^3$). |
| $Mf_{adm} = R_m \cdot (\frac{5 \cdot W_x + 3 \cdot W_y + 1 \cdot W_{45}}{N})$ | Taking into account the orientation of the used profiles |
| $SF = Mf_{adm}/Mf$ | Safety factor, must be greater than 1.5 |

| | W | H | N | Mf | $Mf_{adm}$ | SF |
|---|---|---|---|---|---|---|
| **Rack #1** | 169 | 340 | 9 | 563682,6 | 5833332.5 | 9.28 |

Table 3.9: Calculated safety factor

### 3.1.3 Components

The 19’’-components were attached to the upright grooves with screws and slotted blocks. The brackets of the housings were extended to fit over the grooves for a proper connection. The 2 drawers were attached with M4 screws into the aluminium profiles (no longer allowed for new hardware). All cables were fixed to the rack with cable ties or fabric tape.

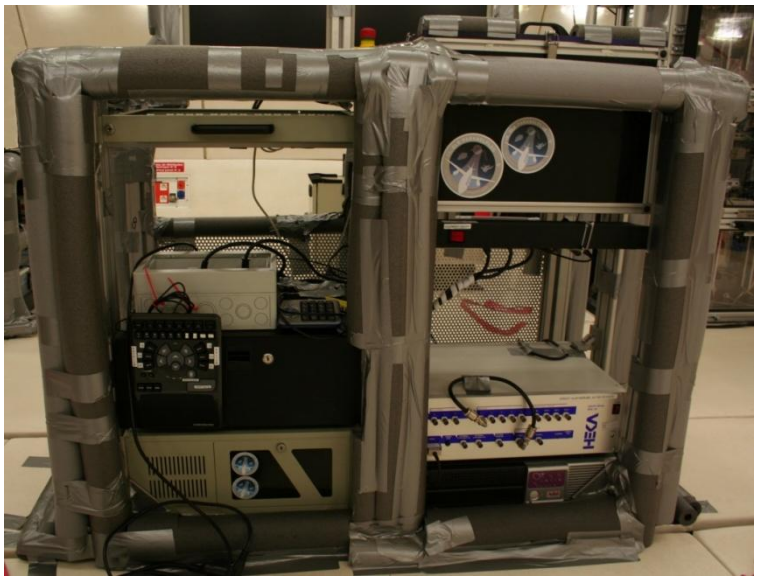

Figure 3.13: The assembled experiment in the A300 Zero-G during the 13th DLR PFC

## Electrical system

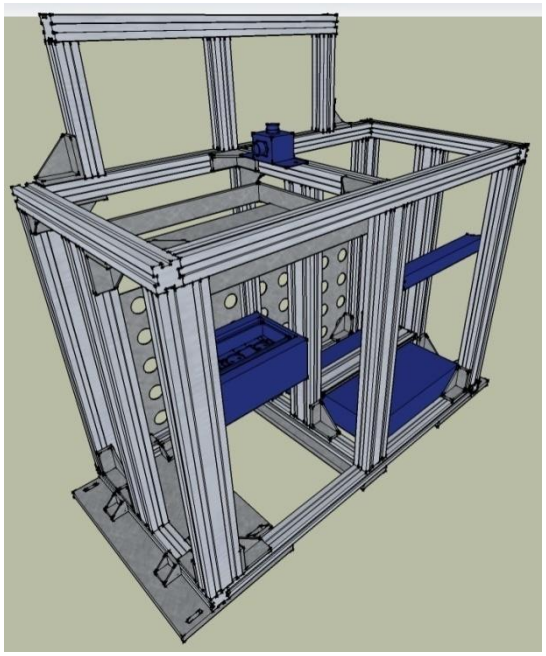

Figure 3.14: Components of the electrical system. Circuitry box, emergency stop button, multi-socket and UPS.

The electrical system evolved the most during the project[5]. It had to meet the strict safety requirements from Novespace and CEV and the electrical requirements, especially shielding (as described in section 2.5.2), for a patch clamp setup. To protect the aircraft and the experimenters, it was mandatory to integrate a ground fault interrupter (GFI), a fast fuse which had to be adjusted just above the maximum electric consumption and a single emergency stop button which had to cut off phase and neutral.

| | **Total power consumption Mean** | **Total power consumption Max.** | **Fast Fuse** |
|---|---|---|---|
| **220 VAC Power supply** | 400 VA | 450 VA | 2.5 A |

Table 3.10: Power consumption and fuse value of the complete setup

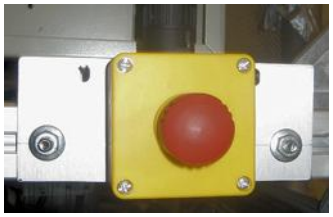

Figure 3.15:
Emergency stop button

The emergency stop button could be attached freely on the aluminium profiles with 2 screws and slotted blocks. After some near-accidents with floating experimenters and reporters, the emergency stop button was moved from a lateral to a central position.

The multi-socket for the complete equipment was a 19'' module with sockets to the inside of the rack and a separate switch. The heavy plug transformer of the patch clamp pump was additionally secured to the multi-socket by cable straps.

Figure 3.16: The circuitry box with mains plug, emergency stop button and multi-socket.

[5] Due to changing regulations concerning the integration and protection of an UPS, the layout of the box changed between the campaigns. 3 different versions were used. The first version was housed in a rackmount container with MIL certified connections and heavy duty components. The latest edition is described above.

The circuitry box was made from a DIN-rail box with standard DIN-rail components. All cable connections were made with safety plugs. The box was attached to the metal drawer.

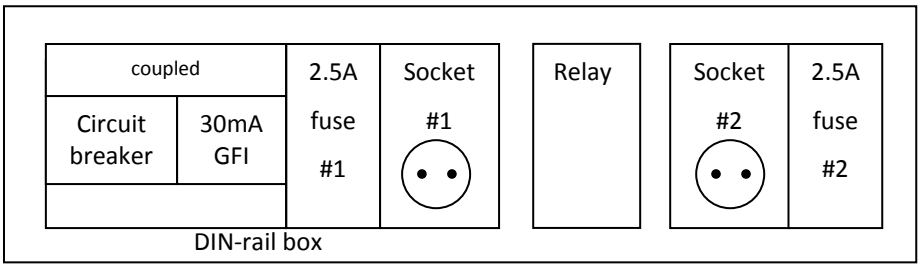


Figure 3.17: Layout of the DIN-rail box

The following components were integrated into the circuitry box (from left to right):

- Circuitry breaker (Moeller) mechanically coupled to main GFI
- GFI 30mA 16A (Moeller)
- Fuse holder #1 & 2 for D-type fuses with internal status LED equipped with 2.5A fuse protecting UPS power-in (#1) and power-out (#2).
- Socket #1 & 2 (Siemens) for UPS power-in (#1) and power-out (#2). The use of sockets made modified cables obsolete, only standard IEC cables were used to and from the UPS.
- Relay (ABB, 230V with status light) with 4 makers controlled by the emergency-stop. When the button was pressed, the relay cut both phase and neutral before and after the UPS powering off the complete setup.

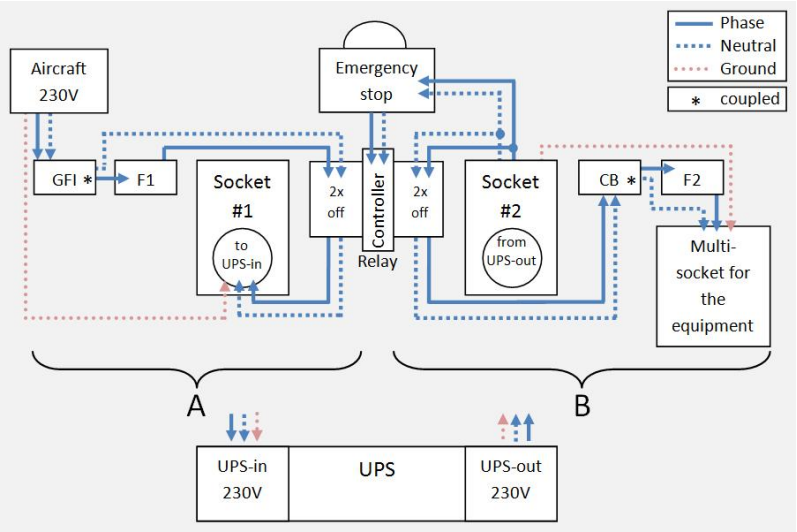


Figure 3.18: Wiring of the components. (A) The circuit before the UPS power-in, (B) after UPS power-out. F1,F2 = fuse, GFI = ground fault interrupter, CB = circuit breaker, UPS = uninterruptible power supply.

The UPS had to be protected by a circuit breaker connected to the GFI, fuse and its power-out had to be connected to the emergency stop button. To ensure the proper function of the UPS in case of a power failure a rather complex wiring was implemented:

| | |
|---|---|
| GFI was triggered: | A & B were disconnected from the mains. The experiment was powered off |
| Emergency stop was used: | The relay cut phase and neutral before and after the UPS, powering off the complete experiment |
| Aircraft power failure: | the UPS powered the experiment |

## Computer system

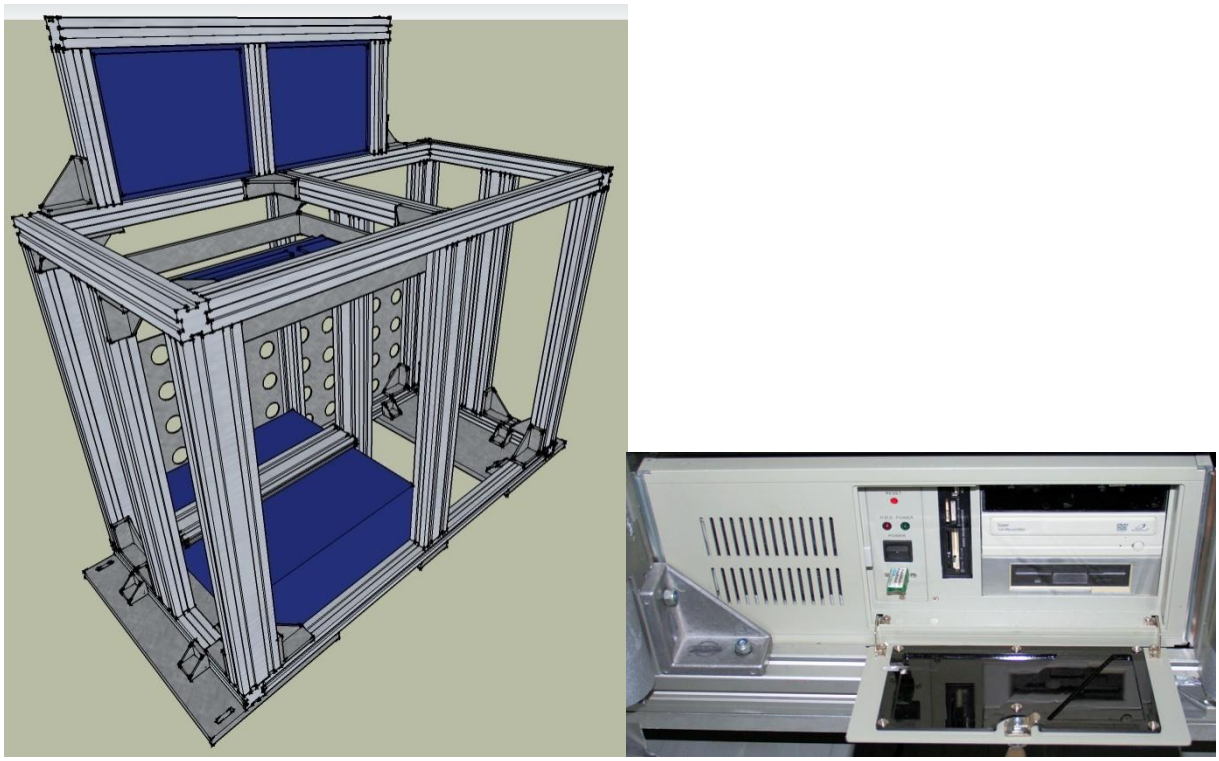

Figure 3.19: The integrated computer system. The computer housing was additionally secured by a 10x90mm aluminium profile fixed with screws bolted in the central cylinder of the profile

A standard computer in a 19'' rackmount steel housing with a 19'' keyboard and integrated touchpad was used. A trackball was connected via USB for faster control. Two 15'' TFT-monitors were used with the Patchmaster software stretched over both monitors. The monitors were chosen because of their small thickness (10mm) as the groove of the

aluminium frame was easily widened to that dimension for a robust integration. The keyboard was fixed with hook and loop fastener.

As a safety precaution, the hard drives were integrated into an alternate frame for quick and easy replacement during the flight. A backup hard disk with all needed software was always stored in the equipment drawer. During the 11th DLR PFC, the main and backup hard disks did not function properly under microgravity at several occasions. Probably the actuator arm could not be positioned correctly. After the campaign, the standard hard disks were replaced by modern solid state hard disks which do not have mechanical components. This solved the problem.

The computer power supply (PSU) was replaced by a high quality PSU after the 11th DLR PFC due to unexplainable restarts of the computer.

In previous campaigns it was observed that in microgravity, the time until the pulse protocols were started took up to 10 seconds (approx. 50% of microgravity) due to the movement of the scientists and the software operation (complex mouse and keyboard inputs were needed to start the protocols). Since the 13th DLR PFC, a special USB keyboard (Revoltec FightPad Advanced, Listan GmbH & Co. KG) was integrated into the system. This keyboard was originally designed for computer games and it could be programmed to run even complex keyboard-mouse operations with a single touch of a button with nearly no delay. For each gravity phase (1g, 1.8g, 0g) the operations were programmed including execution, proper labelling (1g ahead, 1.8g up, 0g, 1.xg down, 1g after) and storage. The saved time was used to extend the pulse protocols for an optimal use of the 20 seconds of microgravity. The keyboard was attached to the equipment drawer with hook and loop fastener and it was removable for operation. Therefore the scientist was not enforced to move to the upper keyboard, he could control the experiment from a prone (or any other preferred) position, saving time and reducing the risk of motion sickness.

Figure 3.20:
The programmable keyboard. During the experiments it was removed from the drawer

## Equipment drawer

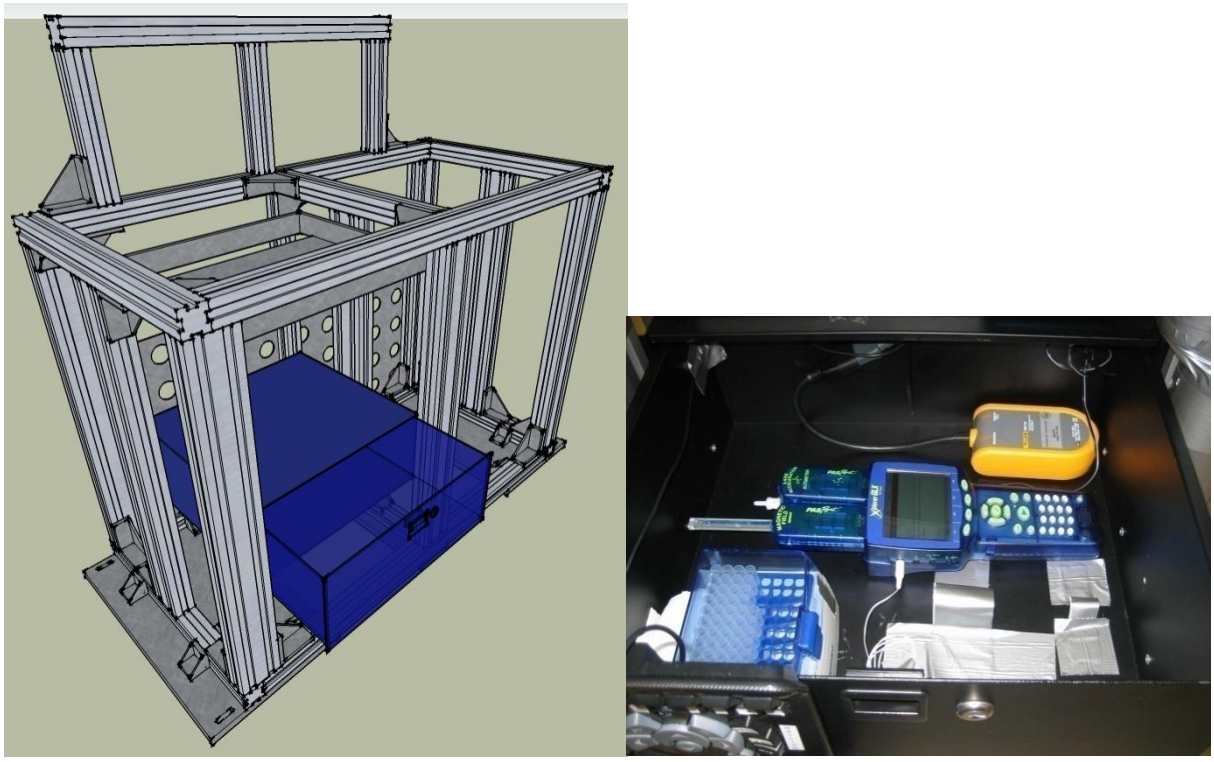

Figure 3.21: The equipment drawer. (left) schematic; (right) detailed picture. Visible are 2 dataloggers and a box with pipette tips.

The drawer was mainly used to store spare parts: a 1000µl pipette with tips, a second hard drive, additional NPC-1 chips and a pair of optical cables for the EPC-10 interface. During the first parabolic flight campaign (November 2007) a vortex shaker was integrated in the experiment to separate the cells during the flight, but this had a negative impact on the vitality of the cells and therefore it was removed after the second flight day.

For the 50$^{th}$ and 52$^{th}$ ESA PFC it was used to store sensory modules and data loggers to monitor different parameters as temperature, vibrations and more (please refer to section 3.2 for details).

## EPC-10 Patch clamp amplifier

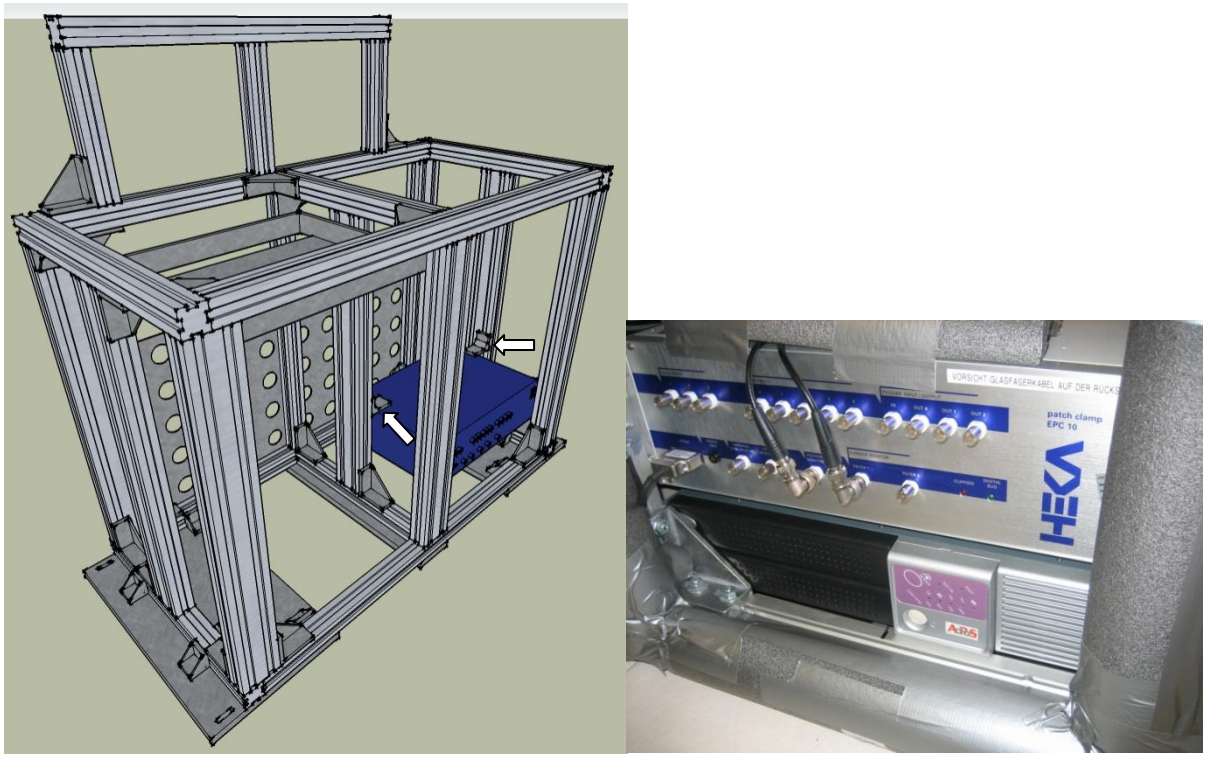


Figure 3.22: The EPC-10. (left) schematic; (right) detailed picture of the EPC-10 above the UPS. It was additionally secured by 2 aluminium brackets from above (arrows)

The EPC-10 (HEKA) was connected to the computer by optical connection to the LIH-1600 interface card. The headstage was integrated into the Port-a-Patch planar patch clamp device (Nanion) in the laboratory box. All cables were carefully fixed with cable ties. It was additionally secured by 2 aluminium brackets from above (indicated in fig 3.22).

## Uninterruptible power supply

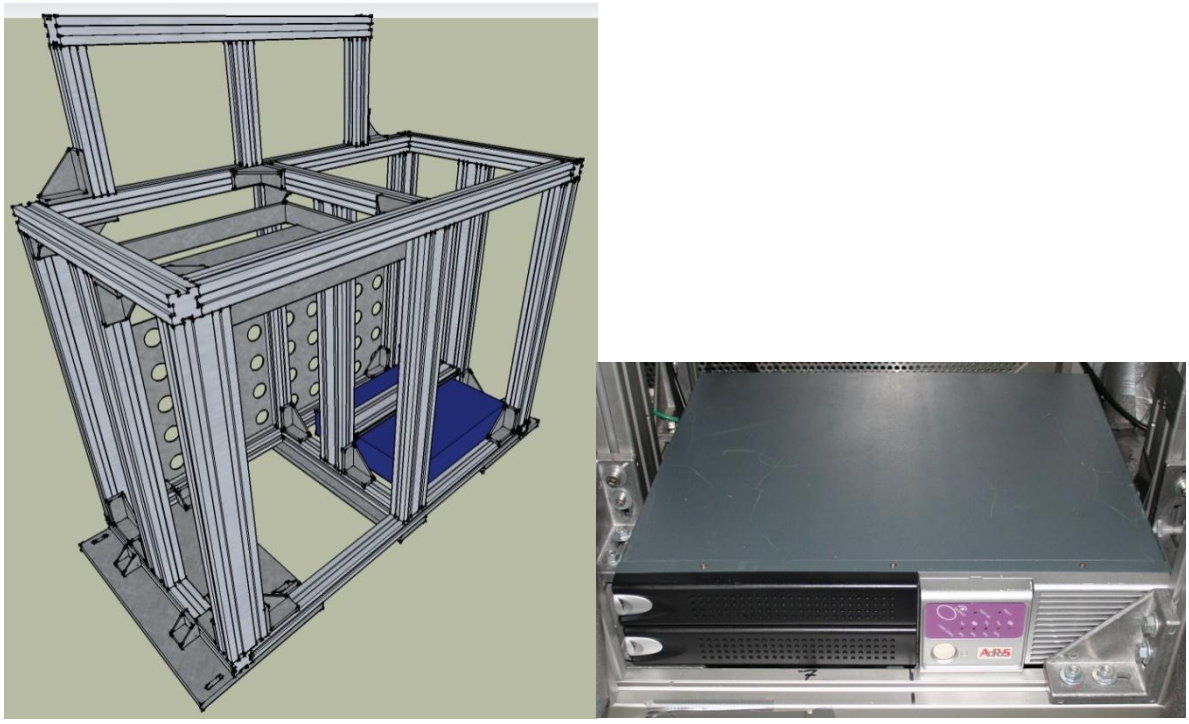

Figure 3.23: The 19''-rackmount UPS. (left) schematic); (right) detailed picture. It was additionally secured by a 10x90mm aluminium profile (fixed with screws bolted in the central cylinder of the profile)

A 1kVA online double conversion UPS (Mini-J RT; AdPoS GmbH & Co. KG) was integrated for several purposes:

1. Data safety. The recorded patch clamp data could be completely lost if the computer system crashes. The power grid for the experiments in the aircraft has been unstable at several occasions in the past, which could, in worst case, mean that a complete flight day is lost. The experiment could be powered by the UPS' batteries for approximately 30 minutes.
2. Stable power output. According to the manufacturer of the EPC-10, the input voltage of 230V may vary ±2% to ensure proper recordings. This could not be achieved by the aircraft converters (for details please refer to section 3.2.5). The UPS complied with the requirement of ±2%.
3. Electrical shielding of the patch clamp hardware. As stated in section 2.5.2, the shielding of the patch clamp hardware from electrical noise is very important. In the A300 up to 3 experiments are connected to the same electric panel as the patch clamp hardware, therefore electrical noise generated by these experiments can influence the patch clamp recordings. The UPS with 2 galvanic separated rectifiers was used to reduce the noise as much as possible.

## The laboratory box

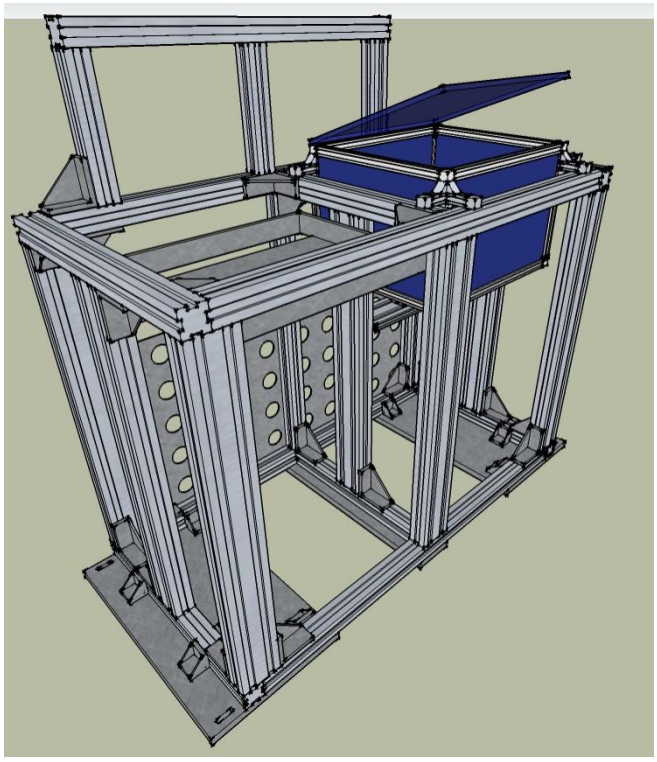

Figure 3.24: Schematic of the laboratory box integrated into the rack.

The actual patch clamp experiments were performed in the laboratory box. It accommodated all needed equipment and samples. During the design process the mandatory safety requirements, the laboratory needs and the adaptations to microgravity (time frame & quick access) had to be brought together.

The lab box was made from 20x20mm Bosch aluminium profiles and 8mm solid aluminium[6] plates. The lid was made from 10mm polycarbonate. When closed, the lid was locked by 3 fasteners. The open lid was locked to the monitor framework (the monitors were used when the box was open, which was the main reason why the lid had to be transparent).

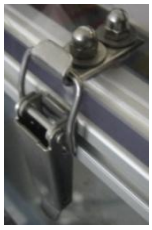

Figure 3.25: One of three fasteners to secure the lid of the laboratory box

[6] Until end of 2009, the laboratory box walls were made from polyoxymethylen (POM) an acetal based plastic due to its resistance to chemicals. Since 2010 POM may no longer be used due to its thermal properties therefore it was replaced by aluminium.

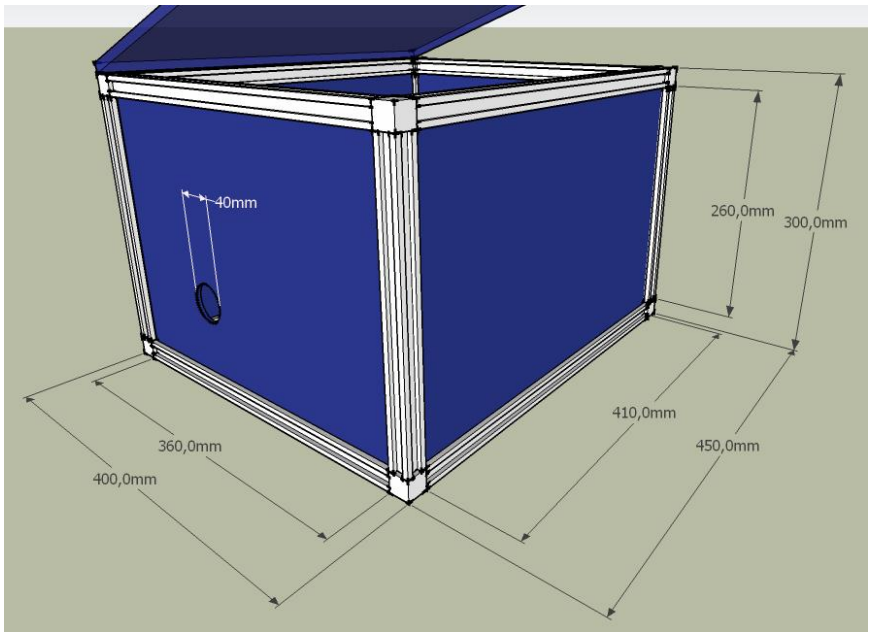


Figure 3.26: Dimensions of the laboratory box.

The lab box contained all needed equipment for the experiment: the Port-a-Patch with the pump and NPC-1 chips, pipettes with tips, the patch clamp solutions, the cell culture and a waste compartment. Since the experiment required liquid handling, the box had to be completely sealed with silicone and a rubber sealing around the lid. To validate the sealing, the laboratory box was completely filled with distilled water. All leaks were marked and sealed with additional silicone until no further leakage was observed.

Furthermore all liquids had to be stored in a mandatory second compartment (Tupperware box).The total volume of stored liquid during the parabolic flight was 8-9ml.

- 2x 1ml external patch clamp solution
- 2x 1ml seal enhancer
- 2x 1ml internal patch clamp solution
- 2x 1ml cell suspension

The different solutions were stored in 1.5ml reaction vessels. For safety reasons each liquid were stored in 2 separate reaction vessels.

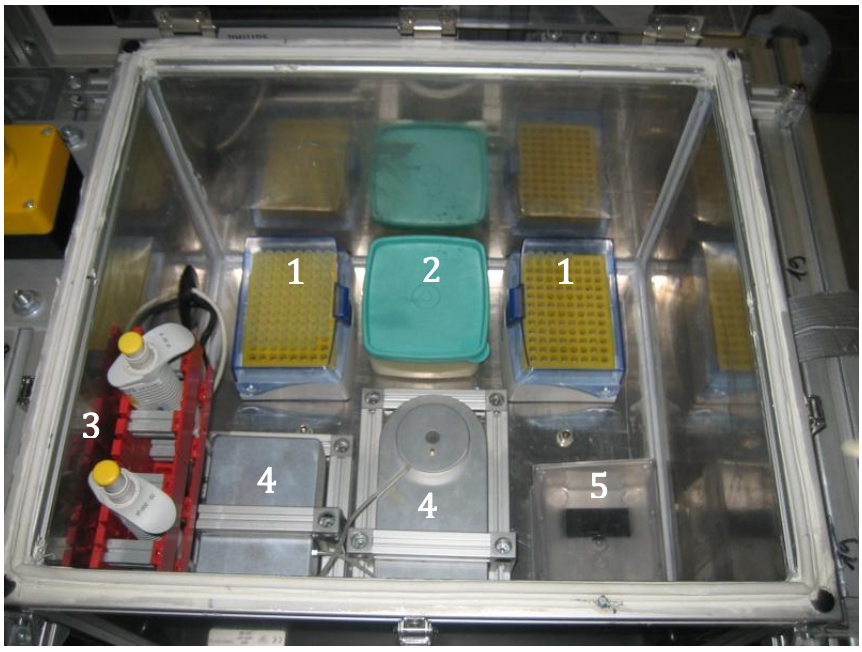

Figure 3.27: View inside the laboratory box. (1) Pipette tips; (2) Liquid storage; (3) Pipettes; (4) Port-a-Patch; (5) Waste compartment (w/o waste bag)

The Port-a-Patch and the pump were secured with an aluminium frame (20x20mm profiles), the pipette tips, the liquid compartment and the waste compartment were secured by hook and loop fastener for quick replacement. The pipettes were stored in a frame (made from glued Fischertechnik modules) on the inner wall. The closed lid secured the pipettes during the microgravity phases. A dispenser for the NPC-1 chips was designed for fast access. It was glued to the inner side of the lid. Once the lid was opened the dispenser automatically was in an optimal position.

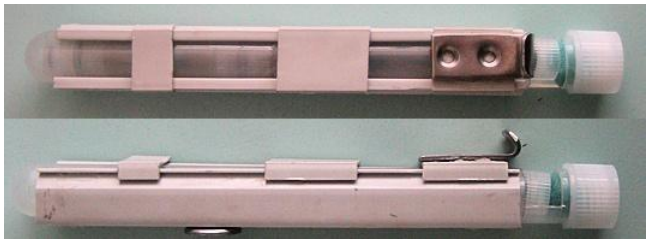
Figure 3.28: The NPC-1 chip dispenser. It was made from a prolonged NPC-1 storage tube and a plastic cable duct. The lid of the cable duct was used to secure the tube and as a movable lid to close the padded dispenser port. The dispenser stored 16 chips. It was refilled by removing the lower cap or by removal of the complete tube.

To connect the laboratory box to the main rack, 6 arms (4 in flight direction) were attached to the box. The connecting arms were made from 20x20mm aluminium profiles (Bosch) with

brackets and cube connectors. M8 screws with slotted blocks were used to connect the arms with the main rack groove.

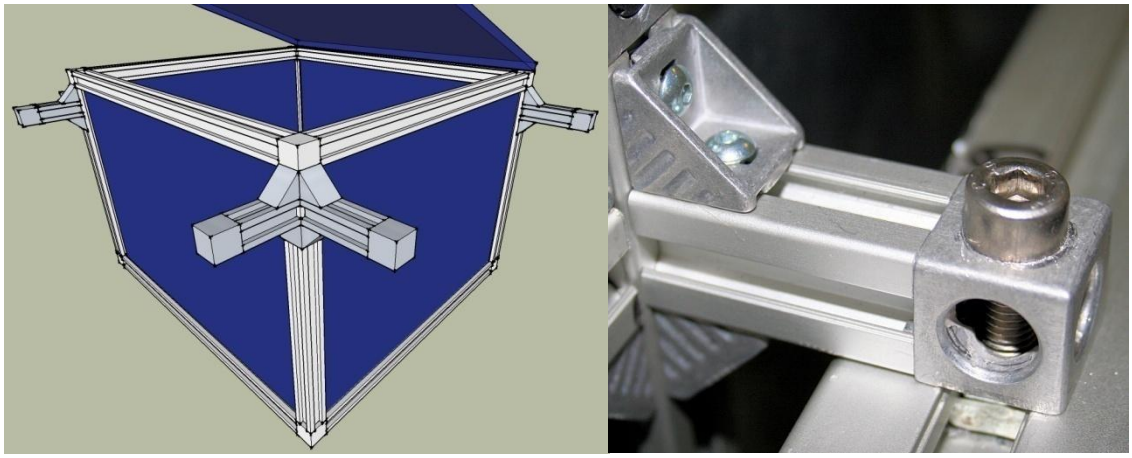

Figure 3.29: (left) Schematic of the fixation. (right) Detailed picture of a connecting arm.

To further secure the lab box, it was mounted on a supporting structure of a 10x90mm horizontal aluminium profile with two 45x45mm uprights. The base of the box was screwed to the uprights. The boreholes were sealed with silicone.

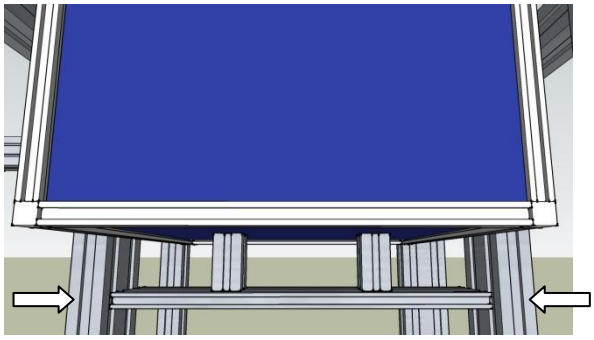

Figure 3.30: The bottom connection to the rack. Arrows indicate screws bolted in the central cylinders of the aluminium profiles.

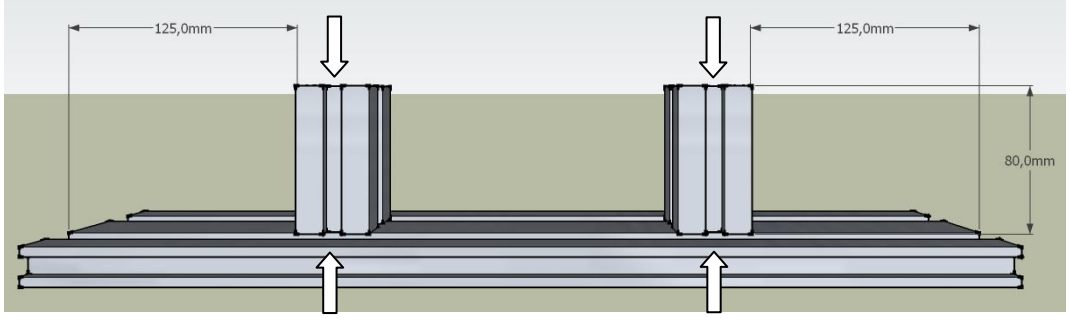


Figure 3.31: Dimensions of the lower lab box connection. Arrows indicate screws bolted in the central cylinder of the aluminium profiles.

To conduct all cables (and the large connectors) in the box, a 40mm hole was cut in the left wall. This hole had to be sealed to fulfil the safety requirements.

Figure 3.32: Removable sealed cable conduct. It was made from a bathtub plug which was sealed by silicone after the cables were put through.

Additionally the hardware had to be removable since it is mainly used in the laboratory without the lab box. For that reason all cables were conducted through an ordinary 40mm bathtub plug which was sealed with silicone afterwards.

## 3.2 Sensory data

During the 50th ESA PFC (May2009), an automated data logger (Xplorer GLX, Pasco scientific) with different sensory modules and a separate automated voltage quality recorder (VR1710, Fluke) have been integrated into the setup to further improve the design and the procedures of the experiment.

### 3.2.1 Temperature

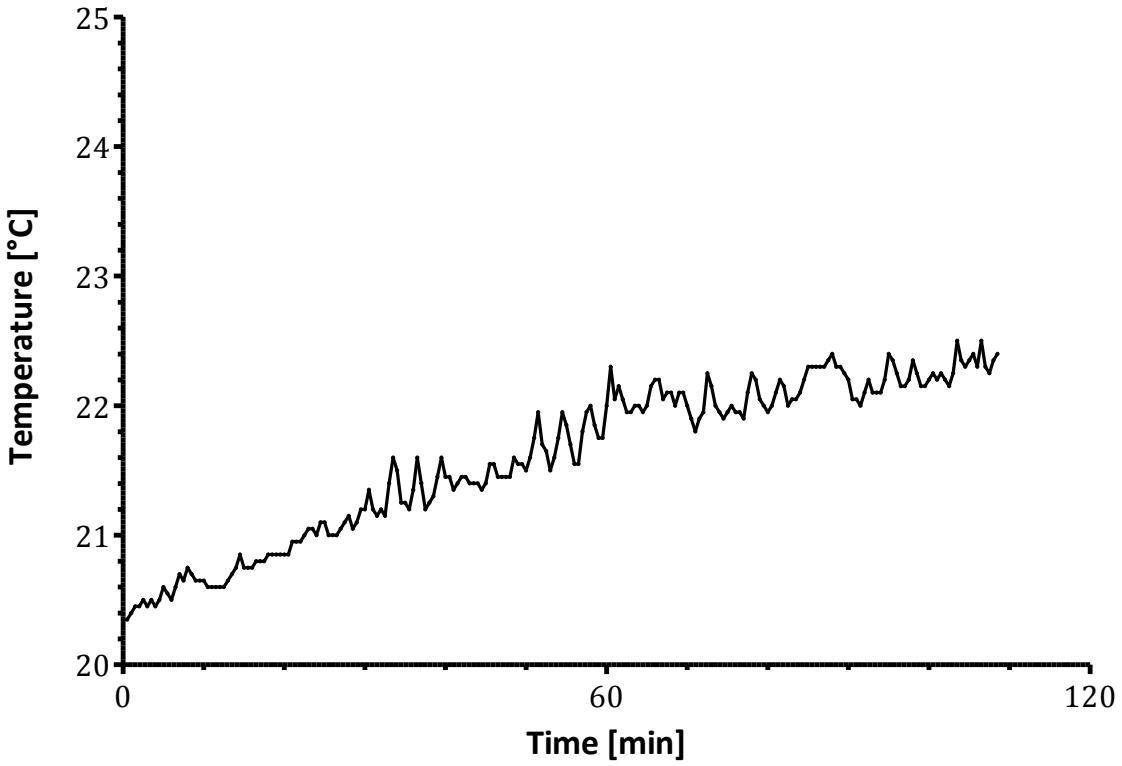


Figure 3.33: The averaged temperature profile of in the A300 Zero G during flight (n=2).

The temperature in the A300 was rising constantly during the flight. The profile in figure 3.33 was recorded during a campaign in May 2009. The starting temperature in the aircraft depended on the season. During the 11th DLR campaign in November 2007, the ambient temperature in the aircraft at $7^{45}$ a.m., 75 minutes before the closing of the aircraft door, was 10.4°C.

### 3.2.2 Pressure

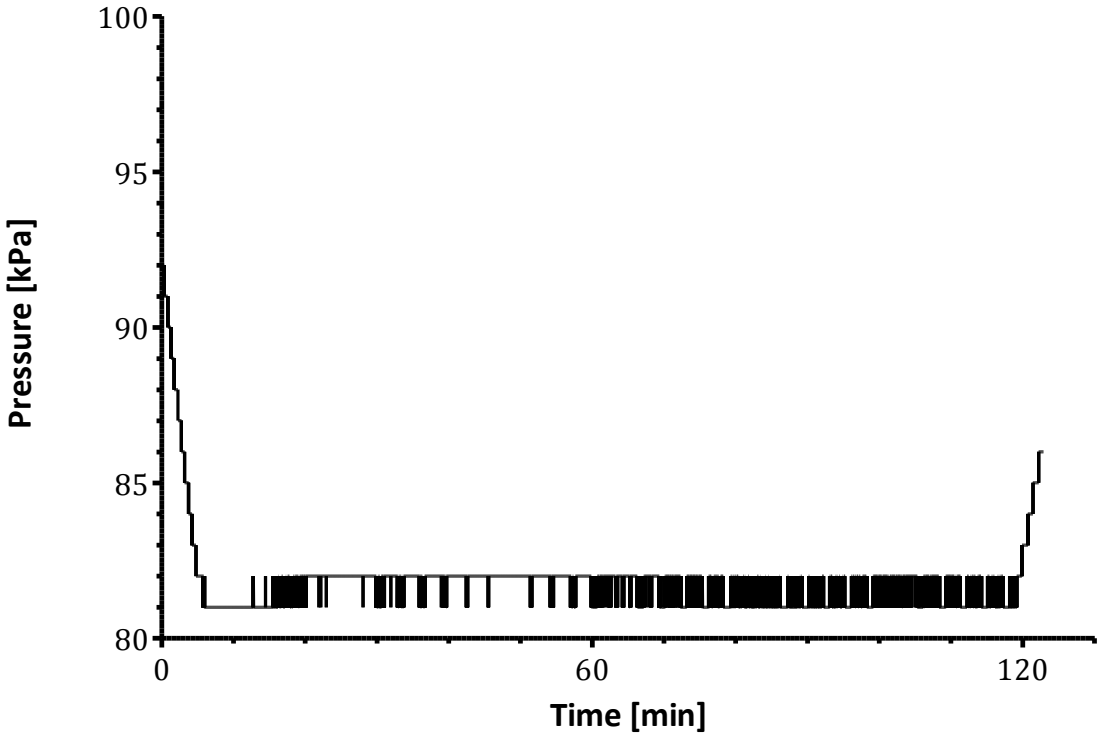


Figure 3.34: Pressure profile in the A300 Zero-G during the flight.

The pressure on ground was 101kPa. During flight the cabin pressure was reduced to 82kPa. According to the pilots this is done to reduce the load on the aircraft during the parabolic flight manoeuvre.

### 3.2.3 Acceleration

The acceleration was recorded in 3 axes (x, y, z) to estimate the quality of the microgravity phases and to monitor unwanted forces.

In fig. 3.35 a recording of 10 parabolas from the second flight day is shown. The dotted line indicates a single microgravity phase in all 3 axes. The lateral acceleration (y-axis) was rather constant except for fast spikes. The acceleration critically depended on the piloting skills and the (often unpredictable) weather conditions. During the first flight day, with a declining storm in the area, intensified lateral forces occurred and could not be compensated by the pilots.

In the z-axis, the hypergravity phases prior to microgravity (nose-up) had a different acceleration profile compared to the hypergravity phase after microgravity (nose-down). Since this could have some relevance for the patch clamp results this finding will be revisited in the patch clamp results and the discussion.

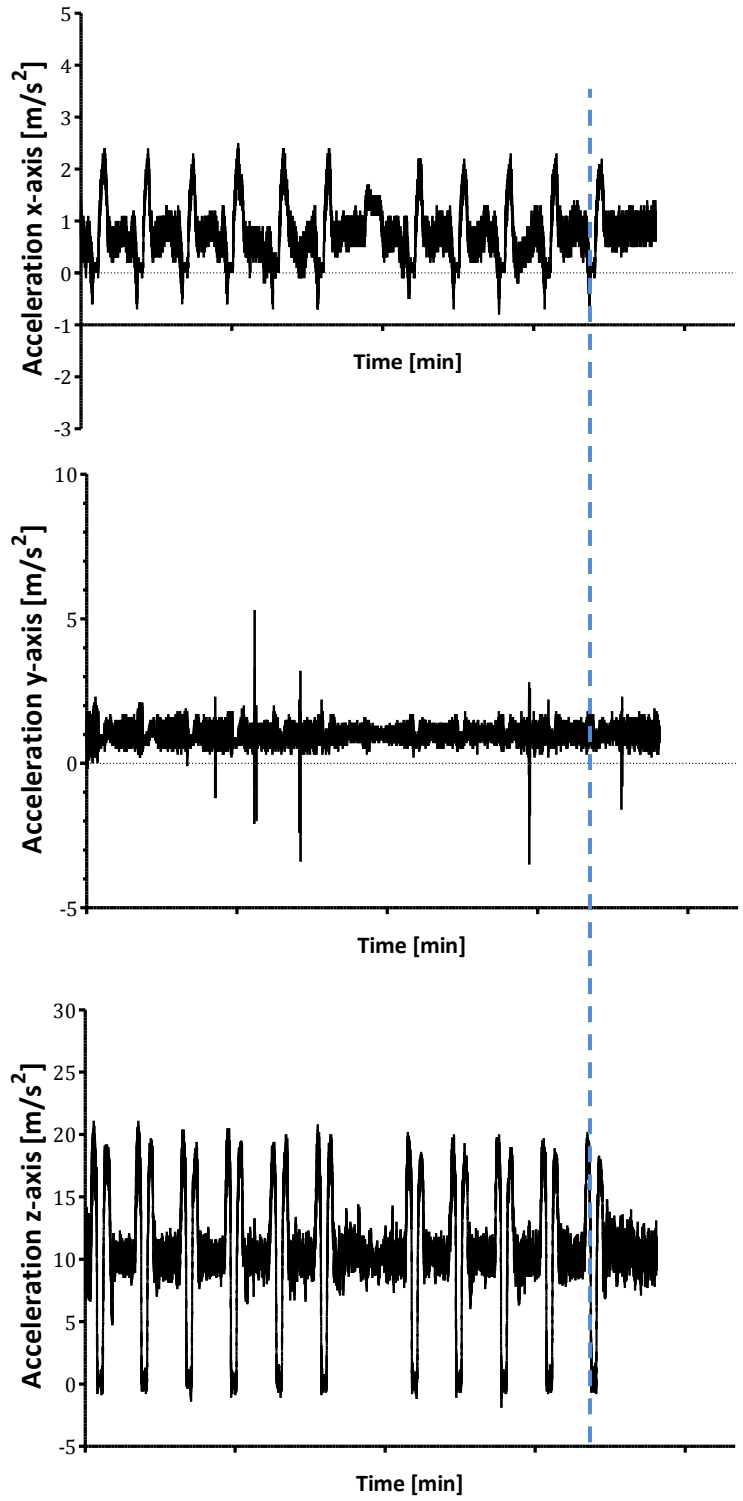


Figure 3.35: Acceleration profile of 10 parabolas (Flight day 2; 13th May 2009). The blue line indicates a single microgravity-phase

### 3.2.4 Magnetic field

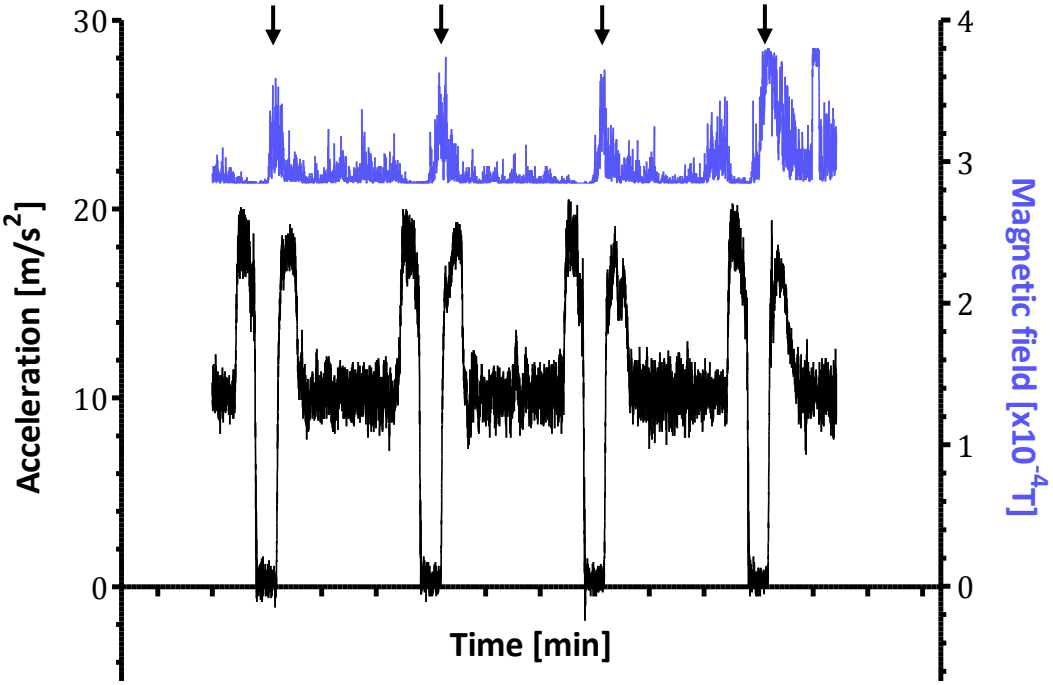


Figure 3.36: The changes in the magnetic field in relation to the g-level in the A300 Zero-G during flight. The arrows indicate the change in the magnetic field which can be assigned to the parabolic flight manoeuvre.

The changes in the magnetic field have been recorded in the z-axis of the aircraft. The data was set in relation with the acceleration data in the z-axis. As indicated in fig. 3.36, the changes in the magnetic field can clearly be assigned to the parabolic flight manoeuvre.

In Europe, the magnitude of Earth's magnetic field is approximately 48µT. The average change during parabolic flight is between 20µT and 50µT. These findings correlate with findings from Prof Dr. W. Schmidt (Univ. Marburg, Germany) which created a flight profile of the A300 Zero-G from GPS-data, magnetic field and acceleration data (personal communication, presented at the Erlanger Gravimeeting 2008). The aircraft moves through Earth's magnetic field and depending on the angle in which it passes through Earth's magnetic field lines, the change in the magnetic field can be measured during the flight. The greatest effect can be observed when the aircraft moves orthogonally through the magnetic field (the angle of Earth's magnetic field lines can be determined for any position). This is indicated in fig. 3.36, the biggest change can be seen in the nose-down phase of the parabolic flight manoeuvre (indicated by arrows). The smaller fluctuation during 1g could come from running experiments in the aircraft.

### 3.2.5 Power supply

Electrophysiological experiments are very sensitive to electromagnetic interferences. Electromagnetic interferences also can have various effects on the hardware, such as damage to components (by heating or power surges) which could lead to a termination of the flight for safety reasons, or communication errors which could eventually result in non-replicable reactions (e.g. unwanted system shutdowns) or even wrong data. Interferences can come from the power source itself (e.g. generators), or more common, from the used hardware components of the individual experiments. A voltage quality recorder (VR1710, Fluke) was connected to the power supply of the A300 at different points in time and several parameters were monitored: Voltage fluctuations (surges and drops) in L1 (phase 1) and N (neutral lead), frequency and transients.

There were 3 different power supplies for the experiments, depending on the position of the aircraft: the public power grid on ground, an external diesel aggregate on ground and the engines during flight.

#### 3.2.5.1 Public power grid

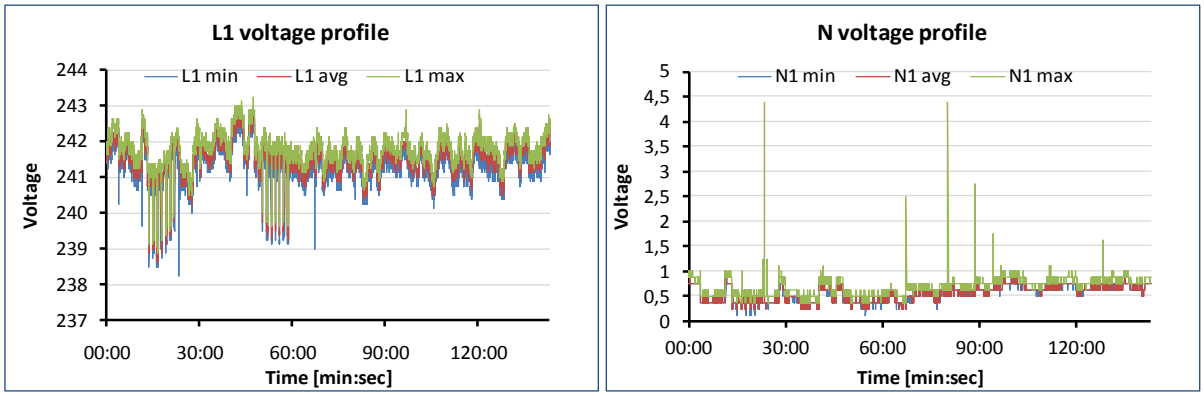


Figure 3.37: A recorded voltage profile of the L1 and N phase in the A300 on ground with running experiments

The voltage ranged between 238.8V and 243V. The minimum and maximum voltage traces are shown to visualize the occurred voltage peaks and drops. There are several peaks above 4V in the neutral conductor. The bar graph shows the distribution of the voltage ($V_{min}$: 0.13; $V_{max}$: 4.38)

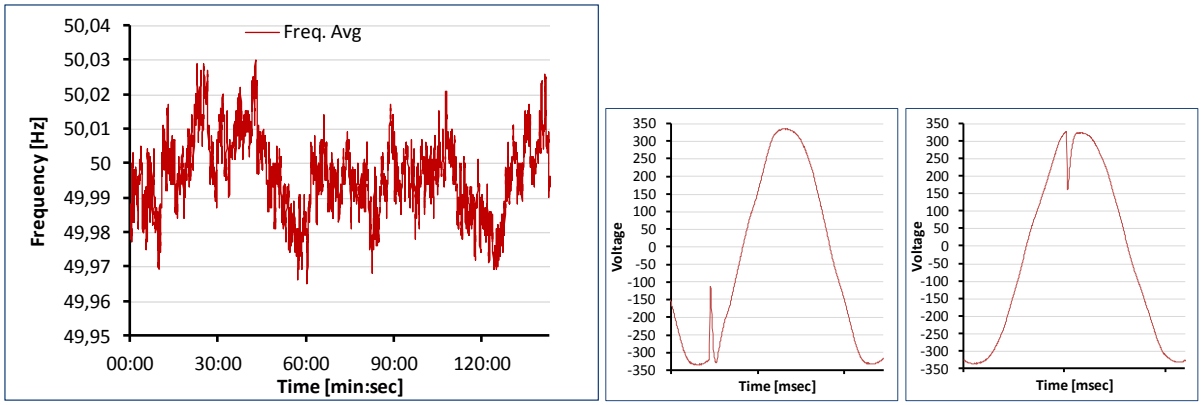


Figure 3.38: Frequency profile and occurred transients with experiments switched on.

With connection to the public power grid, the least transients occurred, but in return the biggest and the shape of the 50Hz sine was not symmetrical. In fig 3.38 two burst transients are shown (here oscillation of voltage) in a 50Hz period.

### 3.2.5.2 Diesel PSU

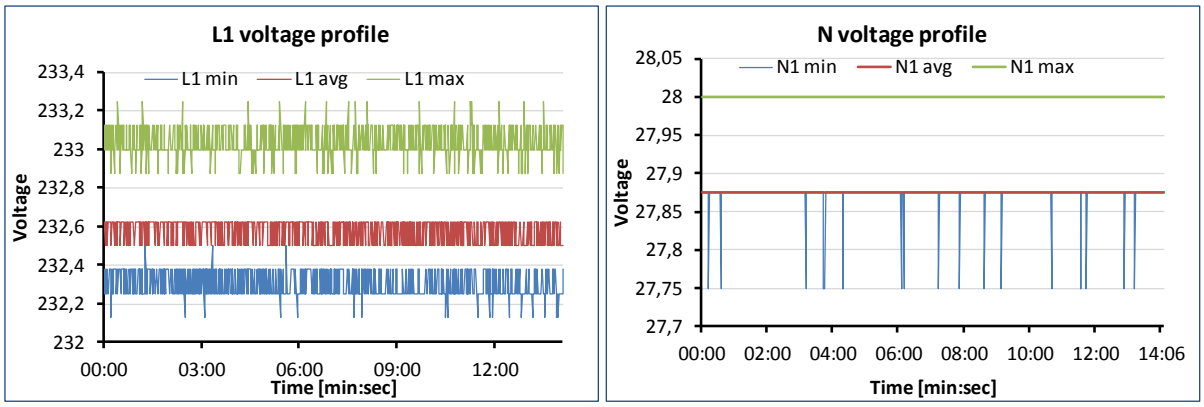


Figure 3.39: The voltage profile of the diesel power generator on ground with no running experiment.

Due to the high amount of events, the memory of the voltage recorder was full after 15 minutes. The voltage fluctuations on L1 are minimal ($V_{min}$: 232.13; $V_{max}$: 233.25). A constant voltage lied on the neutral conductor with nearly no deviation ($V_{min}$: 27.75; $V_{max}$: 28) during the period of measurement.

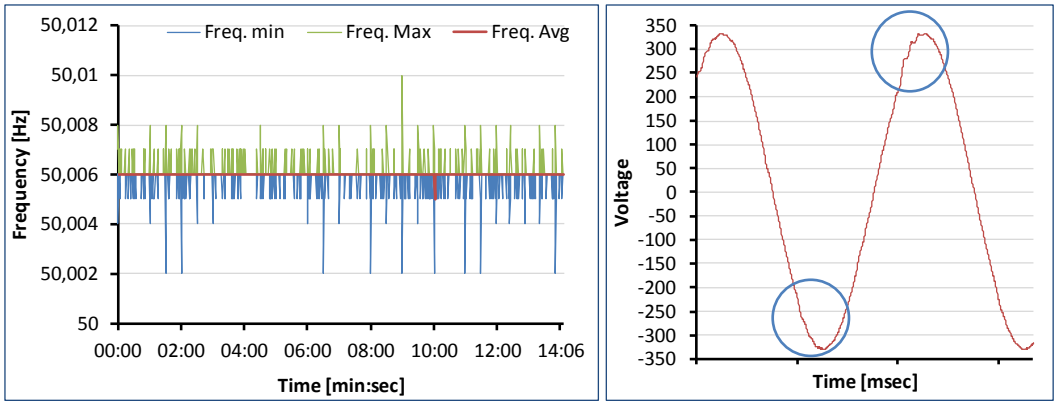


Figure 3.40: The frequency profile of the diesel PSU without experiments

The frequency variations were minimal. Regular impulse packet transients during the complete recording (blue circles in fig 3.40; here oscillation of voltage) in the 50Hz period could be observed. The flanks of the sine were symmetrical.

### 3.2.5.3 A300 PSU during flight

For the power supply during flight, recordings were made with and without running experiments to see the possible influence of the experiments to the power supply.

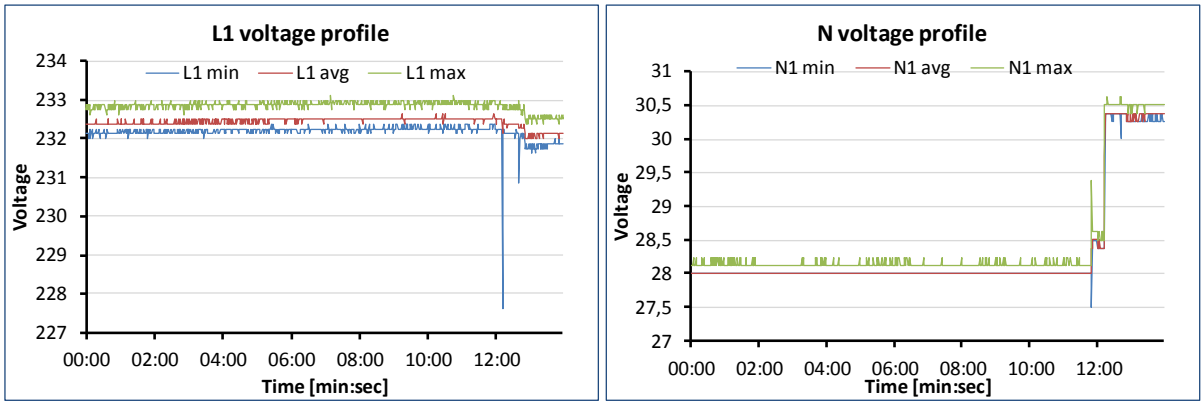


Figure 3.41: The voltage profile in the A300 during flight without running experiments

The short voltage drop after 12 minutes could be a switching artefact where the experiments were powered on. Due to the limited memory of the voltage recorder and the amount of events, only 15 minutes could be recorded ($V_{min}$: 227.63; $V_{max}$: 233.13).

For the first 12 minutes constant ~28V lied on the neutral conductor, afterwards the voltage raised above 30V ($V_{min}$: 27.5; $V_{max}$: 30.63). This could also be an indication of the power-up of the experiments.

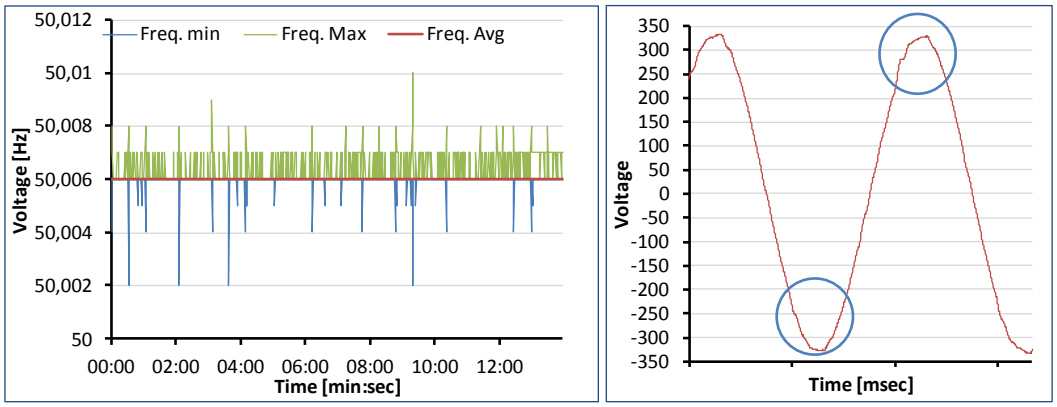


Figure 3.42: The frequency profile during flight without experiments

The frequency variations were minimal. Regular impulse packet transients during the complete recording (blue circles in fig 3.42; here oscillation of voltage) in the 50Hz period were observed. The flanks of the sine were symmetrical.

After storage of the acquired data, the recording was continued.

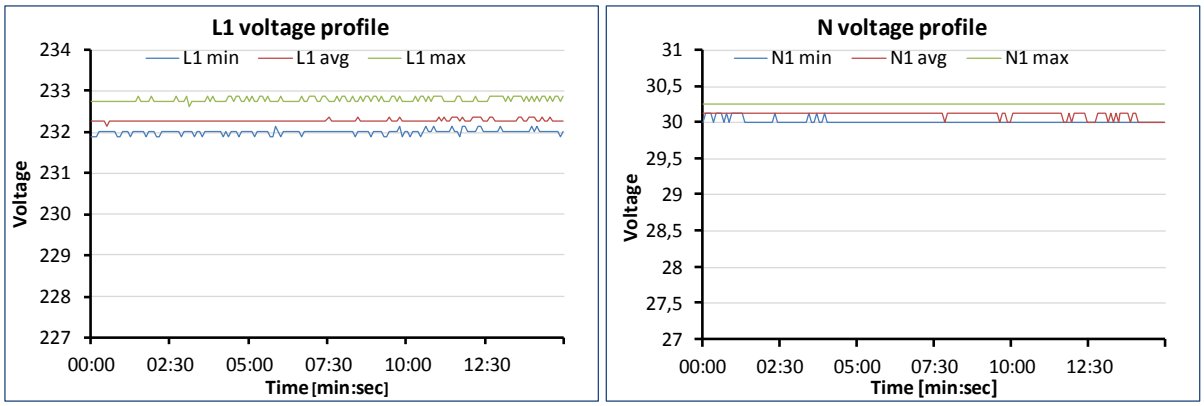


Figure 3.43: The voltage profile of the A300 during flight with running experiments

The mean voltage on L1 was very constant ($V_{min}$: 231.88; $V_{max}$: 232.88). The voltage on the neutral conductor was also very constant ($V_{min}$: 30.0; $V_{max}$: 30.25) with minimal fluctuations.

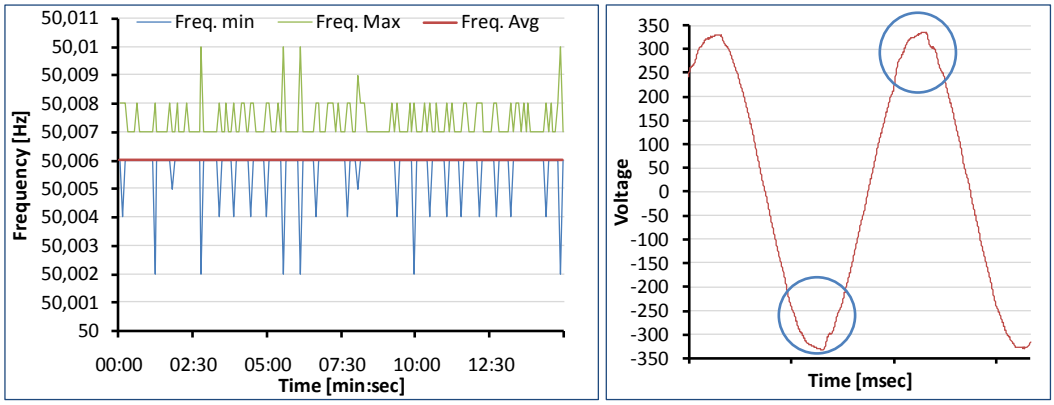


Figure 3.44: The frequency profile during flight with running experiments

The deviation from 50Hz seemed to increase with running experiments, but it was minimal. Regular impulse packet transients during the complete recording (blue circles in fig 3.44; here oscillation of voltage) in the 50Hz period were observed. The flanks of the sine were symmetrical.

### 3.2.5.4 Harmonics

Last monitored parameters were the occurred harmonics for the different power supplies. Harmonics are voltages and currents that appear on the electrical power system as a result of different electric loads (e.g. fluorescent lamps or nonlinear consumers like single-phase power adaptors in screens and computers). Harmonic frequencies are frequent cause of power quality problems. They are (integer) variations of the sinus wave. Especially the orders $N^o$ which are divisible by 3 (3, 9, 12, etc…) have to be considered because these transients are added to the neutral conductor. If the voltage (and current) is bigger than in the L conductor potentially dangerous effects may occur, such as:

- fire hazard by thermal overload of the neutral conductor with un-triggered protection devices since the release currents in the L conductors are not exceeded
- transmission errors within the experiment (control of the experiment and data acquisition)
- malfunctions or damage to components

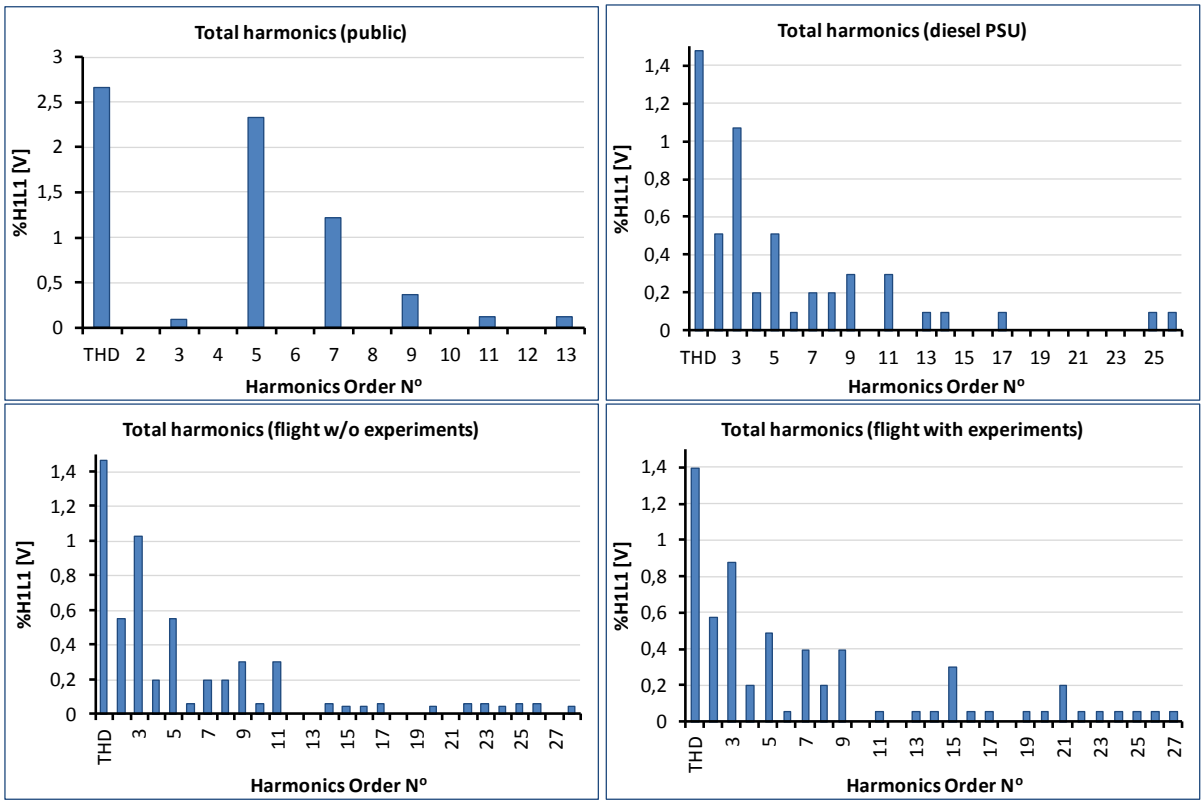


Figure 3.45: Distribution and magnitude of the total harmonics (THD= total harmonics distortion)

For the 2 flight recordings, the ration of detected transients per measuring point was determined to see if the experiments have an influence on the power supply. Figure 3.46 indicates that after power-up of the experiments during the flight, the number of harmonics was increased compared to the flight without running experiments.

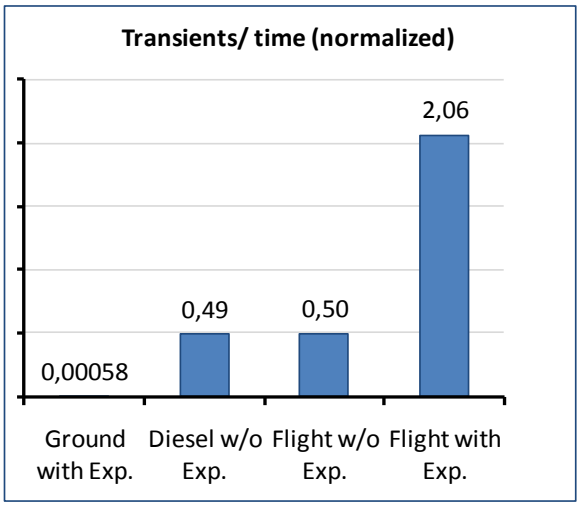


Figure 3.46: Number of transients/time for the different PSU

#### 3.2.5.5 Regulations

The regulations on the quality of power supplies are complicated. For the public power grid it is regulated in IEC 60038 (voltage) and EN 50160 (frequency). For electric and electronic devices EN 61000-3-2 (harmonics) is valid since 2001 where devices are categorized in different groups. Since no regulation of aviation technology could be obtained, no statement is made concerning the quality.

To reduce the possible influence on the experiment, the UPS was integrated in the experiment to provide stable 230V with 50Hz.

## 3.3 Patch clamp experiments under different gravity conditions

Figure 3.47: Preparation of a patch clamp experiment in the A300 Zero-G (© ESA, Anneke Le Floc'h, 2009)

All patch clamp experiments were performed in the whole cell configuration. NPC-1 chips with a resistance of 2-6MΩ were used. The pulse protocols were performed during all gravity phases ($1g_{before}$, $1.8g_{up}$, 0g, $1.xg_{down}$, $1g_{after}$). Since the mean gravity value during the pull out was not very constant compared to the 1.8g pull-up, the data was not used.

### 3.3.1 Current-voltage characteristics of undifferentiated SH-SY5Y cells

To investigate the macroscopic currents of a single cell, voltage step protocols were used. The aim was to record changes in the currents during the different gravity phases.

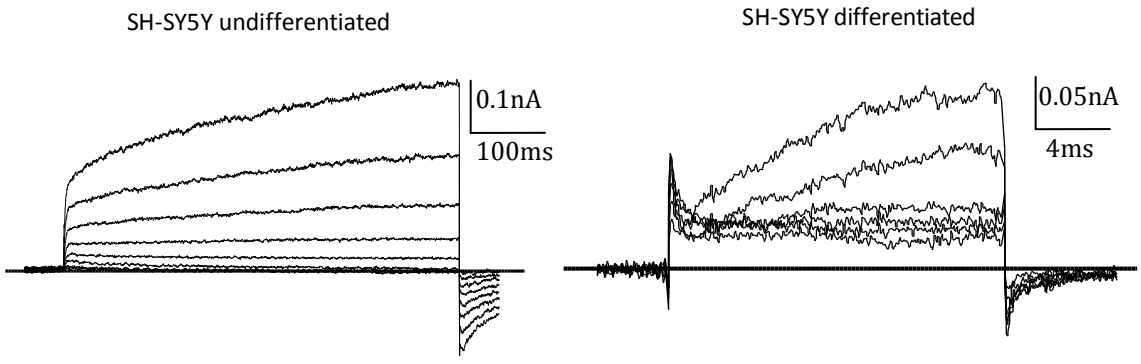


Figure 3.48: Electrical activity of (left) undifferentiated and (right) differentiated SH-SY5Y cells under voltage clamp conditions. Both traces were recorded during a parabolic flight campaign. Unfortunately, no complete set of gravity phases could be recorded with differentiated cells.

Only complete triplets of consecutive recordings (1g, 1.8g, 0g) were used to maintain constant recording properties. All incomplete recordings or recordings where the electrophysiological properties ($R_{seal}$, $R_{series}$, $C_{fast}$, $C_{slow}$) obviously did change were discarded. Unfortunately no complete set of recordings could be recorded with differentiated SH-SY5Y. For measurements of I-V curves of undifferentiated SH-SY5Y cells, potentials of -40 to +30mV were applied in 10mV steps for 500ms with a sweep interval of 2s from a holding potential of -80mV. The resulting currents were measured.

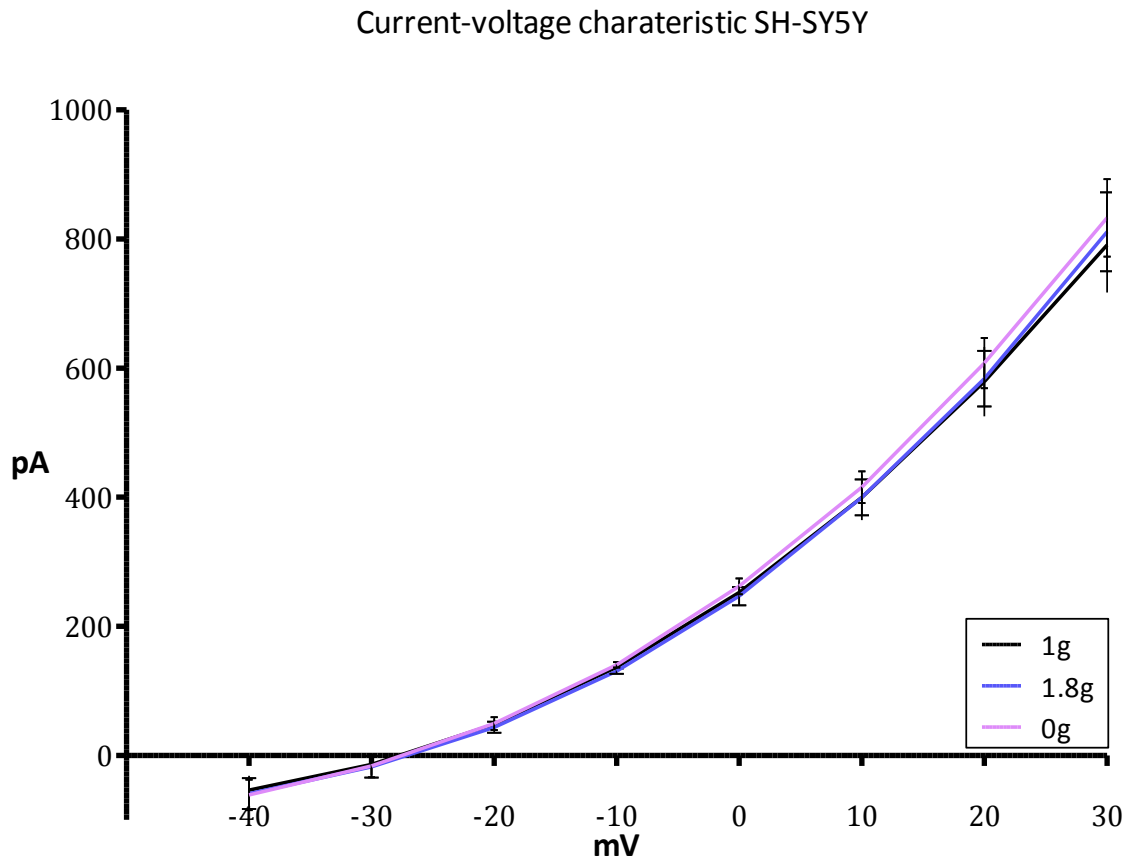


Figure 3.49: The I-V curve of SH-SY5Y cells. Mean ± SEM n = 1 (8 recordings). An increasing deviation from 1g was observed for positive potential.

Compared to the 1g in-flight control, between 0 and +30mV, an increasing rise in the microgravity current was visible. At 0mV, the hypergravity current was decreased and was continuously was increasing between +10 and +30mV.

The I-V curve of SH-SY5Y cells were normalized against the in-flight 1g values to analyze the influence of gravity on the whole cell currents.

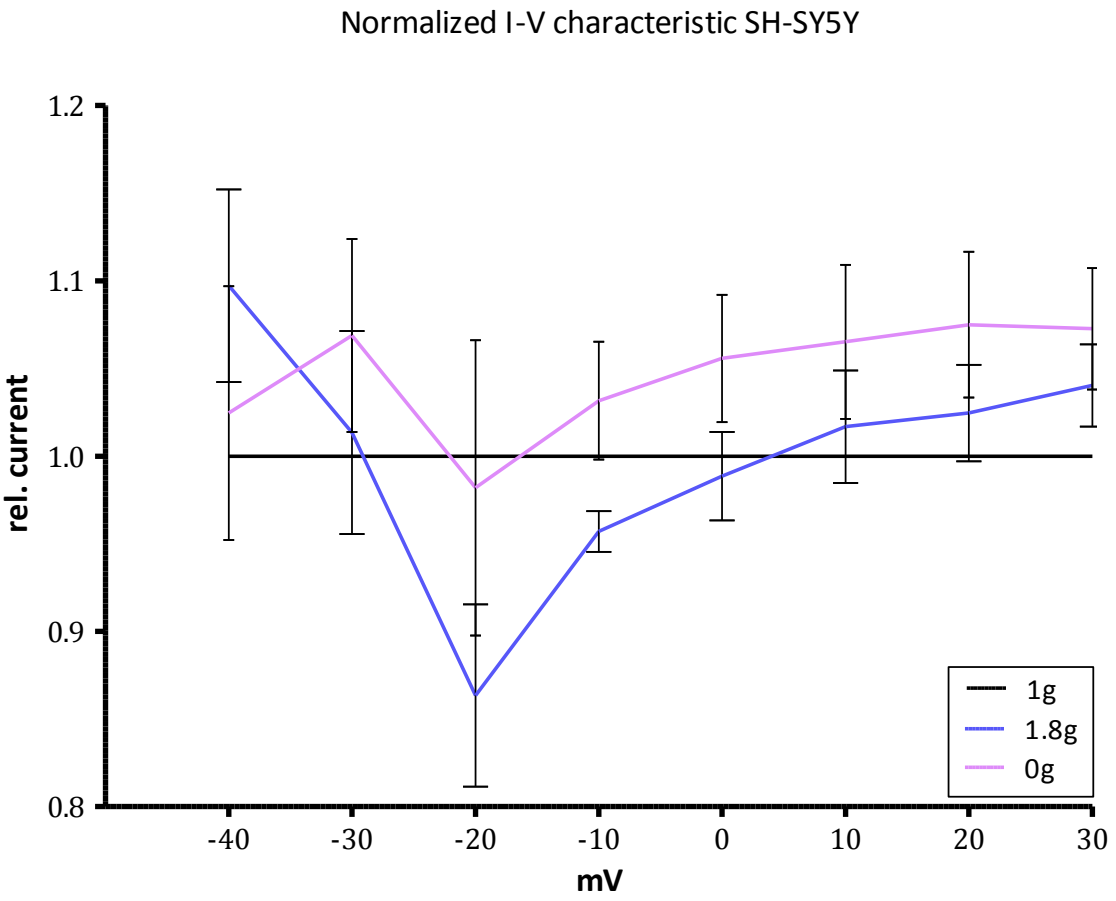


Figure 3.50: Gravity-dependence of the whole cell currents of SH-SY5Y. The currents were normalized against the values from 1g in-flight control. Means ± SEM, n=1 (8 recordings).

In the normalized I-V curve of SH-SY5Y cells, the deviation from the 1g in-flight control was clearly visible: The microgravity current was increased for the complete range of potential, except for -20mV where it was decreased. The hypergravity current had a different pattern. At -40 and -30mV, the 1.8g current was increased, between -20 and 0mV it decreased with a maximum decrease at -20mV. Between +10 and +30mV the hypergravity whole cell current was again increased compared to 1g.

The currents were broken down into the separate voltage steps for a detailed analysis. In the following, the significant deviations are shown. The remaining figures are shown in the appendices.

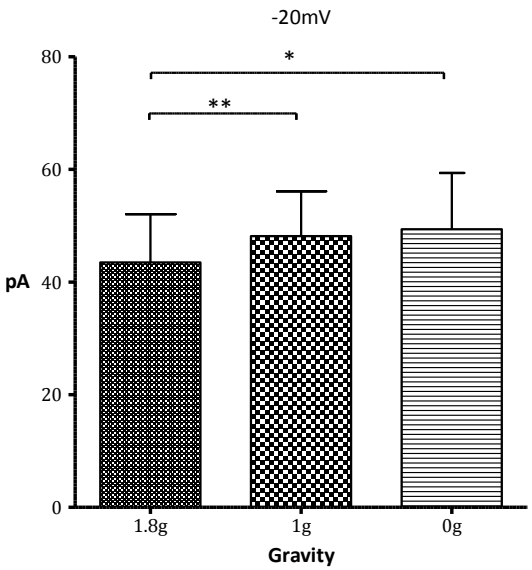


Figure 3.52: Changes in the recorded currents of SH-SY5Y at -20mV. Mean ± SEM, *p= 0.0361, **p = 0.0086, paired t-test. During hypergravity, the mean 1.8g-current was decreased to 90.4% compared to 1g. The 0g-current was increased by 13.5% compared to 1.8g.

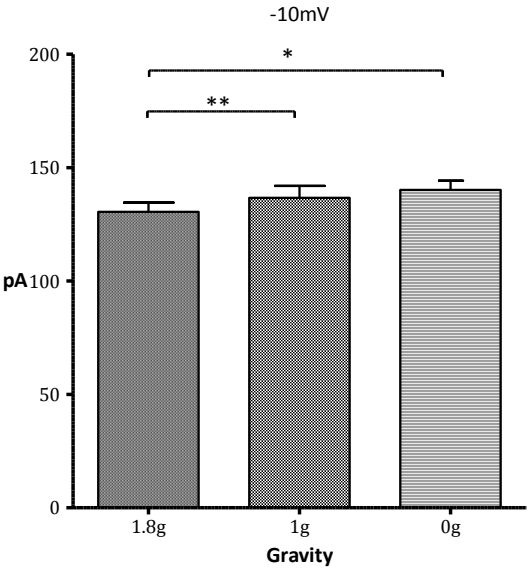


Figure 3.51: Changes in the recorded currents of SH-SY5Y at -10mV. Mean ± SEM, *p = 0.0436, **p = 0.0056, paired t-test. During hypergravity, the mean 1.8g-current was decreased to 95.5% compared to 1g. The 0g-current was increased by 7.4% compared to 1.8g.

At -20 and -10mV, the 1.8g-current was significantly decreased compared to the 1g control. Simultaneously, the microgravity-currents were significantly increased compared to hypergravity.

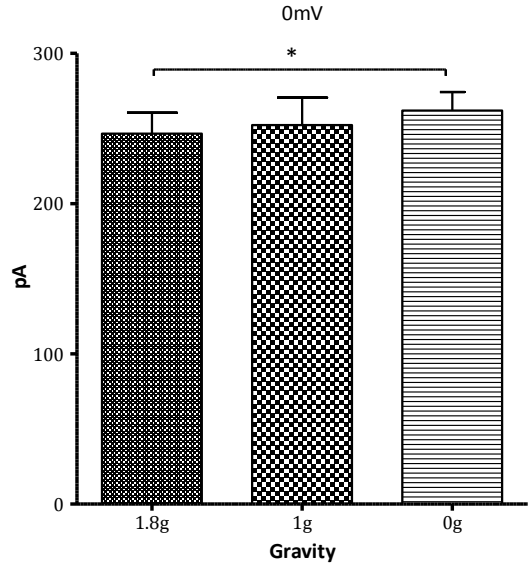


Figure 3.53: Changes in the recorded currents of SH-SY5Y at 0mV. Mean ± SEM, *p = 0.0114, paired t-test. The 0g-mean current was increased by 6.2% compared to 1.8g.

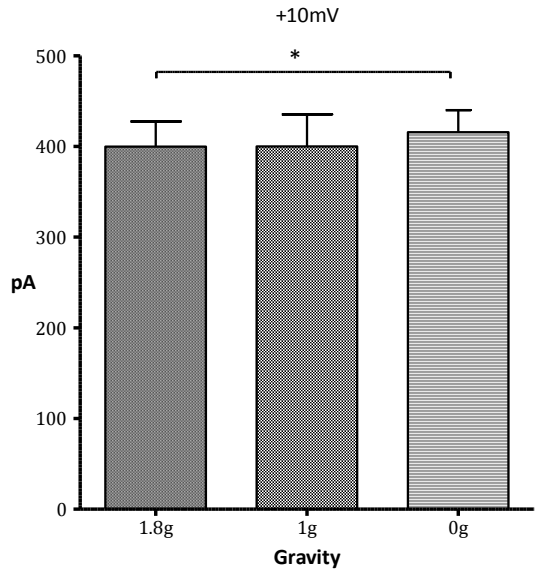


Figure 3.54: Changes in the recorded currents of SH-SY5Y at +10mV. Mean ± SEM, *p = 0.0335, paired t-test. The mean 0g-current was increased to 3.9% compared to 1.8g.

At 0mV and +10mV, the significant increase in the microgravity-current compared to hypergravity could be observed, but the decreased hypergravity current (compared to 1g) was no longer significant.

The significant changes in the whole cell current of SH-SY-5Y are summarized in the following tables.

| | **-20mV** | **-10mV** |
|---|---|---|
| **1.8g** | -9.6% | -4.5% |

Table 3.11: The mean change in the whole cell currents of SH-SY5Y cells compared to 1g during increasing pulse protocols.

| | **-20mV** | **-10mV** | **0mV** | **+10mV** |
|---|---|---|---|---|
| **0g** | +13.5% | +7.4% | +6.2% | +3.9% |

Table 3.12: The mean increase in the 0g whole cell currents of SH-SY5Y cells compared to 1.8g during increasing protocols.

### 3.3.2 Current-voltage characteristics of SNB19 cells

As for the SH-SY5Y cells, the I-V curves of SNB19 cells were normalized against the in-flight 1g values to analyze the influence of gravity on the whole cell currents. As the main focus during the 50th ESA PFC lied on constant pulse protocols, only one I-V protocol was performed, therefore no statistical analysis could be done (n = 1, 1 recording). To measure the I-V curve, potentials between -80 and +60mV were applied in 20mV steps for 500ms with a sweep interval of 2s from a holding potential of -80mV. The resulting currents were measured.

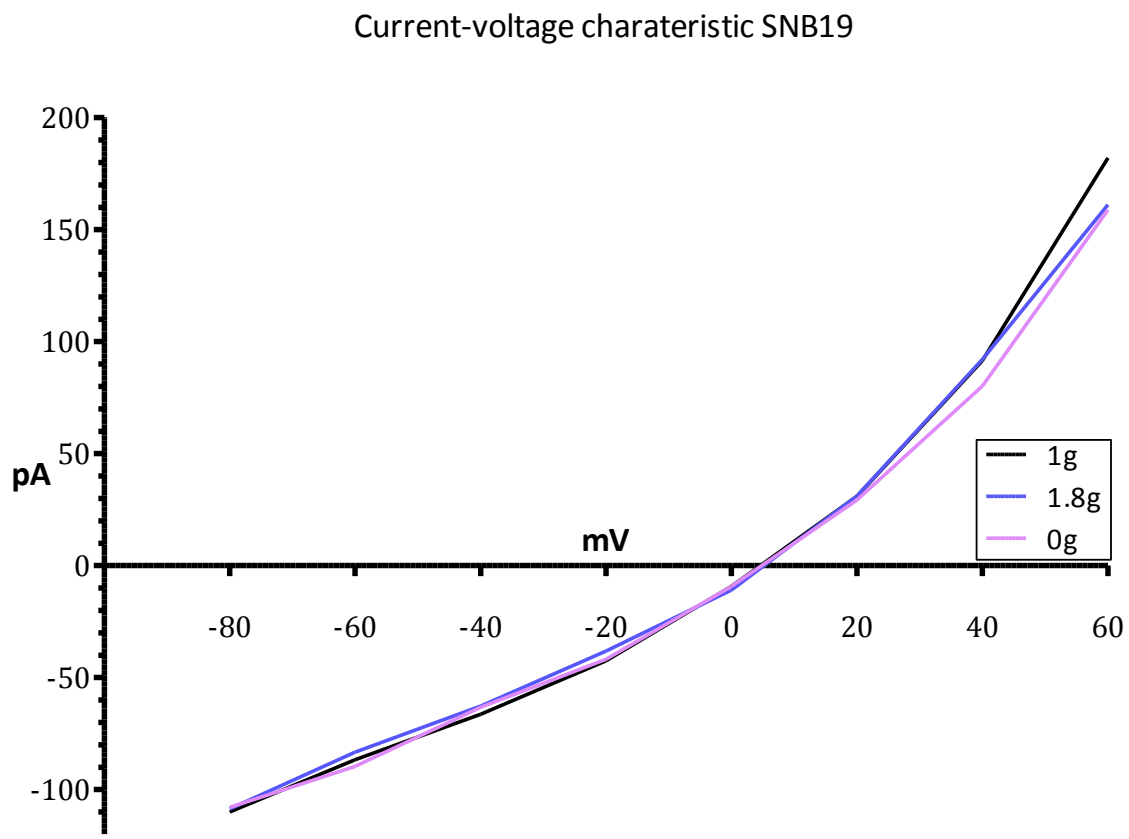


Figure 3.55: The I-V curve of a SNB19 cell. Mean current, n = 1 (1 recording). An increasing reduction of the Δg-currents from 1g can be observed for positive potentials.

At positive potentials, the Δg whole cell currents seemed to be decreased compared to the 1g control.

For a better visualization the I-V curves of the SNB19 cell were normalized against the in-flight 1g values to analyze the influence of gravity on the whole cell currents.

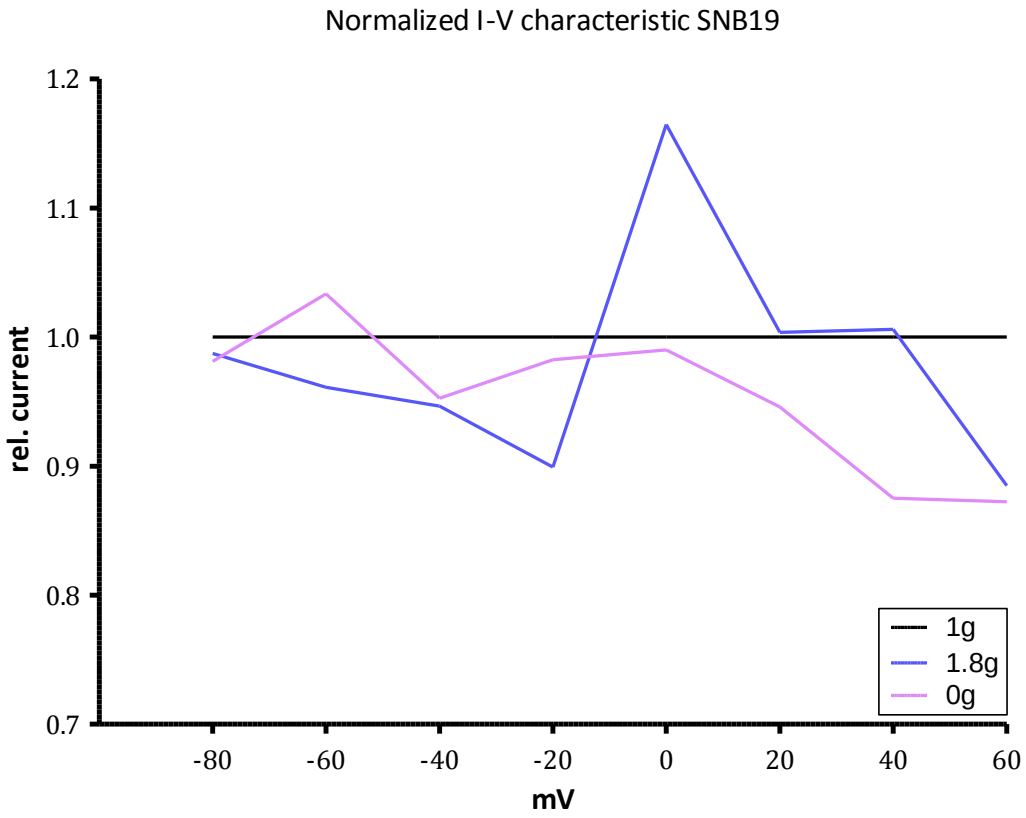


Figure 3.56: Gravity-dependence of the whole cell current of a SNB19 cell. The currents are normalized against the values from 1g in-flight control. Normalized mean current, n=1 (1 recording).

At negative potentials, between -80 and -20mV, the whole cell currents of the Δg whole cell currents were decreased compared to the 1g control, except for an increased microgravity current at -30mV. At more positive potentials, between -20 and +40mV, the hypergravity current increased to values greater than the 1g controls, whereas the microgravity current stayed decreased. At +60mV, the Δg currents were smaller than the 1g control.

At negative potentials, the microgravity current was increased compared to the hypergravity current, which inverted at -10mV. For more positive potentials the hypergravity current was increased compared to the microgravity current.

No statistical analysis could be performed due to the small amount of data therefore the figures of detailed voltage step analysis are shown in the appendices.

### 3.3.3 Constant voltage clamp protocols of SNB19 cells

To investigate whether the electrical properties of the cell membrane changed under different gravity conditions, constant potentials were applied and the resulting currents were recorded during the parabola. Constant potential protocols were performed at -80, -60 and -40mV. The duration of a pulse protocol was 100s (100 sweeps with 1s). It was started 20 seconds before each parabola (announced by the cockpit crew) to include all phases of the parabola (averaged to 20s per gravity phase).

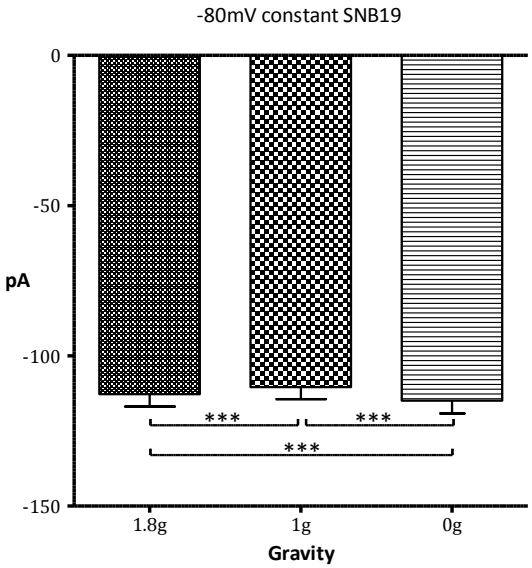


Figure 3.57: Changes in the recorded currents of SNB19 at -80mV. Mean ± SEM, n = 9 (280 recordings), ***p< 0.0001, paired-test. The currents during hyper- and microgravity both were significantly increased. During hypergravity the increase was 2.2%, during microgravity 4.1%.

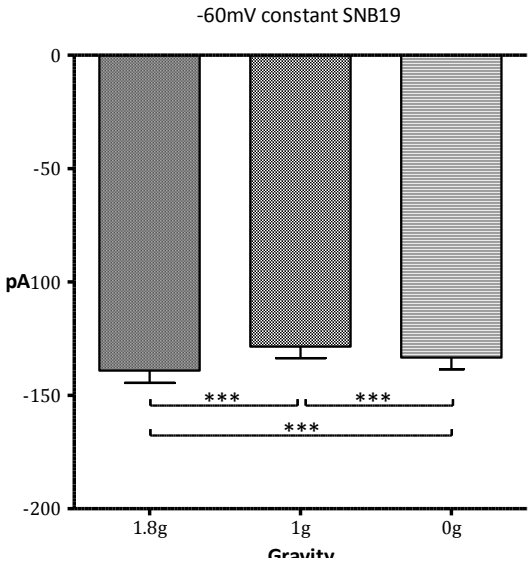


Figure 3.58: Changes in the recorded currents of SNB19 at -60mV. Mean ± SEM, n = 9 (280 recordings), ***p< 0.0005, paired t-test. The currents during hyper- and microgravity both were significantly increased. During hypergravity the increase was 8.2%, during microgravity 3.7%.

For -60 and -80mV, the mean hyper- and microgravity-currents were significantly increased compared to 1g control (the exact values are listed in table 3.13 and 3.14). Furthermore the Δg currents significantly differed from each other. At -60mV the microgravity current was reduced by 4.1% compared to 1.8g. At -80mV, the microgravity current was increased by 1.9% compared to 1.8g.

The significant changes in the whole cell currents of SNB19 at -80 and -60mV are summarized in the following table.

| | **-80mV** | **-60mV** |
|---|---|---|
| **1.8g** | +2.2% | +8.2% |
| **0g** | +4.1% | +3.7% |

Table 3.13: The mean increase in the SNB19 whole cell currents compared to 1g (constant protocols)

| | **-80mV** | **-60mV** |
|---|---|---|
| **0g** | +1.8% | -4.1% |

Table 3.14: The mean deviance of the 0g SNB19 whole cell currents compared to the 1.8g currents (constant protocols).

For -40mV, no significant deviation from 1g could be observed. The figure is shown in the appendix.

# 4 Discussion and outlook

As the interest in manned space flights is increasing, the need of understanding how organisms react and adapt to microgravity becomes more important. Numerous experiments have been performed to investigate how the human body works in microgravity and hypergravity. Especially the central nervous system (CNS) is from utmost importance as the performance of the nervous system has influence on the whole body. Most of the experiments describe cause and consequence, e.g. how muscle tension or the brain activity is changed under microgravity, but the basic principle is still unknown.

All neuronal processes rely on the smallest components of the nervous system, single neuronal cells and its components. The electrical properties of cells are defined by the cell membrane, incorporated ion channels and ionic gradients. The patch clamp technique is a common used tool in investigating these electrical properties. The constructed microgravity patch-clamp hardware and the performed patch clamp experiments shall contribute to the exploration of the basic principle how a single neuronal cell detects gravity up to the aim of how single ion channels are affected by gravity differing from 1g.

Parabolic flights are, up to now, the only possibility to perform patch clamp experiments since it needs experienced operators. But the conditions during a parabolic flight (vibration, time limit) render classic patch clamp nearly impossible. In the past, an attempt to use a classic patch clamp setup in a parabolic flight campaign was discontinued due to the low data yield (Meissner 2004).

The present work showed that the planar patch clamp technique can be used to perform electrophysiological experiments during parabolic flights, the only (by non-astronauts) manned microgravity research platform.

Nevertheless, there were (and still are) limitations which had to be manhandled. The first flight in 2007 (11$^{th}$ DLR PFC) was used to test the first prototype of the complete hardware and it was mainly used to test the planar technique and to accommodate the science team with the procedures of a parabolic flight campaign and, of course, the familiarization with hyper- and microgravity. The focus during the second campaign (2008, 12$^{th}$ DLR PFC) lied on choosing a suitable candidate for microgravity research from the available cell lines in the institute which met the following requirements:

- They must be from human origin, preferably of neuronal origin, to avoid the need for an animal model.
- They must have at least one native family of ion channel which is involved in the generation of action potentials; $Na^+$- or $K^+$- channels. The use of genetic modified organisms (GMO) was not allowed until 2009.
- They must be rather robust since the (biological) working conditions at the Novespace facilities, especially for cell culture, were inadequate at that time.

Three cell lines were in the shortlist, a primary human skeletal muscle cell, a primary human cardiac muscle cell (both provided by Provitro, Berlin) and SH-SY5Y, origination from a human glioblastoma. All cells were tested and the primary cells were dropped since they could not be cultivated properly under the given conditions. Until end of 2008, two small kitchen rooms in the building had to be used as a laboratory. These rooms were shared by all science teams which needed a "lab", therefore space was very limited. The biggest challenge was that a $CO_2$-incubator was not allowed due to safety reasons. HEPES buffered medium was used to maintain a stable pH for the cells. In the lab, this medium is used to the cells for 8 to 12 hours during experiments where it is not possible to maintain a $CO_2$-enriched atmosphere. Even with regular medium exchanges, the long-term use of this medium had a negative impact on the vitality of the cells and reduced the seal probability and stability during the flights, reducing the amount of usable data. To monitor the quality of the seal, standard electrophysiological properties were monitored during the recording ($R_{seal}$, $R_{series}$, $C_{fast}$, $C_{slow}$). If the properties were changed significantly at the end of a parabola, the complete recording was excluded from analysis.

Unfortunately the opening of the laboratory box was restricted by the safety authorities to the breaks after a set of 5 parabolas. This reduced the possible amount of data. When a seal broke during the first parabola of a set, the next 4 parabolas were lost, too. Since the 50$^{th}$ ESA PFC in 2009, the box could be opened between the parabolas under 2 conditions:

- The first 15 parabolas could not be used for good recordings
- Novespace personnel must be present and orders to close the box must be followed with no hesitation.

Since 2009, the lab conditions improved strongly as 2 biosafety level 1 (BSL-1) laboratories were opened at Novespace. Since 2010, a $CO_2$ incubator is allowed for the project and a

small sterile workbench is permanently installed at Novespace (provided by the Dept. of Membrane Physiology, Univ. Hohenheim). For experiments which rely on a healthy cell culture, as patch clamping, this is a big improvement. During a first campaign (52th ESA PFC, 2010) this was greatly appreciated. With a proper cell culture and a new cell line (SNB19), the probability of seal formation and the stability of the seal were greatly improved. The most stable seal was established 10 minutes before the first parabola and was used for nearly 15 parabolas (as the 10µl drop of the external recording solution was evaporated). Three SNB19 cells per flight were successfully used for 7 to 10 parabolas with a seal probability of 70-80%. The option of opening the box between parabolas was not utilized at all.

The performed patch clamp experiments onboard the A300 Zero-G showed that a single neuronal cell reacts to different gravity conditions. At constant potentials at -80 and -60mV, the whole cell currents of SNB19 cells were significantly increased during hyper and microgravity compared to 1g in-flight. Near the estimated resting potential, normally between -80 and -60mV it is assumed that voltage-activated sodium and potassium channels are not activated. As SNB19 cells originate from astrocytes (Gross et al 1988), $K_{(v)}$-channels must be present in these cells, $Na_{(v)}$-channels could also be present (Sontheimer et. Al 1993). The contrary finding from the I-V curve of SNB19 compared to the constant protocols can possibly be explained with the amount of used cells. For the constant protocols 9 cells were used, the pulse protocol was only performed once therefore this I-V curve might only be a snapshot.

The findings from the constant protocols at -80 and -60mV of SNB19 were also visually confirmed with the pulse protocols at -40mV for SH-SY5Y cells. Interestingly the increase of the 1.8g current of SH-SY5Y reversed to a significant decrease at potentials between -20 and -10mV. The normalized current-voltage curve of SNB19 showed a different behaviour, at negative potentials, the microgravity current was bigger than the hypergravity current, which inverted at -10mV. At more positive potentials, the hypergravity current was bigger than the microgravity current.

How can these obviously not corresponding findings be explained?

In experiments with alamethicin doped planar lipid bilayer experiments the gravity dependence of the activity of alamethicin pores was shown (Klinke et al. 2000). The activity

is reduced under hyper- and microgravity. A reduced activity of alamethicin pores implies reduced ionic currents through the membrane. Porins, outer membrane channels derived from E. coli, showed a different behaviour. The opening probability $P_o$ is reduced under microgravity and increased under hypergravity (Goldermann et al. 2001).

Since alamethicin pores as well as porins and ion channels possess different opening mechanisms, the reaction to different gravity conditions cannot be completely compared. Almethicin pores are formed by the aggregation of several alamethicin molecules where the number of molecules defines the size of the pore. Ion channels are complex molecules of constant aggregate size with different opening and closing mechanisms.

Based on the analyzed whole cell recordings, the findings from porins cannot be transferred easily to predict the behaviour of a single cell. The recorded whole cell currents were not only gravity-dependent, but simultaneously showed a voltage-dependence. Based on the porin experiments, a similar opposing reaction during micro- and hypergravity was reasonably expected for the whole cell currents as they are the sum of the cells single channel currents.

Between -40 and -30mV the whole cell currents of SH-SY5Y increased unidirectional during hyper- and microgravity. For potentials between -20 and 0mV the Δg whole cell currents seemed to decrease during hypergravity and increase during microgravity. Different from the findings between -40 and -30mV, the Δg currents between -30 and +30mV maintained a *1.8g-current < 0g-current* relation.

If we look at the ion channels, it is important that the used cell lines were not modified concerning their repertoire of ion channels. For SH-SY5Y, the sodium, potassium and calcium conductances are well described (Toselli et al. 1996 & Tosetti et al. 1998) in the undifferentiated and the differentiated state. It must be assumed that the activity of different families of ion channels could react differently to Δg-conditions, possibly even annulling each other. The acquired I-V characteristic resembled to the respective section of the outward $K^+$- current described for undifferentiated SH-SY5Y cells (Tosetti et al.1998).

For SNB19 cells, little is known about the channel repertoire. A detailed electrophysiological characterization must be performed if these cells are further used for microgravity research.

For the whole cell current of SH-SY5Y the changes under different gravity conditions can be separated into two groups:

- -80 to -40mV with an overall increase under Δg compared to 1g, and
- -30 to +30mV with a decrease under hypergravity compared to 1g and an increased current at 0g compared to 1.8g.

For a possible explanation, we have to look at the existing gating models for ion channels. A kinetic gating model mathematically describes the conformation changes the channel molecule performs to regulate the flow of ions. Voltage-gated ion channels have charged domains to make it sensitive to the electrical field and its variations. The conductance of the ion channel is high ("open") at a particular range of membrane potential and it is low ("closed") for other membrane potentials. The channel protein can have several conformations with varying conductance, and it can switch between the conformations. The activity of the voltage-gated $Na^+$-channel, for example, can be explained with at least 2 closed states (closed-excitable; closed-refractory) and 1 open state. The transition between these states is voltage-dependent. If a gravity-dependence is added to the differential equations which describe the conformation switches, the complex behaviour for such findings as presented in this work can probably be explained.

To further explore the basic principle of how ion channels react to different gravity conditions, more whole cell experiments should be performed with the final goal to perform single channel recordings with suitable cells. One of the drawbacks of SH-SY5Y cell was that a (unwanted) percentage of SH-SY5Y cells naturally differentiated by itself, without retinoic acid treatment. As no optical selection could be made with the Port-a-Patch it was possible to unintentionally patch a cell with different channel repertoire, as the repertoire is different in undiffernetiated and differentiated cells.

Since 2009 genetic modified cells can be used in European parabolic flights (after review by French authorities), therefore cells can be chosen for a) the seal probability and stability on the Port-a-Patch and b) the needed expression of ion channel families. Since classic channel blockers as tetrodotoxin cannot be used (up to now; 2010) due to safety regulations (toxicity), the use of GMO can be an alternative. Either one of the approaches (pharmacology or genetic engineering) must be selected in the future. Also the protocols must be adapted. A wider range of potential (between -100mV and +x mV depending on the cell) must be used to record all relevant activities, as the reversal potential where no net ion flow can be observed. For valuable data, the use of constant pulse protocols and complex

pulse protocols must be weight against one another. The use of constant protocols has the advantage of a high amount of data with the disadvantage of needing more flights to cover all relevant potentials as the number of possible campaigns per year is limited. The complexity of pulse protocols is limited in the 20 seconds of hyper- and microgravity with the advantage of (probably) needing fewer flight opportunities.

It was shown in this work that the developed patch-clamp setup can be used to perform these experiments. A revised hardware will be reduced in size and weight for easier transportation and a more flexible integration in the aircraft. Since hardware design in space research needs time, the redesign already started. It is planned to be able to house additional experiments to investigate several important issues: the changes in cell geometry and its possible influence on ion channels and adaptation.

It was shown that altered gravity has an effect on the actin and microtubule cytoskeleton of SH-SY5Y cells (Rösner et al. 2006) Scattered light experiments with SF21 cell in the drop tower indicated an (not significant) increase in cell volume under microgravity (Meissner 2004). Within the performed patch clamp experiments in the A300 Zero-G, it often could be observed, that the sealing process was better under hypergravity, which could be an indication of a change in cell geometry. Nevertheless the seal properties ($R_m$, $C_{fast}$, $C_{slow}$, $R_{series}$) of the used data were constant during the recording after the seal was established. To further investigate this important aspect, suitable experiments, as with scattered light, should be performed.

To support the whole cell experiments, experiments with voltage-dependent dyes, as DI-4-ANEPPS, could be performed to investigate the membrane potential under different gravity conditions. During parabolic flights, continuous recordings could be performed to monitor possible adaptation effects as they have been observed for retinal spreading depression waves under microgravity (Wiedemann et al 2006).

# 5 Abstract

## 5.1 English abstract

Gravitation influences many physical, chemical and biological processes. Cells and their behaviour are no exception. The gravitational impact on the activity of neuronal cells is very important with the perspective of manned space missions. Previous experiments with vertebrates showed that the velocity of neuronal impulses (action potentials) in nerve fibres is decreasing under zero gravity and is increasing at high gravity. There are many theories about the changed properties of the nervous systems under zero gravity, but the molecular principles are mostly unexplored.

For this dissertation hardware for patch clamp experiments under microgravity was developed. The patch clamp technique is a common used tool in investigating the electrophysiological properties of cells and single ion channels. Since the conditions during parabolic flights render classic patch clamp nearly impossible, advanced chip-based planar patch-clamp hardware, the Port-a-Patch from Nanion Technologies was integrated into a setup. This setup had to comply with the mandatory design and safety regulations to be used in parabolic flights. Two parabolic flight campaigns were used to validate the hardware, adapt the patch clamp procedures to the special conditions during a parabolic flight (as time pressure and vibrations) and to choose a suitable cell line from the available cell lines. As the laboratory conditions on ground were insufficient at the beginning of the project, the main focus had to lie on robust cells. The SH-SY5Y cell line was chosen for their robustness (they already have been used successfully by other teams) and their origin from the human brain (glioblastoma).

During two subsequent parabolic flight campaigns patch clamp experiments were performed and whole cell currents of SH-SY5Y cells were recorded with increasing success rate. Pulse protocols were used to create current-voltage (I-V) characteristics. To obtain 20 seconds of microgravity, two phases of hypergravity, each lasting 20 seconds, had to be endured by the passengers. This fact allowed the subsequent recording of whole cell currents of the same cell during normal Gravity (1g), hypergravity (1.8g) and microgravity (approx. $10^{-3}$g) to compare the I-V characteristics of the different gravity conditions.

For SH-SY5Y cells it was shown that a gravity dependence of the whole cell currents exists. The micro- and hypergravity whole cell currents were changed compared to 1g flight

controls. At -20 and -10mV, the hypergravity current was significantly decreased compared to 1g, by 13.5% at -20mV and by 7.4% at -10mV.

A significant *1.8g current < 0g current* relation could be observed at potentials between -20 and +10mV. At -20mV the microgravity whole cell currents were increased by 13.5%, at -10mV by 7.4%, at 0mV by 6.2% and at +10mV by 3.9%.

The duration and complexity of the used pulse protocols were limited by the time of each gravity phase (20-22 seconds).

In a last parabolic flight campaign, therefore the passive electrophysiological properties of the cell membrane were investigated. As the laboratory conditions at the site were greatly improved in the meantime, especially for cell culture, new cell lines could be tested for their usability. SNB19 cells, also originating from the human brain (astrocytoma) were chosen due to their good sealing quality and stability compared to SH-SY5Y cells and constant pulse protocols near the estimated resting potential (-80 and -60mV) were performed.

At constant -80mV and -60mV, it was shown that the whole cell currents during the variable gravity conditions are significantly increased compared to the 1g in-flight controls. The hypergravity current of SNB19 was increased by 2.2% at -80V and by 8.2% at -60mV. The microgravity current was increased by 4.1% at -80mV and 3.7% at -60mV.

The acquired I-V characteristic of SNB19 differs from the I-V characteristic of SH-SY5Y.

These findings show that the planar patch clamp technique can be used in parabolic flights to investigate the electrophysiological properties of single. Furthermore the findings suggest that the electrophysiological properties of single cells originating from the human brain exist are gravity dependent.

## 5.2 Deutsche Zusammenfassung

Die Schwerkraft beeinflusst viele physikalische, chemische und biologische Prozesse. Zellen und ihr Verhalten bilden dabei keine Ausnahme. Der Einfluss der Gravitation auf die Aktivität neuronaler Zellen ist wichtig, vor allem auch im Ausblick auf bemannte Weltraummissionen. Frühere Experimente mit Wirbeltieren zeigten, dass die Leitungsgeschwindigkeit von Nervenfasern für Aktionspotentiale unter Schwerelosigkeit abnimmt und unter hoher Schwerkraft zunimmt. Es gibt viele Theorien über die veränderten Eigenschaften des Nervensystems in der Schwerelosigkeit, aber die molekularen Grundlagen sind bis heute weitgehend unbekannt.

Für diese Arbeit wurde die Hardware für ein Patch Clamp System entwickelt, welches in der Schwerelosigkeit eingesetzt werden kann. Die Patch Clamp Technik ist ein verbreitetes Werkzeug um die elektrophysiologischen Eigenschaften von Zellen und einzelnen Ionenkanälen zu untersuchen. Da die Bedingungen während eines Parabelfluges klassisches Patchen beinahe unmöglich machen wurde ein planares Patch Clamp System, der Port-a-Patch von Nanion, in einen Experimentaufbau integriert. Der Experimentaufbau wurde nach den Konstruktions- und Sicherheitsregeln entwickelt und gebaut, die für die Teilnahme an Parabelflügen vorgeschrieben waren. Zwei Parabelflugkampagnen wurden verwendet um den Entwurf bezüglich Funktionalität und Sicherheit zu validieren. Des Weiteren wurden die Patch Clamp Prozeduren an die speziellen Bedingungen während des Parabelflugs (wie Zeitdruck und Vibrationen) angepasst, und eine passende Zelllinie wurde aus den zur Verfügung stehenden Kulturen ausgewählt. Da die Laborbedingungen vor Ort zu Beginn des Projekts nicht ausreichend waren musste das Hauptaugenmerk auf der Unempfindlichkeit der Zelllinie liegen. Die Zelllinie SH-SY5Y wurde aufgrund ihrer Robustheit (sie wurde bereits von anderen Gruppen erfolgreich verwendet) und ihrem Ursprung aus dem menschlichen Hirn (Glioblastom) ausgewählt.

Während zwei folgender Parabelflugkampagnen wurden Patch Clamp Experimente mit steigender Erfolgsrate durchgeführt und Ganzzellströme von SH-SY5Y Zellen wurden aufgezeichnet. Spannungsprotokolle wurden verwendet um Strom-Spannungs-Kennlinien (I-V) zu erstellen. Um 20 Sekunden Schwerelosigkeit im Flugzeug zu erhalten waren zwei Hypergravitationsphasen, jeweils 20 Sekunden lang, notwendig. Dies wiederum ermöglichte die aneinandergereihte Aufnahme von Ganzzellströmen derselben Zelle während normaler

Schwerkraft, Hypergravitation (1.8g) und Mikrogravitation (ca. $10^{-3}$g). Dadurch konnten die I-V-Kennlinien der einzelnen Gravitationsphasen miteinander verglichen werden.

Für SH-SY5Y Zellen konnte gezeigt werden, dass eine Schwerkraftabhängigkeit der Ganzzellströme existiert. Verglichen mit den 1g-Kontrollen während des Fluges änderten sich die Ganzzellströme während der veränderten Schwerkraftbedingungen. Bei -20 und -10mV waren die Ganzzellströme signifikant erniedrigt, um 13,5% bei -20mV und um 7,4% bei -10mV.

Ein signifikantes *1.8g-Ströme < 0g-Ströme* Verhältnis konnte zwischen -20 und +10mV beobachtet werden. Im Vergleich zu den Mikrogravitations-Strömen waren die 1.8g-Ganzzellströme bei -20mV um 13,5%, bei -10mV um 7,4%, bei 0mV um 6,2% und bei +10mV noch um 3,9% vergrößert.

Die verwendeten Spannungsprotokolle wurden in ihrer Dauer und Komplexität durch die Länge der einzelnen Gravitationsphasen (20-22 Sekunden) limitiert.

In einer letzten Parabelflugmission wurden deshalb die passiven elektrophysiologischen Eigenschaften der Zellmembran untersucht. Da sich inzwischen die Laborbedingungen vor Ort, vor allem für Zellkulturen, stark verbessert hatten konnten neue Zelllinien getestet werden. SNB19 Zellen, die ihren Ursprung ebenfalls im menschlichen Hirn (Astrozytom) haben, wurden aufgrund ihres, im Vergleich zu SH-SY5Y, sehr guten Sealverhaltens (Wahrscheinlichkeit und Stabilität) ausgewählt. Es wurden konstante Pulsprotokolle nahe des vermuteten Ruhepotentials (-80 und -60mV) von SNB19 Zellen durchgeführt.

Bei -80 und -60mV konnte gezeigt werden, dass die Ganzzellströme von SNB19 Zellen unter Hyper- und Mikrogravitation verglichen mit den 1g-Flugkontrollen signifikant erhöht sind. Die 1,8g-Ganzzellströme waren bei -80MV um 2,2% erhöht, bei -60mV um 8,2%. Die Ströme unter Mikrogravitation waren bei -80mV um 4,1%, bei -60mV um 3,7% erhöht.

Diese Ergebnisse zeigen, dass die planare Patch Clamp Technik im Rahmen von Parabelflugmission erfolgreich verwendet werden kann um die elektrophysiologischen Eigenschaften von einzelnen Zellen zu untersuchen. Weiterhin legen die Ergebnisse nahe, dass die elektrophysiologischen Eigenschaften von Zellen, welche ihren Ursprung im menschlichen Gehirn haben, gravitationsabhängig sind.

# 6 List of used abbreviations

| | |
|---|---|
| **A** | |
| A | ampere |
| A300 | Airbus A300 Zero-G |
| AP | action potential |
| **B** | |
| BSL-1 | biosafety level 1 |
| **C** | |
| C | Capacity |
| $C_{slow}$ | slow capacity |
| $C_{fast}$ | fast capacity |
| $C_m$ | Membrane capacity |
| $Ca^{2+}$ | calcium ion |
| $CaCl_2$ | calcium chloride |
| Cat.No. | catalogue number |
| CB | circuit breaker |
| CEV | Centre d'Essays en Vol |
| CNS | central nervous system |
| $CO_2$ | carbon dioxide |
| $Cs^+$ | cesium ion |
| CsCl | cesium chloride |
| CsOH | cesium hydroxide |
| **D** | |
| DC | direct current |
| DLR | *Deutsches Zentrum für Luft- und Raumfahrt* (German Aerospace Center) |
| DMSO | dimethyl sulfoxide |
| **E** | |
| EDTA | ethylenediaminetetraacetic acid |
| e.g. | exempli gratia; for example |
| EGTA | ethylene glycol tetraacetic acid |
| ESA | European Space Foundation |
| **F** | |
| FBS | fetal bovine serum |
| **G** | |
| g | gram |
| GFI | ground fault interrupter |
| GMO | genetically modified organism |
| **H** | |
| HEPES | (4-(2-hydroxyethyl)-1-piperazineethanesulfonic acid) |
| hERG | human Ether-à-go-go Related Gene |
| HDD | hard disk drive |
| Hz | Hertz |
| **I** | |
| I | current |
| ISS | International Space Station |
| **K** | |
| $K^+$ | potassium ion |
| KCl | potassium chloride |
| kg | kilogram |
| km/h | kilometre per hour |
| kΩ | kilo-ohm |
| kPa | kilopascal |
| **L** | |
| L1 | phase 1 (electric system) |
| LED | light emitting diode |
| **M** | |
| m | metre |
| mA | milliampere |
| mbar | millibar |
| $Mg^{2+}$ | Magnesium ion |
| $MgCl_2$ | magnesium chloride |
| min | minutes |
| ml | millilitre |
| mm | millimetre |

| | |
|---|---|
| mM | millimolar (=$10^{-3}$M) |
| MΩ | megaohm |
| mOsmol | osmolarity |
| ms, msec | milliseconds |
| mV | millivolt |

**N**

| | |
|---|---|
| N | Neutral (electric system) |
| $Na^+$ | magnesium ion |
| NaCl | Sodium chloride |
| $NaHCO_3$ | Sodium bicarbonate |
| NaOH | sodium hydroxide |
| NPC-1 | Nano-Patch-Chip |

**O**

| | |
|---|---|
| OPA | operational amplifier |

**P**

| | |
|---|---|
| PBS | phosphate buffered saline |
| PFC | parabolic flight campaign |
| PSU | power supply unit |

**R**

| | |
|---|---|
| R | Resistance, Resistor |
| $R_f$ | Feedback resistor |
| $R_{acc}$ | Patch resistance |
| $R_{pip}$ | Pipette resistance |
| $R_{series}$ | Series resistance |
| RA | retinoic acid |
| RC-circuit | resistor capacitor circuit |
| rpm | revolutions per minute |
| rSD | retinal Spreading Depression |

**S**

| | |
|---|---|
| s, sec | seconds |
| SEM | standard error of the mean |

**U**

| | |
|---|---|
| U | potential (voltage) |
| $U_{hold}$ | holding potential |
| $U_{pip}$ | pipette potential |
| UPS | uninterruptible power supply |
| USB | Universal Serial Bus |

**V**

| | |
|---|---|
| V | voltage |
| $V_{min}$ | minimum voltage |
| $V_{max}$ | maximum voltage |

**Special**

| | |
|---|---|
| Δg | g-level differing from 1g |
| °C | temperature in Celsius |
| µl | microlitre |
| µT | microtesla |
| 19'' | 19 inches |

# 7 Table of figures

## Introduction



## Material and methods



## Results

## Appendices

# 8 References

Abemayor E; The effects of retinoic acid on the in vitro and in vivo growth of neuroblastoma cells; Laryngoscope 102 (10), pp. 1133-1149, 1992

Bear M.F., Connors B.W., Paradiso M.A.; Neurowissenschaften – Ein grundlegendes Lehrbuch für Biologie, Medizin und Psychologie 3. Auflage; Spektrum Akademischer Verlag, 2009

Behrends J.C.; Fertig N.; Planar Patch Clamping; Neuromethods 38, pp. 411-433, 2007

Biedler J.L., Helson L., Spengler B.A.; Morphology and growth, tumorigenicity and cytogenetics of human neuroblastoma cells in continuous culture; Cancer Res. 33(11) pp. 2643-2652, 1973

Biedler J.L., Roffler-Tarlov S., Schachner M., Freedman L.S.; Multiple neurotransmitter synthesis by human neuroblastoma cell lines and clones; Cancer Res. 38 (11 Pt.1) pp. 3751-3757, 1978

Cegila E. (European Space Agency); Reference Guide to European Low Gravity Platforms Erasmus Centre ESA, UC-ESA-RLG-001 Issue 1 Revision 0, 2007

Cegila E. (European Space Agency); European Users Guide to Low Gravity Platforms; Erasmus Centre ESA, UIC-ESA-UM-0001 Issue 2 Revision 0, 2005

Elbert T.; Slow Cortical Potentials reflect the regulation of cortical excitability; Slow Potential Changes in the Human Brain 235-251, Plenum Press New York, 1993

Goldermann M., Hanke W.; Ion Channels are Sensitive to Gravity Changes; Microgravity sci. Technol. XIII/1, pp. 35-38, 2001

Gross J.L., Behrens D.L., Mullins D.E., Kornblith P.L., Dexter D.L.; Plasminogen Activator and Inhibitor Activity in Human Glioma Cells and Modulation by Sodium Butyrate; Cancer Research 48, pp. 291-296; 1988

Hamill O.P., Marty E., Neher E., Sakmann B., Sigworth F.J.; Improved Patch-Clamp Techniques for High-Resolution Current Recording from Cells and Cell-Free Membrane Patches; Pflügers Arch. 391, pp. 85-100, 1981

Hanke W., Goldermann M., Brand S., Fernandes de Lima V.M; The Retinal Spreading Depression: A Model for Nonlinear Behavior of the Brain; A Perspective Look at Nonlinear Media (227-243); Springer Verlag GmbH, 1998

Hanke W.; The Retinal Spreading Depression, Berichte aus der Biologie 48; Shaker Verlag GmbH, 1999

Hanke W., Fernades de Lima V.M., Wiedemann M., Meissner K.; Microgravity dependence of excitable biological and physicochemical media; Protoplasma 229, pp. 235-242, 2006

Karmali F., Shelhamer M.; The dynamics of parabolic flights: Flight characteristics and passenger percepts; Acta Astronautica 63, pp. 594-602, 2008

Klinke M., Goldermann M., and Hanke W.; The properties of alamethicin incorporated into planar lipid bilayers under the influence of microgravity; Acta Astronautica Vol. 47, No. 10, pp. 771-773, 2000

Kryshtal O.A., Pidoplichko V.I.; Intracellular Perfusion of Helix Giant Neurons Neirofiziologiya, Vol. 7, No.3, pp. 327-329, 1975 (Russian original) (English Version 1976, Plenum Publishing Corporation)

Leao A.A.P.; Spreading Depression of activity in the cerebral cortex; J. Neurophysiol. 7, pp. 359-390, 1944

Machemer H.; Unicellular Responses to Gravity Transitions;Space Forum, Vol. 3, pp. 3-44, 1998

Meissner K.; Elektrophysiologische Charakterisierung neuronaler Prozesse unter veränderten Schwerkraftbedingungen; Dissertation Universitaet Hohenheim, 2004

Meissner K., Hanke W.; Action potential properties are gravity dependent; Microgravity sci. Technol. XVI, pp. 38-43, 2005

Mollemann A.; Patch clamping, an introductory guide to patch clamp electrophysiology; John Wiley & Sons Ltd., 2003

Montmerle T., Augereau J.-C., Chaussidon M., Gounelle M., Marty B., Morbidelli A.; 3. Solar System Formation and Early Evolution: the First 100 Million Years; Earth, Moon, and Planets 98, pp. 39-95, 2006

Novespace; A300 Zero-G Rules and Guidelines; Revision date April 7th 2009

Numberger M., Draguhn A.; Patch-Clamp-Technik, Spektrum Akademischer Verlag Heidelberg, Berlin, Oxford, 1996

Påhlman S., Ruusala A-I., Abrahamsson A., Mattson MEK., Esscher T.; Retinoic acid induced differentiation of cultured neuroblastoma cells. A comparison with phorbolester induced differentiation; Cell Diff. 14, pp. 135-144, 1984

Rösner H. Wassermann T., Möller W., Hanke W.; Effects of altered gravity on the actin and microtubule cytoskeleton of human SH-SY5Y neuroblastoma cells; Protoplasma 229, pp. 225-234, 2006

Ross R.A., Spengler B.A., Biedler J.L.; Coordinate morphological and biochemical interconversion of human neuroblastoma cells; J. Natl. Cancer Inst. 71, pp. 741-747, 1983

Sakmann B., Neher E.; Single-Channel Recording; Plenum Press, New York, 1983

Sieber M.; Elektrophysiologische Untersuchungen der Zelllinie SH-SY5Y; Diploma Thesis (Biology), Universitaet Hohenheim, 2004

Sidell N., Bieshia Chang, Yamashiro J.M., Wada R.K.; Transcriptional upregulation of retinoic acid receptor β (RARβ) expression by phenylacetate in human neuroblastoma cells; Exp. Cell. Res. Vol. 1, Issue 1, pp. 169-174, 1998

Sontheimer H., Waxman S.G.; Expression of voltage-activated ion channels by astrocytes and oligodendrocytes; J Neurophysiol. 70, pp. 1863-73, 1993

Toselli M., Tosetti P., Taglietti V.; Functional Changes in Sodium Conductances in the Human Neuroblastoma Cell Line SH-SY5Y During In Vitro Differentiation; Journal of Neurophysiology Vol. 76, No. 6, pp. 3920-3927, 1996

Tosetti P., Taglietti V., Toselli M.; Functional Changes in Potassium Conductances of the Human Neuroblastoma Cell Line SH-SY5Y During In Vitro Differentiation; Journal of Neurophysiology Vol. 79, pp. 648-658, 1998

Wiedemann M., Rahmann H., Hanke W.; Gravitational Impact on Ion Channels Incorporated Into Planar Liquid Bilayers; Membrane Science and Technology Series, 7, Chapter 24, Elsevier Science B.V., 2003

Wiedemann M., Piffel A., Hanke W.; Effects of different gravity conditions on self organizing biological systems; Signal Transduction 6, pp. 414-421, 2006

Wiedemann M., Kohn F.P.M., Rösner H., Hanke W.; Self-organization and pattern-formation in neuronal systems under conditions of variable gravity; Springer Verlag (In Press), 2010

# 9 Appendices

## 9.1 Laboratory conditions at Novespace

### 2007

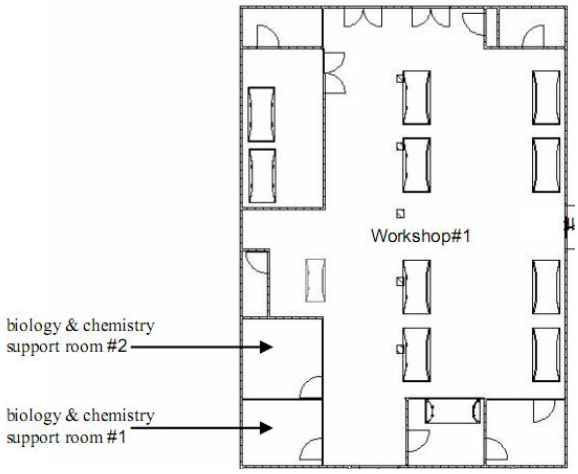


Figure 8.1: The laboratory conditions 2007. Two kitchens were used as biological and chemical support room. They were not certified by any laboratory standard. The total floor area was approximately 6m$^2$ per room. The rooms had to be shared by all science teams. During the 11$^{th}$ DLR PFC, one complete room could be used by the team (Floor plan provided by Novespace).

## 2009

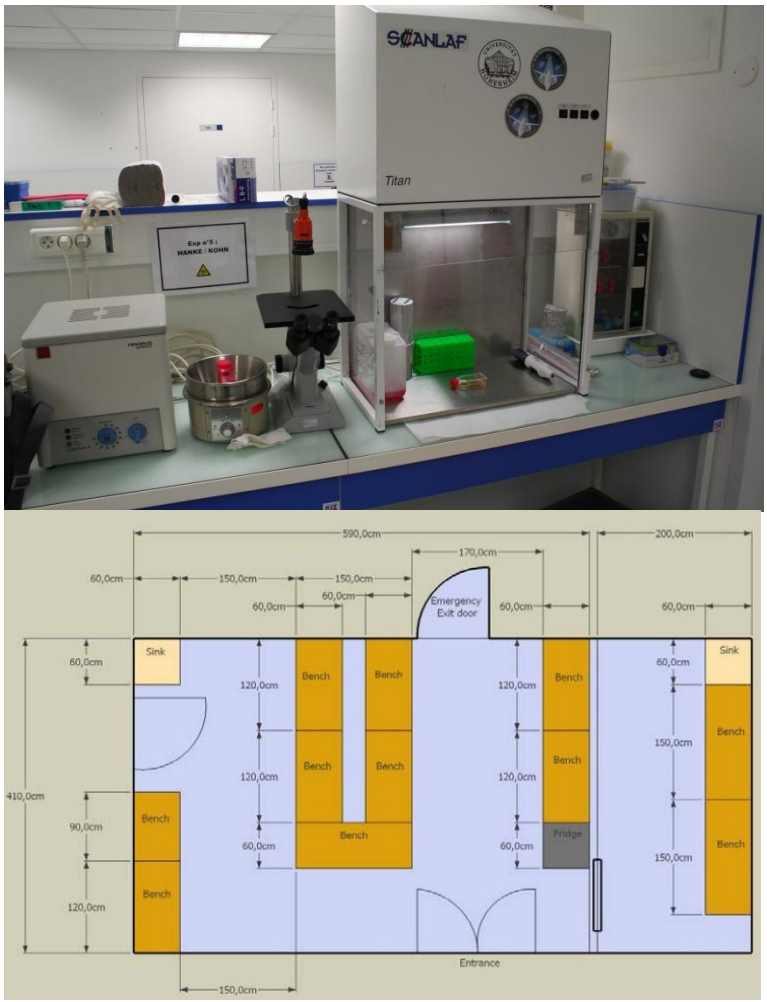


Figure 8.2: The new laboratory rooms since 2009. They are certified to biosafety level 1 (BSL-1). Since 2010, a clean bench is permanently installed in the lab (provided by the Dept. Membrane Physiology, Univ. Hohenheim). Approximately 40m$^2$ with 13m$^2$ of workbench space can be used by the scientists. Depending on the number of experiments, multiple tables can be used by the scientists (Floor plan provided by Novespace).

## 9.2 Non-significant current voltage characteristics of undifferentiated SH-SY5Y

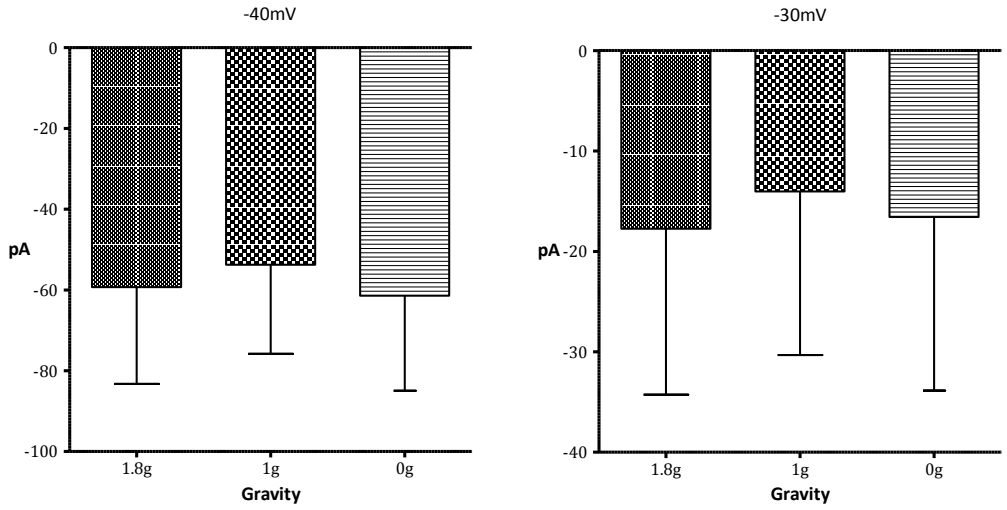


Figure 8.3: Changes in the whole cell currents of undifferentiated SH-SY5Y cells at -40 and -30mV. Mean ±SEM

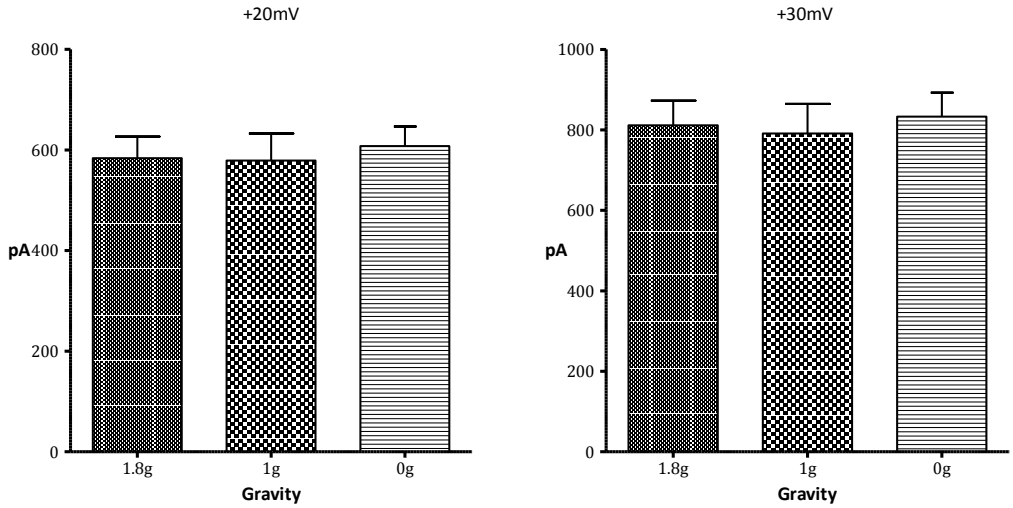


Figure 8.4: Changes in the whole cell currents of undifferentiated SH-SY5Y cells at +20 and +30mV. Mean ±SEM

## 9.3 Non-significant current-voltage statistics of SNB19

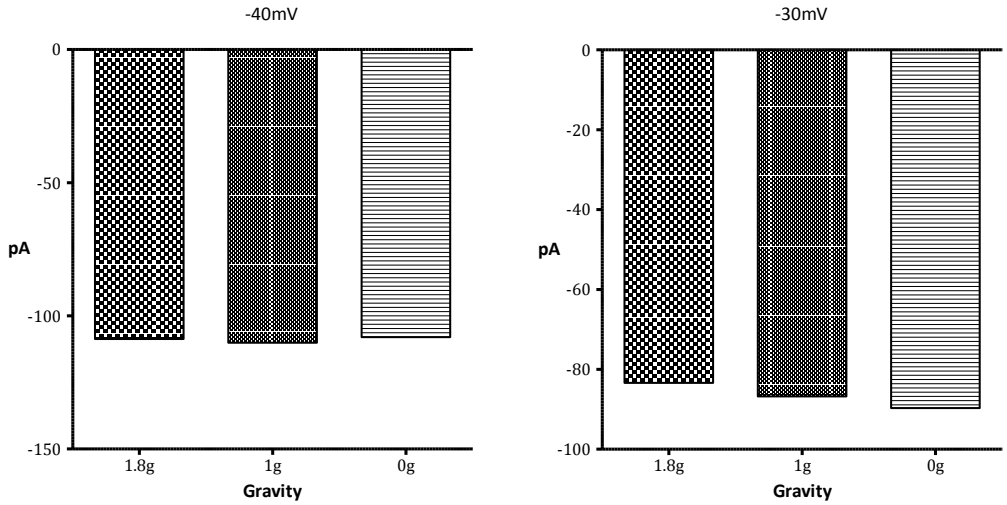


Figure 8.5: Changes in the whole cell currents of a SNB19 cell at -40 and -30mV.

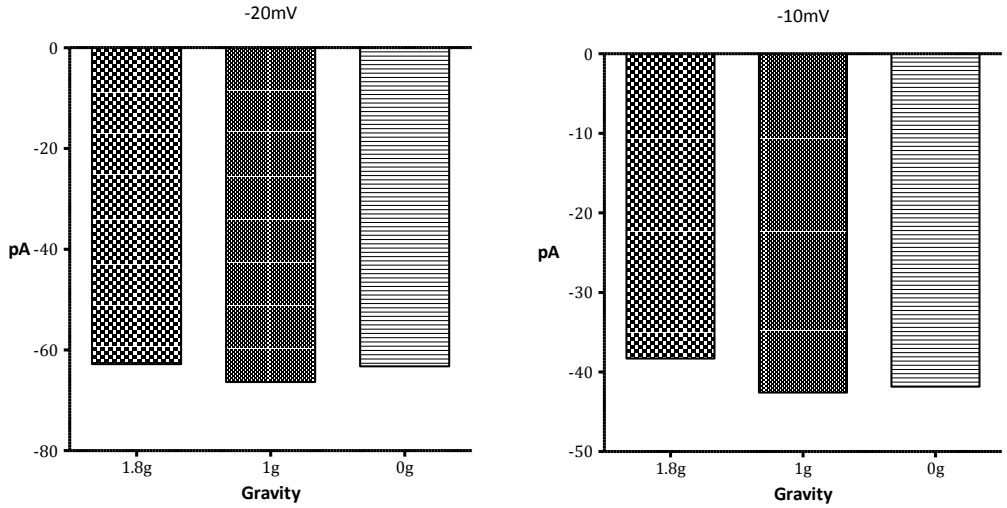


Figure 8.6: Changes in the whole cell currents of a SNB19 cell at -20 and -10mV.

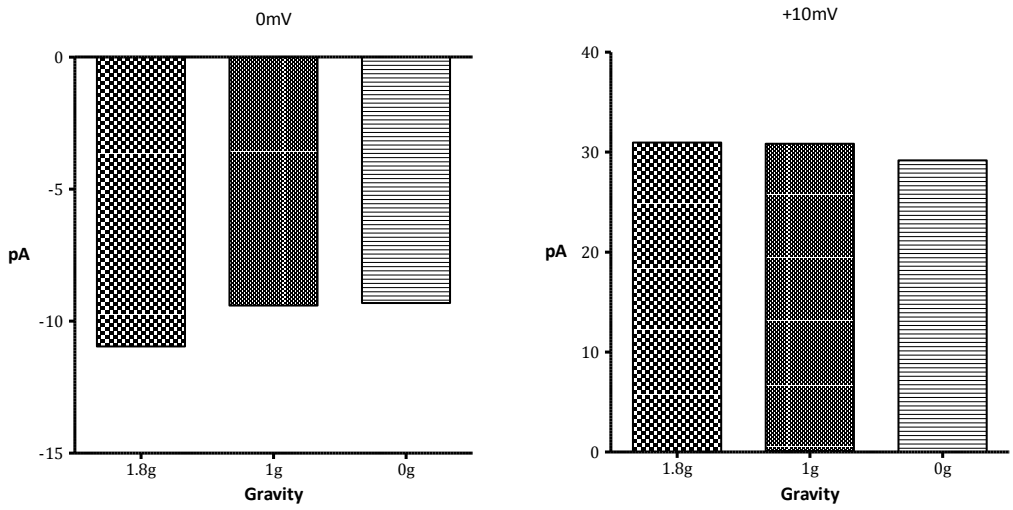


Figure 8.7: Changes in the whole cell currents of a SNB19 cell at 0 and +10mV.

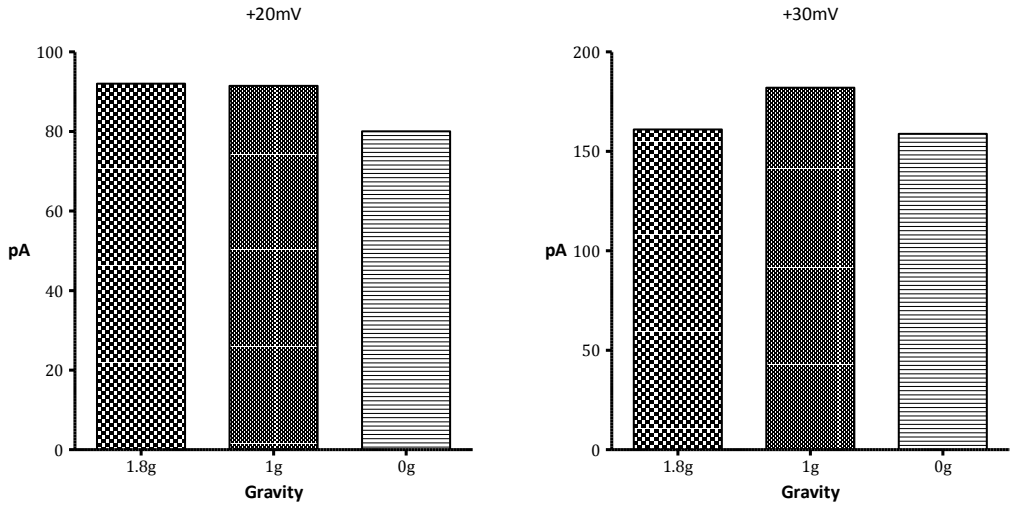


Figure 8.8: Changes in the whole cell currents of a SNB19 cell at +20 and +30mV.

## 9.4 Non-significant constant -40mV protocol SNB19

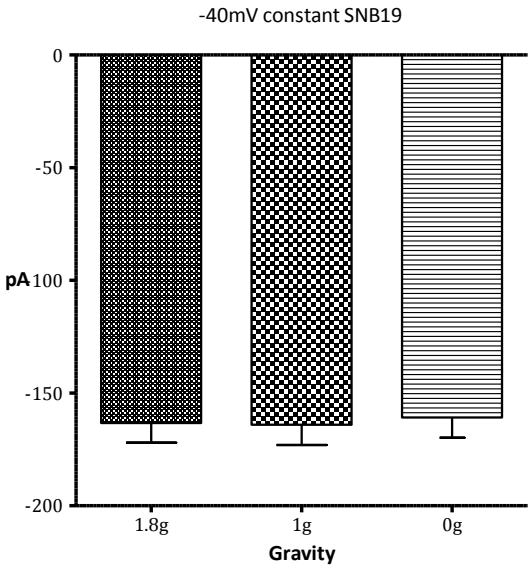


Figure 8.9: Changes in the whole cell currents of a SNB19 cell at constant -40mV.

# 10 Acknowledgments

Ich danke Prof. Dr. Wolfgang Hanke für die Einführung in die Weltraumforschung, einem interessanten und herausfordernden Aufgabengebiet. Ich hätte zu Beginn meines Studiums nie gedacht, dass ich mal „*im Weltraum*“ landen würde. Vielen Dank für Ihr Vertrauen mir die Verantwortung über das ganze Projekt zu geben. Für ihre fachliche und menschliche Unterstützung, egal zu welchem Thema und zu welcher Tages- und Nachtzeit, kann ich mich gar nicht genug bedanken.

Ohne meine Kollegen wäre diese Arbeit überhaupt nicht möglich gewesen. Mein besonderer Dank geht an „*my always charming colleague*“ Michaela Sieber, die mich bei jeder Parabelflugmission unterstützt hat: moralisch, mit Zellnachschub und während der Flüge. Ohne Dich wären die Experimente deutlich schwerer und vor allem deutlich weniger lustig gewesen!

Ich möchte mich bei Meike Wiedemann bedanken, die mich bei der Bewältigung des immensen Papierkriegs, der die Weltraumforschung begleitet, mit aller Kraft unterstützte. Du hast mich während des Papierkriegs für das Projekt sicher durch alle Phasen der emotionalen Zustände begleitet: Irritation, Wut, Verzweiflung, Resignation und letztendlich Ausgeglichenheit.

Stefan Kaltenbach danke ich recht herzlich für die Nacht- und Wochenenddienste an der Uni, um die Parabelexperimente in Frankreich mit frischen Zellen zu versorgen. Ich danke euch allen für eine angenehme Zusammenarbeit und die tollste Arbeitsatmosphäre die man sich wünschen kann!

Des Weiteren danke ich Wolfgang Möller aus der Zoologie für die exzellente Ausbildung in der Zellkultur und für seine Unterstützung in den letzten Jahren!

Ich danke Dr. Hinrich Lühring für unsere Ausflüge in die Biophysik und für die tiefen Einblicke in die Elektrophysiologie. In der kurzen Zeit habe ich viel von Dir gelernt.

Ich möchte auch den vielen Menschen aus den unterschiedlichsten Forschungsgruppen die ich während dieses Projekts kennengelernt habe, für die interessanten Gespräche und die immer positive, beinahe familienartige Stimmung danken, die während der Parabelflugkampagnen und den wissenschaftlichen Meetings herrschte: Prof. Dr. R. Hilbig, Claudia, Miri, Jochen, Peter, Martin und unzählige andere.

Dem DLR, vor allem Dr. Ulrike Friedrich und Dr. Markus Braun, danke ich für die Finanzierung des Projekts, für die Bereitstellung der Fluggelegenheiten und für die Unterstützung der Arbeit.

I like to thank ESA, especially Vladimir Pletser, for providing the flight opportunities and the pleasant atmosphere during the parabolic flight campaigns.

My heartfelt thanks go to the Novespace employees. The engineers who supported this experiment during the whole time, Elisabeth Celton and Patrice Rosier; Ann-Clotilde and Nathalie for the administrative support and all the others which do their best to support the teams and to improve the scientific conditions.

Meinen Eltern und meiner Schwester danke ich dafür, dass Ihr mich bedingungslos bei meinem Lebensweg begleitet und unterstützt. Ohne Euch wäre ich nicht der Mensch der ich jetzt bin!

Mein unendlicher Dank geht an Mara, Du hast mir den Rücken freigehalten wann immer mir die Arbeit über den Kopf stieg; Du hast mich während aller Hochs und Tiefs begleitet und ertragen. Danke, dass Du immer für mich da warst!